RÉPUBLIQUE ALGÉRIENNE DÉMOCRATIQUE ET POPULAIRE

Ministere de l'Enseignement Superieur et de la Recherche Scientifique

Ecole Nationale Polytechnique

Department of Automation

Laboratory of Control of Processes

PhD Thesis in Sciences

Presented, for obtaining the degree of Doctor

of Sciences in Electrical Engineering

Option :Automatic,

by

Samir KHELOUAT

Entitled :

Contribution on Observation and Fault Diagnosis of A Multicellular Converter

Defended, on 10/*July*/2021.

Members of jury :

Chair :	Mr. BOUDJEMA Fares	Professor, ENP
Supervisor :	Mr. BOUKHETALA Djamel	Professor, ENP
Co-supervisor :	Mr. BENALIA Atallah	Professor, Univ. Laghouat
Co-supervisor :	Mme LALEG-KIRATI Taous Meriem	Professor, KAUST (KSA)
Examiners :	Mr. LAGRAA Nasreddine	Professor, Univ. Laghouat
	Mr. BENMANSOUR Khelifa	Professor, ESDAT
	Mr. NAIT SEGHIR Amirouche	Professor, USTHB
	Mr. TADJINE Mohamed	Professor, ENP
Invited :	Mr. DJEMAI Mohamed	Professor, Univ. Valenciennes

ENP 2021

Ecole Nationale Polytechnique (ENP), 10 Avenue des Frères Oudek BP 182, El Harrach16200, Alger

RÉPUBLIQUE ALGÉRIENNE DÉMOCRATIQUE ET POPULAIRE

Ministere de l'Enseignement Superieur et de la Recherche Scientifique

Ecole Nationale Polytechnique

Department of Automation

Laboratory of Control of Processes

PhD Thesis in Sciences

Presented, for obtaining the degree of Doctor

of Sciences in Electrical Engineering

Option :Automatic,

by

Samir KHELOUAT

Entitled :

Contribution on Observation and Fault Diagnosis of A Multicellular Converter

Defended, on 10/*July*/2021.

Members of jury :

Chair :	Mr. BOUDJEMA Fares	Professor, ENP
Supervisor :	Mr. BOUKHETALA Djamel	Professor, ENP
Co-supervisor :	Mr. BENALIA Atallah	Professor, Univ. Laghouat
Co-supervisor :	Mme LALEG-KIRATI Taous Meriem	Professor, KAUST (KSA)
Examiners :	Mr. LAGRAA Nasreddine	Professor, Univ. Laghouat
	Mr. BENMANSOUR Khelifa	Professor, ESDAT
	Mr. NAIT SEGHIR Amirouche	Professor, USTHB
	Mr. TADJINE Mohamed	Professor, ENP
Invited :	Mr. DJEMAI Mohamed	Professor, Univ. Valenciennes

ENP 2021

Ecole Nationale Polytechnique (ENP), 10 Avenue des Frères Oudek BP 182, El Harrach16200, Alger

RÉPUBLIQUE ALGÉRIENNE DÉMOCRATIQUE ET POPULAIRE

Ministere de l'Enseignement Superieur et de la Recherche Scientifique

Ecole Nationale Polytechnique

Département d'Automatique

Laboratoire de Commande de Processus

Thèse de Doctorat en Sciences

Présentée, en vue de l'obtention de grade de Docteur

en Sciences en Génie Electrique

Option : Automatique,

par :

Samir KHELOUAT

Intitulé

Contribution à l'Observation et au Diagnostic des Défauts du Convertisseur Multi Cellulaire

Soutenue, le 10/*Juillet*/2021.

Membres de jury :

Prèsident :	Mr. BOUDJEMA Fares	Professeur, ENP
Directeurs :	Mr. BOUKHETALA Djamel	Professeur, ENP
Co-directeur de thèse :	Mr. BENALIA Atallah	Professeur, Univ. Laghouat
Co-directeur de thèse à l' étranger :	Mme LALEG-KIRATI Taous Meriem	Professeur, KAUST (KSA)
Examinateurs :	Mr. LAGRAA Nasreddine	Professeur, Univ. Laghouat
	Mr. BENMANSOUR Khelifa	Professeur, ESDAT
	Mr. NAIT SEGHIR Amirouche	Professeur, USTHB
	Mr. TADJINE Mohamed	Professeur, ENP
Invitè :	Mr. DJEMAI Mohamed	Professeur, Univ. Valencienne

ENP 2021

Ecole Nationale Polytechnique (ENP), 10 Avenue des Frères Oudek BP 182, El Harrach16200, Alger

Acknowledgements

I would like to express my special appreciation and thanks to following for their help and support, in one way or another in the writing of this thesis.

I sincerely thank my advisor Professor Djamel Boukhetala for directing and encouraging me throughout this work. His pieces of advice and availability have been of great help to me over all my Ph.D. years. I also extend my sincere and lively thanks to my co-advisor Professor Atallah Benalia, for his endless support, encouragement, and guidance as well as his selflessness in sharing his knowledge and being there any time when needed. I would like to express my thanks for his hospitality in receiving me several times in LACOSER laboratory. Words cannot express how I am deeply grateful to him. I also extend my sincere and lively thanks to my co-advisor Professor Meriem Laleg, for her endless support, encouragement, and guidance as well as for giving me the opportunity to do my internship at KAUST. I would like to express my thanks for her generous hospitality, and for being there any time when needed. her help and advice are priceless. Words cannot express how I am deeply grateful to her. I would like also to express my thanks to the committee members of my thesis that agreed to evaluate the work. I also would like to appreciate the help of the all people that are involved closely or remotely, mainly : Prof. Mohammed Djemai, Prof. Ahmed Maidi, Prof. Redouane Kara, and Mr Lahdiri Mohand Arezki. Finally I thank the members of my family, each of them for their way of helping me during all my years of P.hd, my father Belkacem, my mother-in-law Sadia, my sisters, my brothers Khaled and Hamza and my wife Aicha.

Without a doubt they will be very happy for me if they are with us today, unfortunately they left us too early, to my very dear mother Bahia who I really miss and my uncle mohammed whom I will never forget his kindness that I dedicated this work.

الملخص:

يتعلق هذا العمل المقدم في هذه الأطروحة برصد و تشخيص العطب في محول كهربائي ذو ثلاث خلايا، الذي يعتبر نظاما هجينا نظرا لسلوكه التحويلي. و نتيجة لهذا السلوك، تم عرض تحليل قابلية الرصد لمسار زمني هجين باستخدام طريقة هندسية تعتمد على حساب الفضاء القابل للرصد على طول المسار الزمني الهجين. بعد ذلك تم تصميم مرصد ذو نمط انزلاقي للنظام القابل للرصد للمحو الكهربائي. و قد تم إثبات تقارب خطأ الرصد باستعمال نظرية $Lyapunov$. و قد تم أيضا ضبط معايير المرصد عن طريق إيجاد حل لمعادلة LMI. و قد أظهرت نتائج محاكاة المولدات المحصل عليها نتائج جيدة لإعادة بناء التوتر. الجزء الثاني من هذا العمل يتعلق بتشخيص العطب في خلايا المحول الكهربائي. و قد تم أيضا تطبيق طريقة هندسية لحساب الفضاءات الحساسة لمجموعة من الأعطاب و غير حساسة لمجموعة أخرى. و قد تم كشف و تشخيص العطب باستعمال مولدات تعتمد على مراصد ذو نمط انزلاقي. و قد أظهرت نتائج المحاكاة المحصل عليها كفاءة المولدات ذو النمط الإنزلاقي المقترحة لكشف و تشخيص العطب.

الكلمات المفتاحية:

تشخيص الأعطاب، قابلية رصد الأنظمة الهجينة، مرصد ذو نمط إنزلاقي, محول متعدد الخلايا

Résumé :
Le travail présenté dans cette thèse concerne l'observation et le diagnostic de défauts du convertisseur à 3 cellules de commutation qui est considéré comme un système hybride vu son comportement de commutation. De ce fait, l'analyse de l'observabilité a été montré, pour une trajectoire temps hybride, en utilisant une approche géométrique basé sur le calcul de sous espace inobservable le long de la trajectoire temps hybride. Un observateur à mode glissants est ensuite conçu pour le sous espace observable du convertisseur. La convergence de l'erreur d'observation est démontré en utilisant le formalisme de Lyapunov. Les paramètres de l'observateur sont calculés en résolvant une LMI. Les résultats de simulation montrent une bonne reconstructions des tensions flottantes du convertisseur. La deuxième partie, est consacrée pour le diagnostic de défauts cellules du convertisseur. En effet, une approche géométrique a été appliqué pour le calcul des sous espaces sensibles á un ensemble de défaut et insensible á un autre ensemble. La détection et l'isolation des défauts est basée sur la conception de générateurs de résidus à base d'observateurs. Les résultats de simulation ont montré l'efficacité des générateurs de résidus proposés à base d'observateurs à mode glissant.
Mot clés : Convertisseur multi-cellulaire ,obsérvabilité des systèmes hybrides, diagnostic de défauts, observateur á mode glissant.

Abstract :
The work presented in this thesis concerns the observation and diagnosis of faults in the 3-cell converter which is considered to be a hybrid system du to its switching behavior. Indeed, the observability analysis has been shown for a hybrid time trajectory using a geometric approach based on the computation of the unobservable subspace along the hybrid time trajectory. A sliding mode observer is then designed for the observable subspace of the converter. The convergence of the observation error is demonstrated using the Lyapunov theory. Observer parameters are computed by solving a linear matrix inequality (LMI). The simulation results show a good reconstruction of the floating voltages of the converter. The second part is devoted to the diagnosis of converter faults. Indeed, a geometric approach has been applied for the determination of the subspaces sensitive to a set of faults and insensitive to another set. Fault detection and isolation is based on the designing of observer-based residual generators. The simulation results show the efficiency of the proposed residual generators based on sliding mode observers.

Key words : Multi cell converter, observability of hybrid systems, fault diagnosis, sliding mode observer.

Contents

List of figures

List of tables

Nomenclature

List of Abbreviation

FPRG : Fundamental Problem of Residual Generation.
l-NLFPRG : local Non-Linear Fundamental Problem of Residual Generation.
BG : Bond Graph.
HBG : hybrid Bond Graph
ODE : Ordinary Differential Equation.
DAE : Discrete Algebraic Equation.
PN : Petri-Net.
HPN : Hybrid Petri-Net.
DOS : Dedicated Observer Scheme.
GOS : Generalized Observer Scheme.
SOS : Simplified Observer Scheme.
FDI : Fault Detection and Isolation.
LTI : Linear Time Invariant.
LMI : Linear Matrix Inequality.
THD : Total Harmonic Distorsion.
DCC : Diode Clamped Converter.
H-B : H-Bridge.
CH-B : Cascade H-Bridge.
NPC : Neutral Point Converter.
PCA : Principal Component Analysis.
SVM : Support Vector Machine.
SSS : Signal Signature Study.

Notation

R : The set of real number.
R^n : A set of real vector of length n.
$R^{n\times n}$: A set of real $(n \times n)$ matrices.
R^+ : A set of positif real number.
N : A set of natural number.

$||X||_2$: The euclidean norm of the vector X.
$|x|$:Absulute value of x.
X^T : The transpose of X.
$X^\perp$: The orthogonal complement of X.
$ker(X)$: The Kernel or the null space of X.
e^{At} : The transition matrix of A.
N_i^m : The unobservable subspace over the time interval $[t_0, t_m]$.
$\lambda_i\{X\}$: The set of all eigenvalues of the matrix X.
$\lambda_{min}\{X\}$: The minimum eigenvalue of X.
$\lambda_i\{X\}$: The maximum eigenvalue of X.
$oca((\Sigma)^\perp)$: Observability distribution algorithm.
Σ : The conditioned invariant distribution.
Ω : The observability codistribution.

Introduction

Most practical control systems require both analog and logic components. A hybrid system is a generic term for such systems. Switched systems are a class of hybrid systems, where the continuous and discrete dynamics are interacting and cohabit. These systems arise naturally in many automatic applications of control and becoming more and more complex due to the emergence of complex control techniques. The execution of switched systems can be defined by a sequence of transitions between modes (sub-systems), in each mode, the system state evolves continuously according to a dynamical control law until a discrete transition occurs which drives it to the other modes. The continuous dynamic of each mode may be continuous or discrete-time but generally is given by differential equations. The discrete variable dynamic is governed by a digital automaton with a countable number of states.

The multilevel voltage converter systems are considered as switched systems and are required more and more in many applications in industry for their improved performances. These systems are not a new topologies, some of them are known since 1960 [1], but they were not used until recently because of certain technical barriers, that have disappeared mainly due to the improvement of the control theory of switching systems and the intensive computer use in the control of the process [2]. One of these multilevel voltage converters is the flying capacitor also reported as an imbricated cell converter or the multicellular converter. It has been introduced in the early 1990s for energy conversion and it consists of a series of elementary cells of semiconductor devices that operate in commutation mode, makes it possible to share the constraint in tension and improve the harmonic contents of the output waveform and also allows the reduction of different losses due to commutation of power semiconductors. For all these offered features and benefits, the multicellular converter becomes more attractive in industrial applications, especially in renewable energy and automotive high-power applications [3]. These advantages are acquired when the converter operates in optimal conditions, i.e., it is necessary to ensure a particular distribution of the voltage for every cell of the converter. To this end, a suitable control sequence for switches must be applied. Consequently, the convergence of the floating capacitor voltages to their references. These properties are lost if the capacitor voltages deviated from their references, caused by different anomalies that can affect the functioning of the converter. However, it is important to measure the floating capacitor voltages, and the use of sensors increases the cost and the complexity of the system.

The estimation of the floating voltages by using an observer is then an interesting alternative. Many observers are proposed in the literature to overcome a problem of state estimation of the multicellular converter. In the two last decades, the sliding mode observer has been intensively studied thanks to its interesting features and its robustness.

The observability is an important property that should be studied before designing observers for any system. For the hybrid three cell converter, the observability matrix is never full rank for each operating mode, but it does not imply the unobservability of the system in a classical sense. Indeed, new concepts have been recently introduced to analyze the observability of the states for hybrid systems. First, the $Z\{T_N\}$ observability which is introduced in [4] for switched hybrid systems gives the condition under which there exists a hybrid time trajectory that makes the system observable [5]. The second method, based on a geometrical condition is more recently introduced in [6] and it is based on determining the unobservable subspace along the hybrid time trajectory.

Safety and reliability are crucial for the operation of power electronic converters. Indeed, the continuous increase in the use of power converters in complex and sensitive industrial plants, and the emergence of complex control techniques make it necessary to ensure its safety and reliability. In power electronics, we distinguish two types of faults, parameter faults, and discrete faults. Parameter faults depend mainly on the variation of certain parameters of the converter from their nominal values [7]. Such faults are of low dynamics and can often be detected before the breakdown of the converter. Capacitance degradation of the 3-cell converter, due to multiple causes such as high ambient temperature, high humidity [8] and aging of the capacitance are some examples of parameters faults. Discrete faults which include short and open-circuit of the converter cells are considered as hard faults and lead to a breakdown of the component if the fault is not detected on time. These faults are of high dynamics and are often difficult to handle to save the entire component [9]. Therefore, it is necessary to have reliable diagnostic tools to ensure the good functioning of the converter and to protect not only the electrical devices that are connected to it and avoid the shutdown of the production, but also to protect the human operators around. Fault diagnosis is the process of determining the type, size, location, and the occurrence time of the faults. Indeed, detecting a fault returns to point out its occurrence, i.e., determine if the current state of the system and its components are in normal functioning, signaling any deviation from the expected behavior. While the isolation task consists of analyzing the events to be able to determine the source of the fault. In the literature, several approaches have been developed to perform a reliable diagnosis procedure. Methods based on the analytical model consist of knowledge of the system constituted by the explicit formulation of the analytical model (for example differential equations). These methods consist of comparing the current behavior of the real system characterized by the collected information to the theoretical behavior provided by an analytical model. Consequently, a set of indicator signals are generated so-called "residual signals". A temporal or frequency analysis of these signals and their evolution should not only detecting any abnormal behavior of the system but also localize its origin.

Developed results

The main contribution of this thesis can be summarized as follow :

- Application of geometrical approach based hybrid observability to a hybrid 3-cell converter model to demonstrate the observability of the floating capacitor voltages under a known hybrid time trajectory.
- Reconstruction of the floating capacitor voltages of the 3-cell converter using a sliding mode observer.
- To establish the diagnosis procedure using an analytical model, a faulty model that takes into account discrete faults in a 3-cell converter is proposed.
- Application of the geometric approach based on observability co-distribution to the detection and isolation of discrete faults of the 3-cell converter.
- Two diagnosis strategies are proposed. The first is based on the Luenberger residual generator, while the second is based on the sliding mode residual generator. A comparison between the two proposed strategies is done in terms of robustness to highlight the best suited to fault diagnosis of the converter.

Thesis organization

The thesis is organized as follows :

Chapter 1 : Throughout this chapter, basic concepts of hybrid systems are presented to familiarize with hybrid systems, since the three cell converter is considered as a hybrid system, and different tools that are used to analyze or to control the converter are related to hybrid systems. Different observability criteria for linear time-invariant, nonlinear affine, and switching linear time-invariant systems are also presented, and some observation structures for hybrid systems are given. The end of this chapter is devoted to basic concepts of the fault diagnosis to familiarize with the diagnosis concepts that will be used in chapter five for fault diagnosis of the 3-cell converter.

Chapter 2 : Is devoted to a 3-cell converter which will be the subject of observability analysis and observation in chapter three and fault diagnosis in chapter five. First, properties and control requirements of the multicellular converter are presented. Thereafter, different mathematical model of the converter are introduced, and our attention will be focused on instantaneous and hybrid models, this is the fact of their use along of this thesis. Finally, some control strategies of the 3-cell converter will be presented.

Chapter 3 : Addresses the observability analysis and observation of the 3-cell converter. First, a state of art on observability and observation of hybrid systems is presented. Then, observability analysis of the 3-cell converter is demonstrated using the ZTn-observability which is the most known for the observability analysis of the hybrid systems. Recently, a geometrical approach is introduced for the observability of the hybrid systems, we have applied it to show the observability of the floating capacitor voltages of the 3-cell converter. Under a

control sequence input that made the floating capacitor voltages observable, a sliding mode observer will be designed for the observable subspace of the converter. The Lyapunov theory will be used to demonstrate the finite-time convergence of the designed observer. Observer parameters are derived from a Linear Matrix Inequality solution. The reconstruction of the capacitor floating voltages is then made from the designed sliding mode observer.

Chapter 4 : First, we present an overview of different methods used for fault diagnosis, either physical redundancy methods or analytical redundancy methods. Then, the nonlinear geometric approach to nonlinear fault detection and isolation, which will be applied to the 3-cell converter in chapter five, is introduced. An academic example will be considered to highlight the approach.

Chapter 5 : This chapter is dedicated to the application of the nonlinear geometrical approach to the diagnosis of switch faults of the 3-cell converter. First, a nonlinear model that takes into account the discrete faults of the converter is introduced. Based on this faulty model, a functional analysis of the capacitor flying voltages is given for each fault situation. This latter will be useful to study the capacitor floating voltages behaviors in failure mode, which will depend on the remaining operating modes after the appearance of the fault. Then, we apply the geometric approach presented in chapter four to switch faults detection and isolation of the 3-cell converter. The application of the method seems impossible for the ideal case. For this, we propose a way to ensure the solution to the Fundamental Problem of Residual Generation (FPRG). Consequently, two types of residual generators are proposed. The first is based on Luenberger observer assuming that all state variables of the converter are available to measurement. While the second is based on sliding mode observer assuming that only the load current is available to measurement. In this case, a sliding mode observer is designed to estimate the capacitor floating voltages. A comparison between the two strategies is carried out in terms of robustness to multiple noises and parameter uncertainties.

Finally, concluding remarks and suggestions for future research ideas are discussed in conclusion.

Chapter 1

Generalities

Contents

1.1 Introduction

The control of processes consists on the study of the dynamic of different kinds of systems (Electrical, mechanical, chemical,...,etc) in order to take decision and then make a desired behavior of the system. A dynamical system can be represented by a mathematical model. This model is described by means input-output or input-state relations. These relations allow to design actions to be carried out to impose a desired behavior to the system. Usually, two kind of systems are distinguished according to a nature of state variables, continuous and discrete. Continuous dynamic may be represented by a continuous time control system as a linear system with the state $x(t)$ and the control input $u(t)$. As an example of discrete dynamics, one can consider a finite-state automaton with discrete states, $q_i \quad (i = 1, ..., N)$, taking value in some finite set Q, and where transitions between different discrete states are triggered by suitable value of an input variable $\sigma(t)$. When the input $u(t)$ of the continuous dynamics is some function of the discrete states q_i, and similarly, the value of the input $\sigma(t)$ to the discrete dynamics, is determined by the value of the continuous state $x(t)$, a hybrid system is then arisen. The importance offered by a system modeled as hybrid model is that it consists of two dynamics (continuous and discrete) which cohabits, defining for each operating mode a region that limits the system to evolve within of a subspace. For that, several techniques of control and analyze (stability, controllability, observability) are appeared, mainly with the technological increase and the intensive computer use in control. This chapter is dedicated to present some basic definitions used along of this thesis. First, some definitions related to hybrid systems are presented, mainly, the different classes of hybrid systems as well as their different modeling formalisms. Followed by the observability and observation issues of hybrid systems. Finally, some diagnostic tools are given to succeed the designing of diagnosis procedure of physical systems.

1.2 Basic concepts of hybrid systems

1.2.1 Definition of hybrid systems

A hybrid systems are dynamical systems composed by discrete and continuous states. Their evolution is given by equation of motion that generally depends on both. The execution of hybrid system can be defined by a sequence of steps ; in each step, the system state evolves continuously according to a dynamical law until a discrete transition occurs. The continuous dynamics of each sub-system may be continuous time, discrete time but is generally given by differential equations. The discrete variable dynamics of hybrid system is generally governed by a digital automaton with a countable number of states [10]. The continuous and discrete dynamics interact at "event" or "trigger" times when the continuous state hits certain prescribed sets in the continuous state space.

Example 1.1 : The heating system is considered as a hybrid system with two commutation modes. Figure (1.1) represents the graphical representation of hybrid automaton of a heating system. The system exhibits the continuous dynamic represented by the temperature $x(t)$ while the discrete dynamic is represented by switching on and off the heating. The tempe-

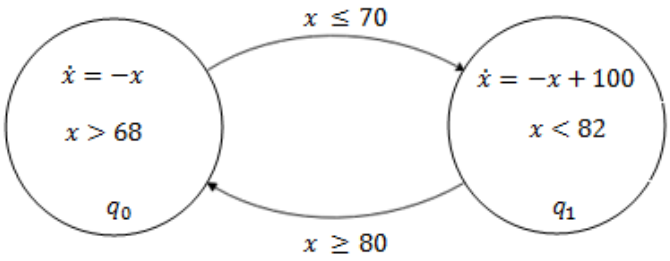

FIGURE 1.1: The graphical representation of hybrid automata of heating system.

rature is regulated around 75^o by turning the heating on when the temperature is between 68^o and 70^o and turning the heating off when the temperature is between 80^o and 82^o. The discrete mode of the heating is changed in response to a discrete control command event sent by a discrete controller. As an example, if the initial discrete mode of the heating is q_0, in this mode, the continuous dynamic is governed by the following differential equation $\dot{x}(t) = -x$ with $x > 68$. Ones the temperature is around 68^o and 70^o, the control command event "Heating ON" will change the discrete mode to q_1, and the continuous dynamic evolution is given by $\dot{x} = -x + 100$ with $x < 82$.

1.2.2 Applications

The reasons to study hybrid systems can be quite diverse. Here, we will provide three sources of motivation, which are related to [11] :

1. Design of technological systems,
2. Networked control system,
3. Physical processes exhibiting no smooth behavior.

These three sources find its origin in many field, namely :

- Air traffic management : A finite set of manoeuvres, such as speed change, short cut and detor are used by the air traffic controller to obtain a conflict-free flight environment [11], [12],
- Simulation of complex process composed by several continuous modes operation [13],
- The supervision of processes and reliability (Safety) of multi-model systems [13],
- Modeling of the dynamic behavior of the systems of response time constrained by their environment [13],
- Chemical process control : as an example keeping a reference temperature while chemical reaction take place [12],
- Communication network : Large data flows are conveniently modeled as continuous variables, while traffic control mechanisms such as routing induce discrete variables [12],
- Embedded control : as computer disk drive [10],
- Robotic : As example, modeling of the co-operation of two robot manipulators [14].

1.2.3 Classes of hybrid systems

Research on hybrid systems has a strong multidisciplinary flavor, and different communities have developed different viewpoints. The researchers in computer science concentrate on studying the discrete behavior of the system, while the continuous dynamics are assumed to take relatively simple form [15]. In this case, the discrete model such as automata or finite state machines, need to be extended concept like time, clocks and continuous evolution to capture the mixed discrete and continuous evolution in hybrid systems [11]. On the other hand, the researchers in system and control science, tend to regard hybrid systems as a continuous system with switching. Indeed, continuous models represented by differential or difference equations have to be extended to be suitable for describing a hybrid system [11]. The main issues, in this case, become then, stability analysis and control synthesis [15]. Let consider a system given by its differential equation of the form :

$$\dot{x} = f_\sigma(x(t)), \tag{1.1}$$

where $x(t) \in R^n$ is the state vector. $f(x(t))$ is a vector field and σ is the switching signal. Then the switching events on hybrid systems can be classified into :

- Autonomous switching of the dynamic.
- Controlled switching.
- Autonomous state-jump.
- Controlled state-jump.

a- Autonomous switching of the dynamics

Autonomous switching are phenomena which appears when the dynamic of the system change discontinuously. The switching can be caused by a clock if the vector field f depends explicitly on the time t. As an example :

$$\dot{x} = f(x(t), t) = \begin{cases} f_1(x(t)) & if \quad t \in [2kT, (2k+1)T], \quad k \in N \\ f_2(x(t)) & if \quad t \in [(2k+1)T, (2k+2)T], \quad k \in N \end{cases} \tag{1.2}$$

In this example we have a commutation between two different modes of operation with a period $2T$. This kind of hybrid dynamical system is called ***time-dependent switching***. In other hand, if the switching is invoked when the continuous state x reaches a specific surface on the continuous state space, the system is considered as ***state dependent switching***. This surface is usually called the "commutation function". As an example, let consider the following hybrid system

$$\dot{x} = f_\sigma(x(t)) = \begin{cases} f_1(x(t)) & if \quad h(x) = x \leq h_1 \\ f_2(x(t)) & if \quad h(x) = x > h_1 \end{cases} \tag{1.3}$$

$h(x)$ is the commutation function. It can also represent the imposed state variable limits [16]. The figure (1.2) represents an autonomous state dependent switching of a hybrid system.

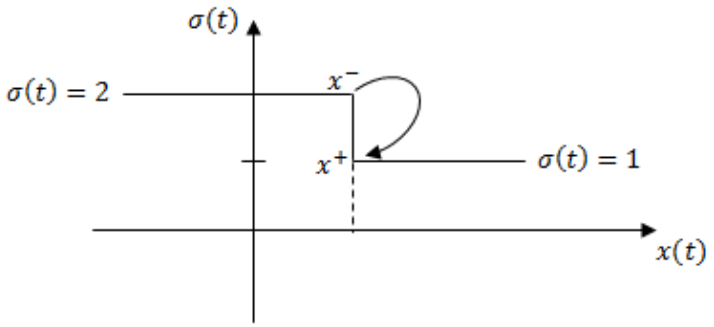

FIGURE 1.2: Autonomous state-dependent switching

b- Controlled switching

This occurs if the system has a discrete input σ that is used to invoke the switching among different continuous dynamics. Then the vector field of the system of equation (1.1) becomes $f(x(t), \sigma(t))$ and it changes abruptly when the input $\sigma(t)$ is changed. A switched system with controlled switching can be described by a controlled switching model. The DC-DC converter is a simple example of such systems.

c- Autonomous state jump

In this case, when the continuous state reaches a certain sub-space of the state space, the commutation of the dynamic passes from its current value to an other discontinuously [16]. Figure bellow illustrates the autonomous state jump phenomena.

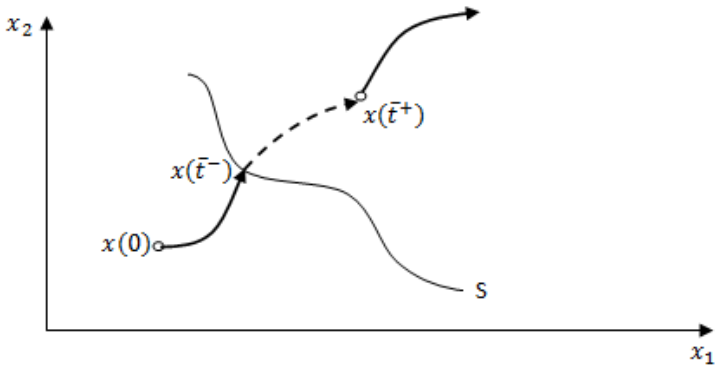

FIGURE 1.3: Autonomous state-jump

A simple description of state jump is given as follow. An autonomous jump set is a set S on which a state jump is invoked [11]. Some relation R, which often called ***reset map*** determines when the state jump is produced as depicted by figure (1.3).

$$x((\bar{t}^{-}), x(\bar{t}^{+})) \in R \tag{1.4}$$

$\bar{t}$ is the time instant at which the trajectory $x(t)$ reaches the set S. Then in this case, the system is described by the extended model.

$$\begin{cases} \dot{x} = f(x(t)), \quad for \quad x(t) \in S \\ x((t^-), x(t^+)) \in R(q(\bar{t}^-)) \quad for \quad x(t) \in S \end{cases} \tag{1.5}$$

An illustrative example is a bouncing ball. If the ball touches the ground at time $\bar{t}$, then its velocity is instantaneously reversed.

d- Controlled state jump

Are discontinuities in the state trajectory that occur as a response to a control command. An example in which such a state jump is necessary for satisfying performance requirements in the automatic gearbox. A state jumps in the gearbox controller must be invoked when the gearing is changed in order to avoid a jump in the acceleration of the vehicle.

1.3 Modeling of hybrid systems

1.3.1 Hybrid Bond-Graph

The bond graph methodology provides a systematic framework for building consistent and well-constrained models of dynamic systems across multiple domains. It is a topological representation that captures the energy-based interactions among the different components that make up the system. It is a powerful modeling tool, especially when multiple physical domains are combined to define the system dynamics (electrical, mechanical, hydraulic, thermodynamic,...etc). The bond graph models based on two principles :

1. Conservation of energy and continuities of power.
2. A lumped parameter approach that converts the physical system configuration to a set of generic interacting process.

The bond represents the energy connection between two components. There are two power related variables, effort and flow, associated with each bond. Energy transfer is represented by *power=effort* $\times$ *flow*, the rate of change of energy is $\frac{\partial_E}{\partial t}$. The bonds are represented as lines with half arrowheads, the direction of the arrowhead representing the direction of energy flow. The edges, called also signals, represent the signal flows between subsystems which can either be a flow, an effort, function of effort and flow variables or an external signal [17]. The bond graph were mainly developed to obtain a mathematical model of system as ODEs or DAEs for simulation, for analysis of structural observability and controlability or for the design of the controller.
Besides, various proposals to extend the bond graph modeling framework to represent discrete discontinuities events have evolved during the past two decades. Hybrid Bond Graph (HBG) extends Bond Graph (BG) by incorporating switched junctions to enable discrete changes in system configuration. The BG junction may be dynamically switched on (active) and off (inactive) as system behavior evolves. An active junction behaves like a regular BG junction, whereas in the off state, all bonds incident on the junction are inactivated. Therefore, an inactive junction and the connected bonds do not play any part in determining the system dynamics.

Example (Hybrid bond graph for the one tank system) : Figure (1.4) represents one tank water level system. Its hybrid bond graph is depicted by figure (1.5). The input flow into the tank ensured by the pump, is represented as flow source **SF**. The two pressures are : the input flow **Op** and the output flow **Ov**. A 0-junction defines each of these variables (pressures) and connect to the storage element that represent the tank capacity **C** according to the section **St** of the tank. The dissipation element represented by the valve section **Sv** is connected to the 1-junction to represent the emptying of the tank through the valve.

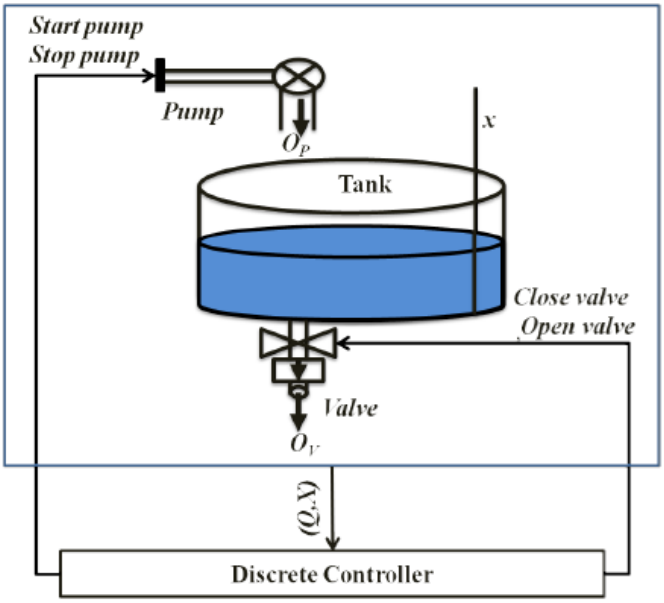

FIGURE 1.4: One tank water level control system

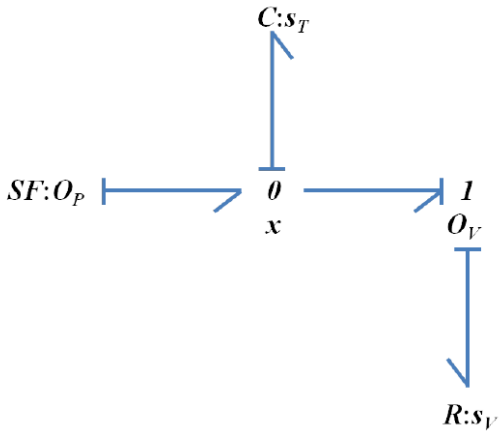

FIGURE 1.5: Hybrid bond graph for the one tank system.

1.3.2 Hybrid Petri-Net

Petri Nets (PNs) are widely used to model discrete event dynamic systems (computer systems, manufacturing systems, communication systems,...etc). A hybrid petri net can be obtained if one part is discrete and an other part is continuous. According to [18], a hybrid petri net is a sextuple :

$$Q = \{P, T, Pre, Post, m_0, h\}; \tag{1.6}$$

such that

- $P = \{P_1, ..., P_n\}$ is a finite, not empty, set of places ;
- $T = \{T_1, ..., T_n\}$ is a finite, not empty, set of transition ;
- $h : P \cap T = \{D, C\}$, called hybrid function, indicates for every node whether is discrete mode (sets P^D and T^D) or a continuous node (sets P^C and T^C) ;
- $Pre : P \times T \to R^+$ or N, is input incidence mapping ;
- $Post : P \times T \to R^+$ or N, is output incidence mapping ;
- $m_0 : P \to R^+$ or N, is the initial marking.

Example (Hybrid petri net for the one tank system) : Hybrid petri net for the one tank system is depicted in figure (1.6). It consists of one continuous place P_1 represented by a double circle, two continuous transitions represented by the empty bars T_1 and T_2, four discrete places P_2, P_3, P_4 and P_5 represented by a circle and four discrete transitions represented by full bars T_3, T_4, T_5 and T_6. P_1 describes the level x of the tank, P_2 and P_3 represent respectively the position closed and opened of the valve and P_4 and P_5 describe, respectively the OFF and ON of the pump. Continuous transition T_1 and T_2 describe, respectively the filling and the emptying of the tank. Discrete transitions T_3, T_4, T_5 and T_6 describe, respectively the controller commands to open and close the valve and to start or to stop the pump.

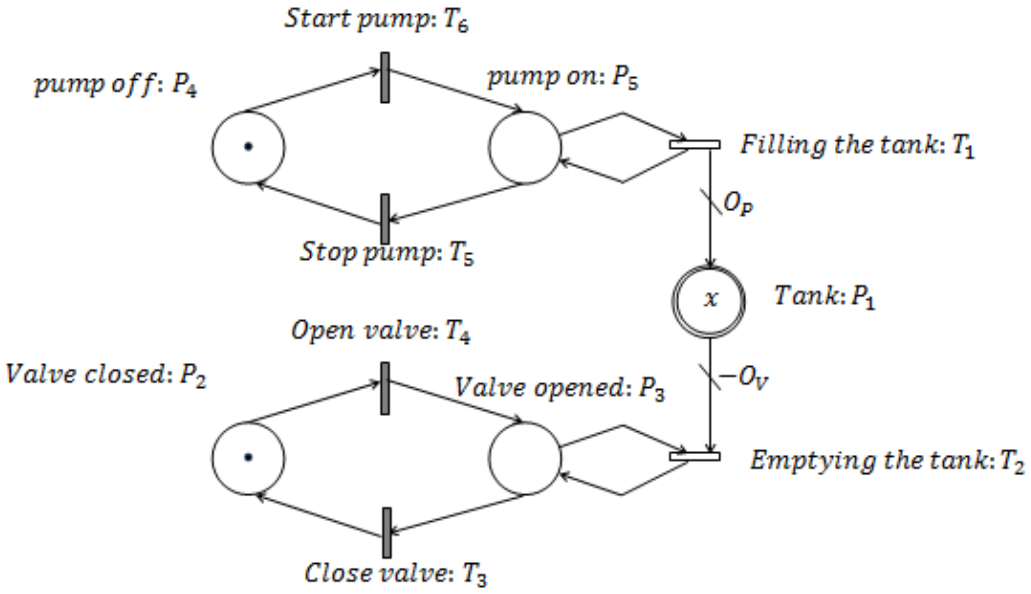

FIGURE 1.6: Petri net for the one tank system.

1.3.3 Hybrid automata

A hybrid automaton is a dynamical system that describes the evolution in time the value of the set of discrete and continuous state variables.

Definition 1.1 : A hybrid automaton H is an 8-tuple

$$H = (Q, X, f, Init, Inv, T, G, R), \tag{1.7}$$

where :

- $Q = \{q_1, q_2, ..., q_k\}$ is a finite set of discrete states ;
- X is the continuous state space ;
- $f : Q \times R^n \rightarrow R^n$ is a vector field ; defines the evolution of the continuous states. Generally given by differential equation.
- $Init \subset Q \times R^n$ is the set of initial hybrid states ;
- $Inv : Q \rightarrow 2^{R^n}$ describes the invariants of the locations ; which describes the conditions that the continuous state has to satisfy at this mode ;
- $T \subseteq Q \times Q$ is a set of all possible discrete transitions ;
- $G : T \rightarrow 2^{R^n} \times 2^{R^n}$ is a set of guards, prescribing when a discrete state transition occurs.
- $R : T \times X \times U \rightarrow 2^{R^n}$ represents a reset map, which specifies how new continuous states are related to previous continuous states for a particular transition.

Definition 1.2 (Directed graph of H) : An oriented graph of a hybrid automaton defined by H is obtained by associating to each mode $q_i \in Q$ a node, and to each transition $T_{i,j}$ an oriented arc from the node of mode q_i to the node of mode q_j .

It is often convenient to visualize hybrid automaton as directed graph (Q, T), with modes $q_i \in Q$ and transitions $T_{i,j} \in T$. For each mode $q_i \in Q$ we associate, a vector field $f_{q_i} : R^n \rightarrow R^n$ which describes the evolution of the continuous state in mode q_i, and an invariant set $inv(q_i)$, which describes the condition that the continuous state has to satisfy. A transition $T_{i,j} \in T$ starts at $q_i \in Q$ and ends at $q_j \in Q$. With each transition we associate a guard $G(q_i, q_j)$ and a reset function $R(q_i, q_j)$. Invariant and guard play a complementary roles ; whereas invariants describe when a transition must take place, the guards serve a enabling conditions that describe when a particular transition may take place. The reset map is, in general, a set valued function that specifies how continuous states are related to previous continuous state for a particular transition.
As an example of a hybrid automaton, figure (1.7) depicts a schematic representation of a hybrid automaton consisting of three discrete modes. The hybrid state of the system is given by $(q, x) \in Q \times X$. Starting from an initial value $(q_0, x_0) \in Init$, the continuous state x evolves according the differential equation

$$\begin{cases} \dot{x} = f(q_0, x) \\ x(0) = x_0, \end{cases} \tag{1.8}$$

while the discrete state q remains constant $q(t) = q_0$. The continuous evolution can go as long as x remains in the invariant set of the location q_0. If at some point, the continuous state x reaches the guard condition $G(q_0, q_1) \subseteq R^n$, the discrete state may change value to q_1. At the same time the continuous state gets reset to some value in $R(q_0, q_1, x) \subseteq R^n$.

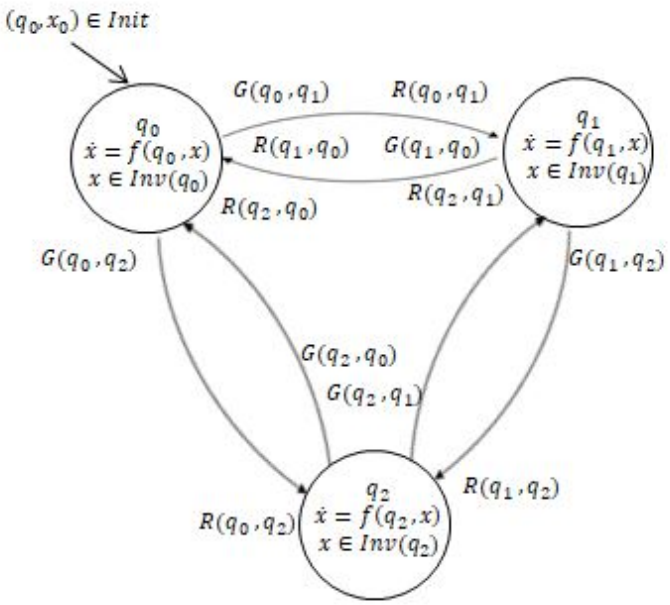

FIGURE 1.7: Schematic representation of a hybrid automaton with three discrete states.

After this discrete transition, continuous evolution resumes and the whole process is repeated.

Example : Figure (1.8)depicts the topology of dc-dc boost converter, it is considered as hybrid system since it works in commutation mode due to the opening or closing of the switch (SW) and the conduction or non conduction of the diode (D). It consists of a resistance R, an inductance L, a capacitor C, a controlled switch SW and uncontrolled diode (D). In the modeling, all the resistances like equivalent series resistance of the capacitor r_c, inductor series resistance r_L, switch on time resistance r_s, and the diode on time resistance r_d have been considered. The output voltage and the capacitor voltage are different due to the ESR of capacitor, but if the ESR is negligible then we can assume that the output voltage is equal to capacitor voltage. The state variables are then $x_1 = i$ and the output voltage $x_2 = v$.
The dc-dc boost converter is modeled by three operation modes, which depend on the the switch position (opened or closed) and the conduction or the non conduction of the diode. All sub models are linear of the form $\dot{X} = A_q X + B_q U$, where $X \in R^2$ is the state vector. A_q and B_q are the state and input matrices respectively, where $q = 1, 2, 3$ denotes the mode of operation. $U = E$ is the source voltage. The hybrid automaton diagram of the dc-dc boost converter is depicted by figure (1.9), and its dynamic can be described by the following 7-tuple hybrid automaton :

$$H = (Q, X, f, T, G, inv, Init), \tag{1.9}$$

where

- $Q = \{q_1, q_2, q_3\}$: represents a set of 3 discrete modes, according to the position of the switch (SW) and the diode (D).
- $X \in R^2$ is the the continuous space, the state vector is then $x = [i, \quad v]^T$.
- $f : Q \times R^2 \to R^2$ is the vector field that assigns to every discrete mode q_i $(i = 1, 2, 3)$,

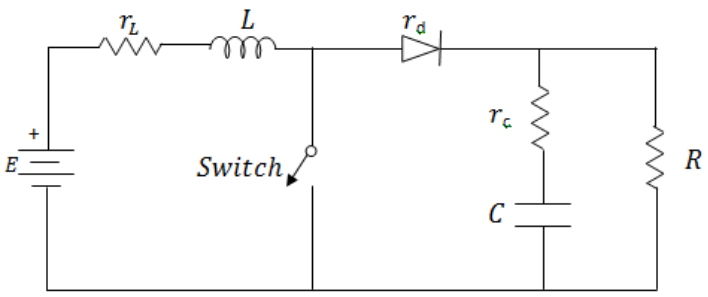

FIGURE 1.8: Circuit diagram for dc-dc boost converter

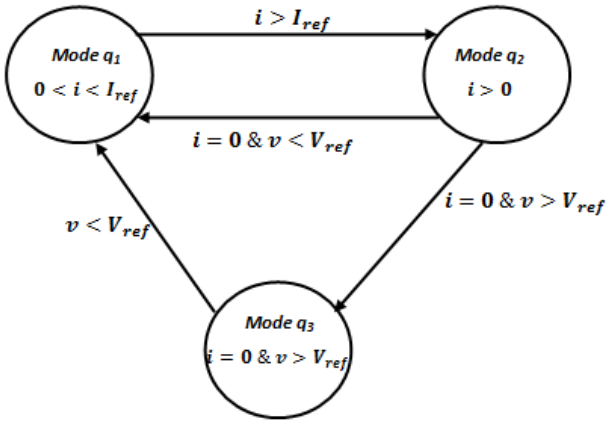

FIGURE 1.9: Hybrid automaton for the dc-dc boost converter.

a linear continuous dynamic described by the following equation

$$f_{q_i}(x) = A_{q_i}x + B_{q_i}, \quad q_i \in Q, i = 1, 2, 3; \tag{1.10}$$

with

$$A_1 = \begin{bmatrix} -\frac{r_L+r_s}{L} & 0 \\ 0 & -\frac{1}{(R+r_c)C} \end{bmatrix}, \quad B_1 = \begin{bmatrix} \frac{1}{L} \\ 0 \end{bmatrix},$$

$$A_2 = \begin{bmatrix} -\frac{r_L+r_d}{L} & -\frac{1}{L} \\ \frac{R}{R+r_c}(\frac{1}{C} - \frac{r_c(r_L+r_d)}{L}) & -\frac{R}{R+r_c}(\frac{r_c}{L} + \frac{1}{RC}) \end{bmatrix}, \quad B_2 = \begin{bmatrix} \frac{1}{L} \\ \frac{R}{R+r_c}\frac{r_c}{L} \end{bmatrix},$$

$$A_3 = \begin{bmatrix} 0 & 0 \\ 0 & -\frac{1}{(R+r_c)C} \end{bmatrix}, \quad B_3 = \begin{bmatrix} 0 \\ 0 \end{bmatrix}.$$

- $T = \{T_{1,2}, T_{2,1}, T_{2,3}, T_{3,1}\}$ is the set of all possible transitions between modes.
- $G : T \to 2^{R^2}$ is the guard that associates to each edges a condition that enables the transition between two modes. The guards are as follow :

$$
\begin{aligned}
G(T_{1,2}) &= \{X \in R^2 : i > I_{ref}\},\\
G(T_{2,1}) &= \{X \in R^2 : (i = 0) \quad \wedge \quad (v < V_{ref})\},\\
G(T_{2,3}) &= \{X \in R^2 : (i = 0) \quad \wedge \quad (v < V_{ref})\},\\
G(T_{3,1}) &= \{X \in R^2 : v < V_{ref}\},
\end{aligned}
$$

where I_{ref} is the desired reference current of the inductor and V_{ref} is the desired reference of the output voltage.

- The invariant set of different modes are :

$$
\begin{aligned}
Inv(q_1) &= \{X \in R^3 : 0 < i < I_{ref}\},\\
Inv(q_2) &= \{X \in R^3 : i > 0\},\\
inv(q_3) &= \{X \in R^3 : (i = 0) \quad \wedge \quad (v > V_{ref})\},
\end{aligned}
$$

- $Init \subseteq R^2 \times Q$: gives the initial states. As example :

$$
Init = q_1 \times \begin{pmatrix} v_0 \\ 0 \end{pmatrix}, \tag{1.11}
$$

where v_0 represents the initial state of the capacitor voltage.

1.4 Solution of switched system

Consider a switched system given by the following equation :

$$
\dot{x}(t) = A_{q_i}x(t) + B_{q_i}, \quad i = 1, ..., N. \tag{1.12}
$$

Suppose that the switching signal is given as follow

$$
S_{q_i}^{[t_0,t_f]} = \{x_0, (t_0, q_1), (t_1, q_2), ..., (t_{N-1}, q_N)\}; \tag{1.13}
$$

where q_1 is the initial activated mode during the time interval $[t_0, t_1]$ and x_0 is the initial continuous state. It is well known that the solution of a linear time invariant system (LTI) of the form $\dot{x} = Ax(t) + Bu(t)$ over the time interval $[t_0, t_1]$ is :

$$
x(t) = e^{A(t-t_0)}x_0 + \int_{t_0}^{t} e^{A(t-\tau)}Bu(\tau)d\tau; \tag{1.14}
$$

where e^{At} is the transition matrix. It can be seen from (1.14) that the most difficult part in the solution is the evaluation of the integral. If a certain transformation is introduced to remove the B term, the solution to the original problem can be significantly simplified. For the switched system, $u(t) = 1$, an extra-state $x_{n+1}(t) = u(t)$ can be introduced. Clearly, $\dot{x}_{n+1}(t) = 0$. Thus the state space equation of the switched system can be rewritten as follow :

$$
\begin{bmatrix} \dot{x}(t) \\ \dot{x}_{n+1}(t) \end{bmatrix} = \begin{bmatrix} A_{q_i} & B_{q_i} \\ 0 & 0 \end{bmatrix} \begin{bmatrix} x(t) \\ x_{n+1}(t) \end{bmatrix} \tag{1.15}
$$

Let $z(t)$ be the augmented state vector, and F_{q_i} a matrix of dimension $(n+1) \times (n+1)$, such that :

$$z(t) = \begin{bmatrix} x(t) \\ x_{n+1}(t) \end{bmatrix}, \qquad \text{and} F_{q_i} = \begin{bmatrix} A_{q_i} & B_{q_i} \\ 0 & 0 \end{bmatrix}.$$

Then, the augmented system (1.15) can be rewritten as :

$$\dot{z}(t) = F_{q_i} z(t), \quad i = 1, ..., N. \tag{1.16}$$

Since for each operation mode q_i, the continuous dynamic given by equation (1.16) represents an autonomous equation, then its solution on the time interval $[t_0, t_1]$ is

$$z_1(t) = e^{F_1(t-t_0)} z_0 \tag{1.17}$$

with $z_0 = z(t_0) = [x(t_0), x_{n+1}(t_0)]^T = [x(t_0), 1]^T$. And its solution over the time interval $[t_1, t_2]$ is :

$$z_2(t) = e^{F_2(t-t_1)} z_1 \tag{1.18}$$

by substituting (1.17) on equation (1.19), $z_2(t)$ becomes :

$$z_2(t) = e^{F_2(t-t_1)} e^{F_1(t_1-t_0)} z_0 \tag{1.19}$$

Following the same reasoning as above, the solution of the augmented switched system (1.16) according to the ordered sequence $S_{q_i}^{[t_0,t_f]}$ can be computed as follow :

$$z(t, t_0, z_0) = e^{F_N(t-t_{N-1})} e^{F_N(t_{N-1}-t_{N-2})} .....e^{F_2(t_2-t_1)} e^{F_1(t_1-t_0)} z_0 \tag{1.20}$$

Then the solution of the original switched system (1.12) is given by the n first equations of the solution (1.20).

1.5 Observability and observation of hybrid systems

In many industrial applications, the knowledge of state variables of the system is of great utility either for control purposes, monitoring or even for fault diagnosis. For this, two methods can be distinguished. The first consists of implementing sensors to measure the state variables. Unfortunately, using multiple sensors involves extra hardware cost and extra weight, and the system can become bulky, or for technical reasons, the measurement can not be performed. To overcome all these drawbacks, other option can be used to accomplish the same objectives, this second method is based on state estimation using observers. State estimation is a fundamental problem in many areas of control engineering and has always been the objective of intensive investigations since the pioneering works of Kalman (1960) and Luenberger (1964). Many observers are proposed in the literature to overcome a problem of state estimation of dynamical systems, high gain observer, Luenberger observer, sliding mode observer, adaptive observer..., etc. The observability of the system is a very important characteristic that should be checked before any observer designing. By definition, the observability is the ability to reconstruct the state vector from the available signals of the system. Hence, if the state vector can be reconstructed, then an observer can be designed to estimate the state variables.

The rest of this chapter will be devoted to the observability, observation, and diagnosis of dynamical systems. First, we recall the observability of linear and nonlinear continuous systems and then we treat the case of switching systems. Also, we give an overview of different criteria presented in different researches for the observability of both continuous and discrete states of hybrid systems. Then, we move to cite different observation structures that allow the reconstruction of the continuous and the discrete states of a hybrid system, followed by an overview of different works that address the observation of hybrid systems. Finally, we recall some principle definitions about the diagnosis of dynamical systems.

1.5.1 Observability of linear continuous systems

In this section we recall observability analysis criteria of both linear and nonlinear continuous systems before pointing our attention on the observability of linear hybrid systems. Let consider the continuous linear system

$$\begin{cases} \dot{x}(t) = Ax(t) + Bu(t) \\ y(t) = Cx(t), \end{cases} \tag{1.21}$$

where $x(t) \in R^n$ is the state vector, $u(t) \in R^p$ is the input control vector and $y(t) \in R^q$ is the output vector. A, B and C are matrices of appropriate dimensions.

Definition 1.3 : The continuous state of the system (1.21) is said to be observable if for any initial state $x(t_0) = x_0$ and for $t_1 > 0$, the availability of the input and the output of the system on the time interval $[t_0, t_1]$ allows the reconstruction of the initial state $x(t_0)$.

generally, to check the observability of linear continuous system, we use the Kalman criterion given by the following theorem.

Theorem 1.1 : System (1.21) is said to be locally weakly observable if the observability matrix is of full rank, i.e.,

$$rank(O) = rank \begin{bmatrix} C \\ CA \\ \vdots \\ CA^{n-1} \end{bmatrix} = n \tag{1.22}$$

1.5.2 Observability of nonlinear continuous systems

Consider a continuous nonlinear affine system of the form

$$\begin{cases} \dot{x}(t) = f(x(t)) + g(x(t))u(t) \\ y(t) = h(x(t)), \end{cases} \tag{1.23}$$

where $x(t) \in R^n$ is the state vector, $u(t) \in R^p$ is the input control vector, $y(t) \in R^q$ is the output vector, $f(x(t))$ and $g(x(t))$ are smooth vector fields and $h(x(t))$ is smooth application.

Theorem 1.2 : The system (1.23) is said to be observable if

$$rank \begin{bmatrix} dh \\ dL_f h \\ \vdots \\ dL_f^{n-1} h \end{bmatrix} = n, \tag{1.24}$$

where $L_f h$ is the Lie derivative of $h(x(t))$ along the direction of the vector field $f(x(t))$.

1.5.3 Observability of switched linear system (classical sense)

Let consider a linear switching system given as follow :

$$\Sigma : \begin{cases} \dot{x}(t) = A_{q_i} x(t) + B_{q_i} u(t) \\ y(t) = C_{q_i} x(t) + D_{q_i} u(t), \quad i = 1, ..., m. \end{cases} \tag{1.25}$$

where $x(t) \in R^n$, $u(t) \in R^p$ and $y(t) \in R^q$, are respectively the state vector, the control input vector and the output vector. $q_i \in Q = \{q_1, q_2, ..., q_m\}$ represent the index of the switching signal $\sigma(t)$, which indicate the active mode of the hybrid system. $\sigma(t)$ is a piecewise and right continuous function, where its value changes each switching time $t_k \in R^+, \quad k \in N$. Between two commutations, the discrete state of the switching system is defined by :

$$\sigma(t) = q_i \in Q, \quad t_{i-1} \leq t < t_i, \text{with} \quad t_0 = 0. \tag{1.26}$$

In the case of switching systems, it is often introduced the dwell time between two consecutive commutations. It represent the stay time in an operating mode, where the continuous states evolve under external input $u(t)$, and the switching signal remains constant. The dwell time play a crucial role either in control or in the observation of dynamical hybrid systems. Indeed, almost all works, assume that there exists a constant time less than the dwell time, such that the error stabilization is guaranteed. Hence, we assume for the rest of this thesis that the inequality (1.27) holds and verify the minimum condition of the dwell time.

$$T_d \leq t_{i+1} - t_i, \quad i \geq 0. \tag{1.27}$$

In literature, many approaches are presented to analyze the observability of switched systems. In this chapter, we give the classical sense of the observability in term of the rank condition of observability matrix before presenting other approaches in chapter three. Assuming that the switching signal is well known, we said that the continuous state of the switched system (1.25) is observable in classical sense, if and only if, the observability matrix of each mode $O_{q_i}, \quad i \in I_m$ is of full rank, i.e.,

$$Rank(O_{q_i}) = Rank \begin{bmatrix} C_{q_i} \\ C_{q_i} A_{q_i} \\ \vdots \\ C_{q_i} A_{q_i}^{n-1} \end{bmatrix} = n. \tag{1.28}$$

This rank condition is a weak condition for the observability of the continuous states of

switched system, i.e., the non satisfaction of the above rank condition does not imply that the state of the switching system can not be reconstructed. Other approaches treat the case where some modes are not observable in classical sense, that we introduce some of them in chapter three.

1.5.4 Overview on observability of hybrid systems

In the majority of cases, only partial information about the internal state of the hybrid system can be measured, and the most of the control strategies need the knowledge of all state variables of the system, in order to establish a control law based on state feedback, or to design a diagnosis procedure to detect and isolate any abnormal behavior of the system or to supervisor the system. For all these purposes, the design of an observer to estimate the internal states of the hybrid system becomes necessary. However, the observability is a concept of fundamental importance that establish the conditions for the reconstruction of the states. For the hybrid systems, the observability involves both the discrete as well as the continuous dynamic of the system. A hybrid system is said to be observable, when it is possible to reconstruct both the discrete and the continuous states of the system from the observed output information [19]. In the two last decades, many researches have addressed the observability of hybrid systems, and several criteria have appeared in the literature. However, the main difference between these approaches is how the switching signal is viewed ; some consider it as a fixed and known function of times, others viewed it as an unknown external signal, others consider it as a result of a discrete dynamical system or it is controlled and therefore an input [20]. In [21], sufficient conditions for final state observability are given, and a methodology to design a dynamical observer for a class of hybrid system is presented in [22]. While the hybrid observer consists of two parts ; a location observer that identifies the location of the hybrid plant, while the continuous observer produces an estimate of the continuous states evolutions. The authors assume that all modes of the hybrid system are observable to guarantee the exponential convergence of the hybrid observer. In [16], [23], [24], the authors give algebraic conditions for the discrete state observability based on the switch function reconstruction for a linear hybrid system of two modes. The switch equation is a function of output and input signals and their times derivatives. The determination of the sign of the switch function allows to distinguish the active mode at any time. Using the same reasoning, i.e., the computation of a switch function, they give geometrical conditions for the observability of the discrete mode of a non linear hybrid system, assuming that the two sub systems are observable and verifying the transversality concept. While the authors in [25] give weak conditions, based on the concept of indistinguishability, that are sufficient to guarantee the uniqueness of the reconstruction of the state trajectory of an autonomous switched linear system, even if the individual sub-systems are unobservable. They also give a way to reconstruct the continuous state trajectory, the discrete state trajectory and the switching times. In [26], observability of switched systems has been investigated. Indeed, the authors introduce the notion of critical observability for safety critical switching systems, where a set of critical states must be reconstructed immediately, since they correspond to hazards that may yield catastrophic events. In [27], the authors treat the strong observability for a class of hybrid

systems with periodic jumps, they introduce the concept of weak unobservable sub space, and then provide a structural properties in term of algebraic and geometric conditions to a strong observability, which can be guaranteed if the weakly unobservable space is restricted to zero. The authors in [28], deal with switching time observability and switch observability for both homogeneous and inhomogeneous switched systems, unlike in the work of [25], where the observability is studied for a homogeneous hybrid systems. Indeed, they characterize the strong observability by rank condition relaxing then the rank condition given in [25].
In [4] and [29], the authors propose a new concept for characterizing the observability of switched systems w.r.t the hybrid time trajectory, called $Z\{T_N\}$-observability. They also give practical conditions for checking the $Z\{T_N\}$-observability of the switched system. Different works are presented as an application of the $Z\{T_N\}$-observability approach for several switched system. In [4], [30], [31], [32], [33], [5] and [34], the $Z\{T_N\}$-observability have been applied to analyze the observability of the floating voltages of the series 3-cell converter. In [35], the authors apply the $Z\{T_N\}$-observability approach to analyze the observability of the 3-cell converter, it is also considered the case when a dc-motor is coupled with a multi-cell converter. They also show that under certain admissible assumptions, the floating voltages of the converter and the speed of the dc-motor can be estimated with an acceptable error due to the fact that the dynamic of the electrical part (multi-cell converter) is much faster than the one of mechanical part (dc-motor). The author in [36], applied the $Z\{T_N\}$-observability to analyze the floating voltages of the parallel multi-cell converter. In [37], the approach has been investigated to deal with the left invertibility of switched linear system.
In [38] and [39], a geometrical conditions for the observability of hybrid systems are presented. The authors introduced an algorithm to compute the unobservability subspace of a hybrid system along of a hybrid time trajectory. Then, they proved that if the unobservable subspace is restricted to zero, then the hybrid system is observable along of the hybrid time trajectory, i.e., an uncorrect application of the switching signal, the system losses the observability characteristic. The approach has been applied to a multicellular converter as in [40], [41], [2] and [42]. In [20], the authors give relaxed geometrical conditions for observability of the continuous state of a hybrid system comparing with the works of [38] and [39].
Recently, the almost always observability is introduced and characterized for an autonomous hybrid system in [43]. Indeed, the authors give a geometrical condition for the possibility reconstructing the current continuous component of the state, from the observable output, for almost switching time. They also investigate the optimal location of additional sensors that make the system almost always observable. In [44] a geometrical condition for the observability of the multi-cell converter is investigated. Indeed, the authors give a new results to compute the unobservable sub space along of a hybrid time trajectory, based on the intersection of all unobservable sub space of each mode. In [45], the authors design an output feedback control of the multi-cell converter using a super twisting observer. They establish a switching control strategy that guarantee the existence and the finite time stability of a limit cycle. Also, they show that the repetitive switching sequence of the limit cycle guarantee the continuous state observability. The authors in [46] have addressed the observability of the discrete state of a switching discrete time linear systems. They show that the mode-observability problem return to the existence of a discerning control sequence.

1.5.5 Observation of hybrid systems

Several observer structures are proposed in order to estimate the continuous or the discrete states or both for a switching systems. The main difference between these structures is related to knowledge of the continuous state or the discrete state [47]. Figures (1.10), (1.11), (1.12) depict these structures.

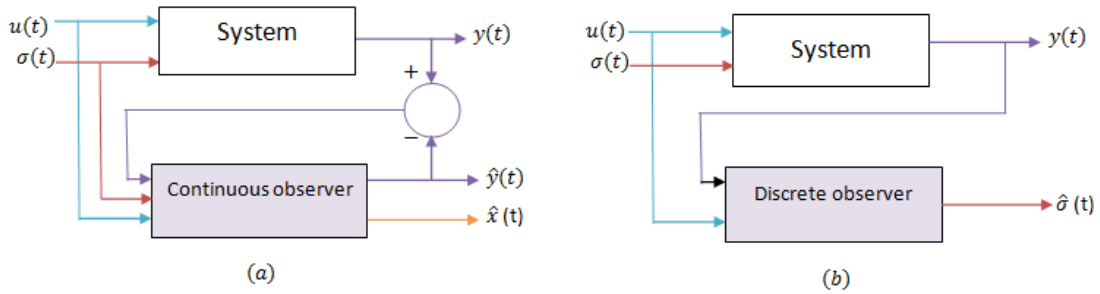

FIGURE 1.10: a- Observation of the continuous state when the switching signal is known. b- Observation of the discrete state when the continuous state is available to measurement.

Figure (1.10.a) depicts the first structure for the continuous state estimation of the hybrid system when the switching signal is known. Where (1.10.b) depicts the second structure for the estimation of the switching signal assuming that the continuous states are available to measurement.

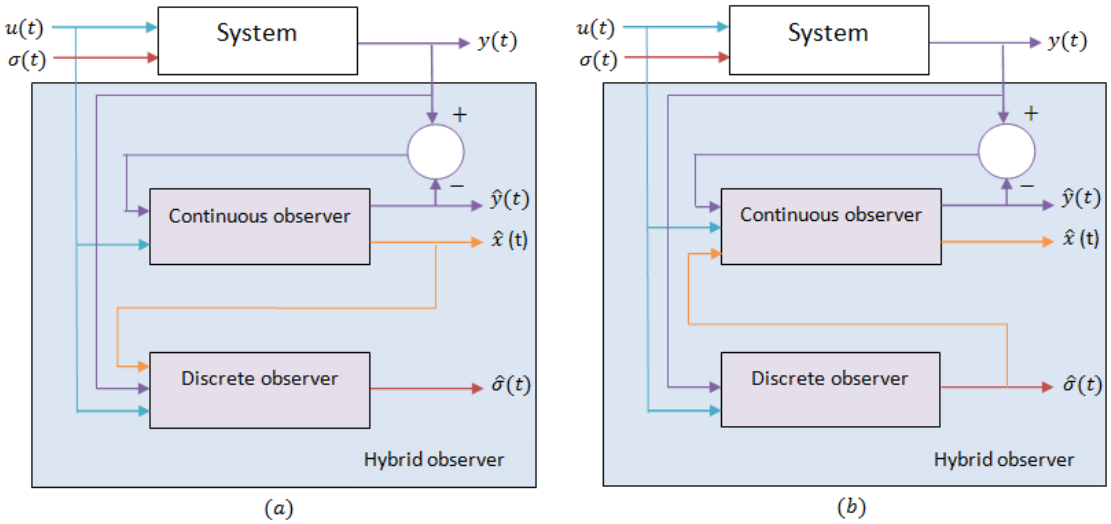

FIGURE 1.11: a- Identification of the switching signal using the continuous state estimation. b- Estimation of the continuous states after identifying the switching signal.

Observer structure based simultaneous estimation of the continuous and discrete states of a hybrid system is given by figure (1.11). Indeed, figure (1.11.a) depicts the observation structure of the discrete state using the estimation of the continuous state, provided by the continuous observer. While figure (1.11.b) depicts the observation structure of the continuous state using an estimation of the discrete state provided from the discrete observer.

Figure (1.12) show an other structure for the simultaneous estimation of continuous and

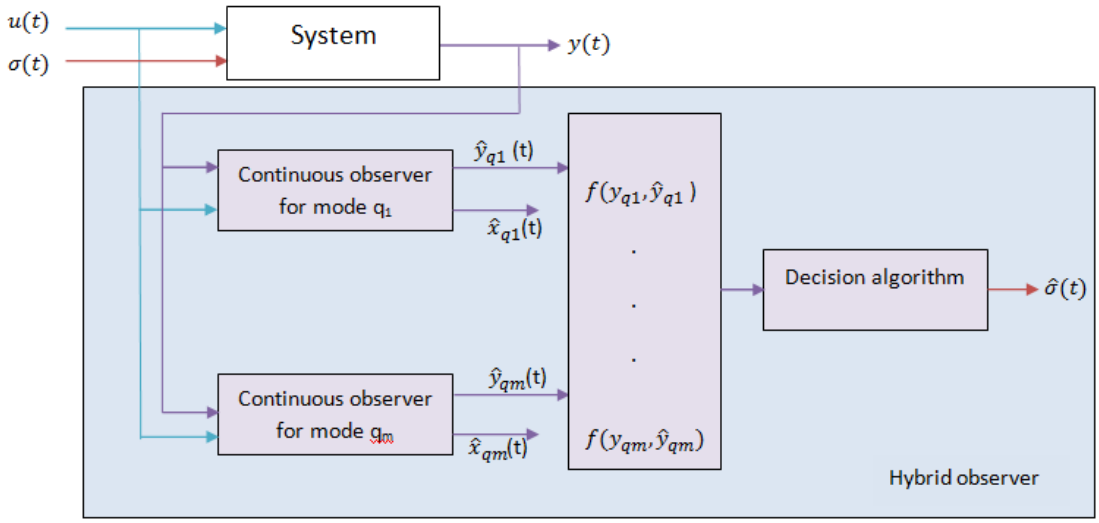

FIGURE 1.12: Identification of the switching signal using a stuck of continuous observers and an identification algorithm

discrete states of a hybrid system. The strategy based on the designing an observer for each mode. A decision algorithm is then designed to reconstruct the switching signal.

1.6 Basic concepts on fault diagnosis

With the massive growth of the technologies in the last decades, more expected from automatic systems, where these systems are expected to perform more complicated and complex tasks. However, whatever the productivity and effectiveness of these systems, they are still subject to malfunctions. There are many factors that can cause these malfunctions. They can be external factors that physically damage the components or sensors of the systems (ex : under harsh weather condition), or they could just be an ordinary degradation of the overall performance of the systems, i.e., the internal part of the manufacturing machine that has not been maintained for a long time. All these factors can be the origins of the appearance of faults on the system. A fault is said to have occurred, whenever the systems start to behave abnormally and are not able to perform the task well. If the system does not have a fault detection procedure to handle the faults at the occurrence time, these faults can lead to negative consequences such as the damage of the system, injuries or loss of valuable human life, economic loss, and also unhealthy effects on the environment. To avoid these heavy consequences, a reliable diagnosis procedure is necessary. The main purpose of a diagnosis procedure is determining the type, size, location, and the occurrence time of the faults, we refer then to fault detection and isolation procedure (FDI). In this section, the basic concepts of fault diagnosis will be given. We also give an overview of existing structures dedicated to fault diagnosis that are developed over the years. Starting by clarifying the definition of some concepts specific to fault diagnosis.

Fault : A fault is an unpermitted deviation of at least one characteristic property (feature) of the system from the acceptable usual standard condition [48].

Failure : A failure is a permanent interruption of a system's ability to perform a required function under specified operating condition [48].

Malfunction : A malfunction is an intermittent irregularity in the fulfillment of a system's desired function, i.e., a temporary interruption of a system's function [48].

Residual : Signal designed as an indicator of functional or behavioral anomaly [49].

Fault diagnosis : The task of fault diagnosis consists in determining the type, the size and the location of the most possible faults, as well as its time of detection [49].

1.6.1 Diagnosis performances criteria

The performance of a diagnosis technic is characterized by a number of important and quantifiable criteria. These performances describe the efficiency of the diagnosis procedure.

Detectability : defines the ability of the diagnosis procedure to detect the fault occurrence. This criterion is related directly to the residual signals, that must be sensitive to the considered faults.

Sensitivity : characterizes the ability of the diagnosis system to detect faults of certain magnitude (faults that have their effects on residual closed to zero). It depends not only on the residual structure but also on the ratio of the measurement noise magnitude to that of the fault. According to [50], the residuals are sensitive to a fault, if this latter has an impact on the output signals of the system.

Isolability : consists on the ability of the diagnosis system to distinguish between faults. i.e., locate which part of the system has been affected by the fault. This criterion is related to the residual structure which must allow the discrimination between multiple faults to locate their origins. Multiple simultaneous faults are in general more difficult to isolate than a single fault. Also, the interplay between faults and disturbances, noise, and model errors may lead to uncertain or incorrect isolation decision. Furthermore, some faults may be non-isolable from one another because they act on the system plant in an indistinguishable way [51].

Speed reaction : consists on the ability of the diagnosis system to detect the faults with reasonable small delay after their occurrence. In practice, this criterion can be a determinant factor to avoid a disaster (ex : in nuclear stations and aeronautic applications).

Robustness : determines the ability of the diagnosis procedure to detect the fault independently of unknown inputs (disturbances, parameter uncertainties and modeling errors). Fault detection and isolation (FDI) methods that are able to handle these unknown inputs are referred to as robust. Robust diagnosis approach avoid false alarms.

1.6.2 Type of faults

A fault is a behavior anomaly within a physical system. It's corresponds to a deviation from the normal behavior of the system, of its control system, or of its instrumentation system (sensors). Then we distinguish :

Actuator fault : actuator fault is a failure representing a total or partial loss of an actuator leading to the loss of a control action on the system [52]. This type of fault act directly on the system and will therefore influence the whole process affecting the system variables. It can be considered as additive fault as described by figure (1.13).

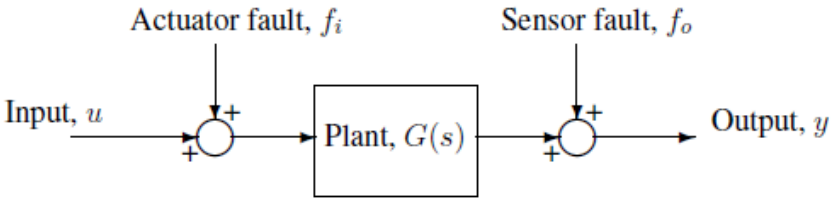

FIGURE 1.13: Additive actuator and sensor faults onto the system

The input to the system is expressed by $u_i^f = u_i + f_i$. As an example of an actuator fault, the damage of the pitch control of an aircraft, which causes great difficulty in controlling the pitch speed and the pitch angle of the aircraft [53].

Sensor faults : A sensor fault represents an error in the measurement of a physical quantities, and it can be partial or total [52]. Basically, sensor faults do not affect the process of open loop systems, such as the one shown in figure (1.13). However, in closed loop systems as shown in figure (1.14), where the output is used to generate the control signal, sensor faults will indirectly affect the operation of the system.

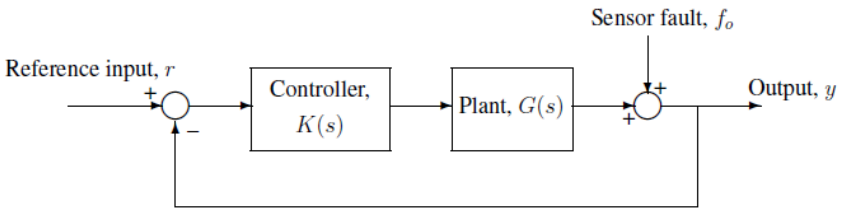

FIGURE 1.14: sensor fault affects a closed-loop system

The cause of sensor faults might be due to wear and tear of the sensors leading to inaccurate measurement or total failure of the sensors yielding zero measurement [53].

System faults : System faults are all those that affect the system components other than actuator and sensors. They act on changing system parameters. This type of faults is difficult to diagnosis because of variety of failure situations [52].

1.6.3 Different structures of diagnosis using an observer

The diagnosis of physical systems that are described by a mathematical model in the form of state equations, consists on studying the behavioral coherence of the model with respect to the real system. Diagnosis based observer approaches allow comparing the measured variables to the estimated variables provided from an observer. Figure (1.15) depicts the principle structure of fault diagnosis using an observer.

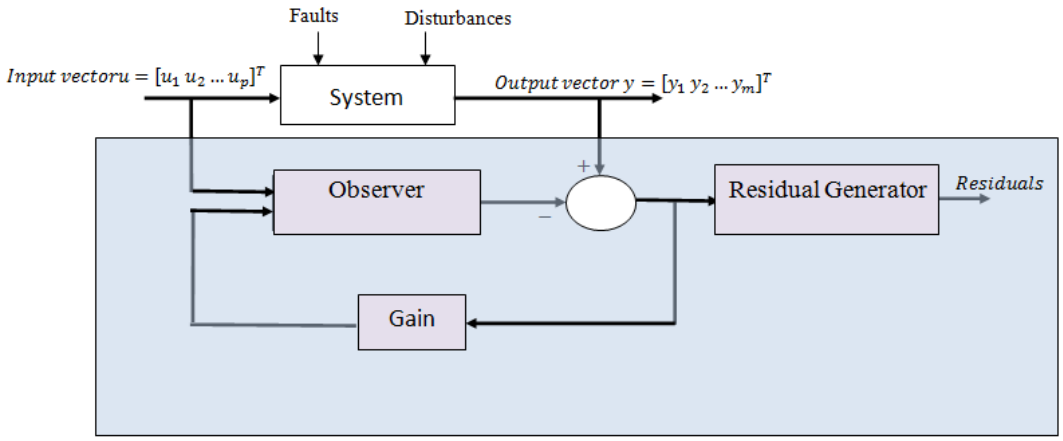

FIGURE 1.15: Observer-based diagnostic principle

An observer-based diagnosis is a technique that has been the subject of several developments. This involves state estimation from the knowledge inputs and outputs of the system and using the output estimation error as residual. Ideally, in free-faults conditions, this residual should be substantially zero, and deviate significantly from zero when a fault occurs on the system. Detecting the occurrence of faults is generally always feasible ; however, its isolation is more delicate. Hence, a bank of observer piloted by a set of different input and output signals is then frequently designed. The analysis of the generated residuals by these observers associated with a decision logic allows the isolation of the faults. Different diagnostic structures using a bank of observers can be used for isolating sensor and actuator faults.

Dedicated Observer Scheme (DOS) :

In the case of dedicated observer scheme (DOS), as many observers as faults are synthesized, each one is considered as a residual generator sensitive to only a specific fault. Thus, the occurrence of the fault is indicated by the observer of bad estimation which allows fault detection and isolation. Figure (1.16) shows the principle of the DOS structure.

Simplified Observer Scheme (SOS) :

In the case of a simplified observer structure, only one observer is designed such as will be sensitive to a set of faults. If one of the faults in which the observer is sensitive occurs, the observer provides bad estimation, then the generated residuals deviate from zero indicating the presence of a fault. Figure (1.17) shows the principe of the SOS structure.

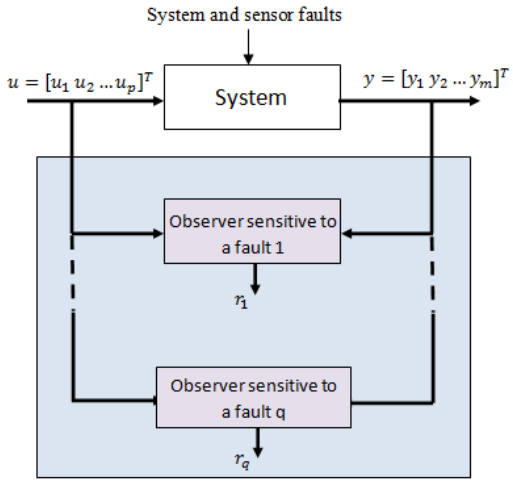

FIGURE 1.16: Dedicated observer scheme (DOS)

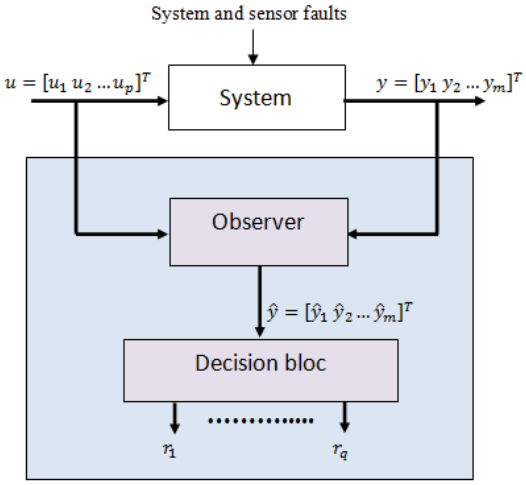

FIGURE 1.17: Simplified observer scheme (SOS)

Generalized Observer Scheme (GOS) :

In the case of a generalized observer scheme, q observers are designed, each one is sensitive to one fault. Figures (1.18) and depicts the generalized observer structure for both sensor and actuator faults detection and isolation. If a fault occurs, the estimation of the sensitive subspace will be bad. Hence, all residuals except one will be sensitive to the occurred fault.

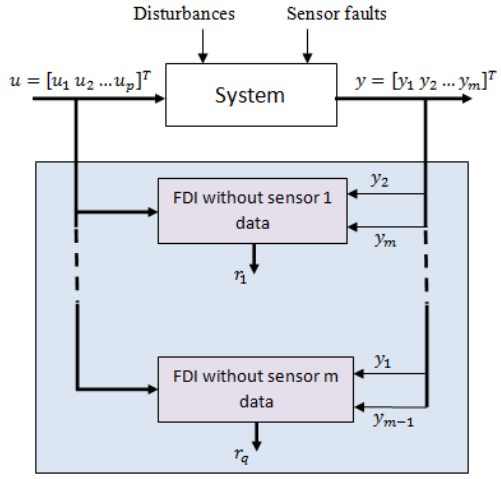

FIGURE 1.18: GOS-based sensor FDI

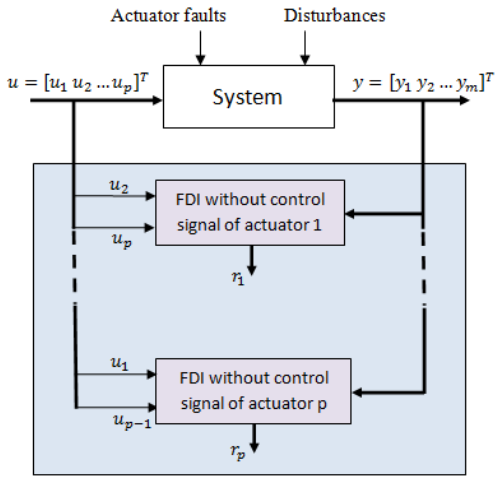

FIGURE 1.19: GOS-based actuator FDI

1.7 Conclusion

The aim of this chapter is to familiarize with the basic concepts of hybrid systems. These systems that arise in many industrial applications, which has attracted the community of researchers to develop the theory for hybrid systems. This is mainly due to advances in computer technology in recent years, which allowed the implementation of very complex modeling and control algorithms. In the literature of hybrid systems, several modeling formalisms have

been developed, three types are presented, Bond Graph, Petri Net and Hybrid automaton. This later is adopted along of this thesis and used to model the three cell converter in chapter two. Also, the observability of hybrid system in classical sense is presented, and different structures of observation of hybrid system is discussed. These two issues of concern will be studied convenably for the three cell converter in chapter three. The end of the current chapter is dedicated to introduce some basic concepts of fault diagnosis, mainly, diagnosis performance criteria, type of faults and different structures of fault diagnosis based on observers. This will be as a tool for chapter four and five where the diagnosis of the 3-cell converter is performed.

Chapter 2

Multicellular converter : Modeling and control

Contents

2.1 Introduction

Many industrial applications require more and more the use of the multi-level voltages converter for performance improvements on one hand and costs reducing on the other hand. The multi-level voltages converter is not a new topology, some of them are known since 1960, but they were not used in industry until recently because of certain technical barriers. These converters have been reappeared mainly due to the improvement of the control theory of switching systems and the intensive computer use in the control of the processes. This chapter is devoted to the study of the 3-cell converter, which can generate several voltage levels in the output voltage signal. The mathematical modeling of the converter is a primordial step to analyze its behavior and before designing any controlling law, or the designing of an observer, or carrying out a diagnostic task. For this, we present the different existing models of the 3-cell converter. Thereafter, we present some control law using these different models.

2.2 An overview on control of multicellular converter

The multicellular converter shares the constraint in elevated tension of the power source by dividing it over several cells, this limits the voltages that sustained by the semiconductors. The later operate in switching mode, it can be either closed or opened, which allows changing the operating mode of the converter according to the switch states, that allows generating several voltage levels on the output voltage signal, which is increasingly requested more and more by industrials. The switches are considered as ideal [54], so their behavior can be modeled by a discrete state(0 for closed and 1 for opened). Therefore, it can be considered as a hybrid or switching system. The main objectives of the control strategy of the multicellular converter consist of computing a control law to have a desired average output voltage and the desired load current to supply electric machines. This is obtained by a commutation between different operating modes at an appropriate switching frequency of the semiconductors. Consequently, the different signals are chopping at the switching times, and this allows the appearance of several undesirable harmonics on the output signal. This is why it is necessary to design control techniques minimizing the appearance of this unwanted phenomenon. Mathematical modeling is of a particular interest step before any study designing of the control law. However, the multicellular converter can be described by continuous variables (generally the load current and floating voltages), but also with discrete variables (cell states). In literature, the multicellular converter is described by different mathematical models such as the average model, harmonic model, instantaneous model, and hybrid model. On the first one, the discrete variables are replaced by their average values over the switching period [54]. The obtained model is well defined as the switching period is less than the time constant of the converter, and it is continuous which allows the possibility of several linear and nonlinear control design. Whereas, the instantaneous model called also direct model, represents accurately the state of each commutation cell, i.e., with their real values(0 or 1) over the switching period, and takes into account the instantaneous state of the state variables. Thus, all harmonics of high frequency related to the switches commutation will be represented in this model. Furthermore, the nonlinear behavior of the converter can be captured using the

nonlinear instantaneous model [3]. However, the hybrid model of the converter has been attracted the attention of several researchers in recent years, while fully justifiable since the dynamic behavior of the converter is based on both continuous and discrete state variables. The choice between these different models depends mainly on its use(control design, observability analysis, observer design, diagnosis). In the literature, several control approaches have been proposed. However, the proposed control techniques are based on all cited mathematical models. In [54] several control techniques are proposed. Nonlinear approaches have been applied to the average model. The first, based on the exact input-output linearization of the nonlinear average model. However, several drawbacks are associated with this approach. Indeed, a singularity point can appear in the neighborhood of an average value of the current close to zero, and the saturation of the control signal. But, the main limitation of this control technic is that it requires precise knowledge of the converter parameters [54]. To overcome these disadvantages, another approach based on the Lyapunov theory is proposed. All these proposed technics require the complete knowledge of all state variables using additional sensors. A pseudo-observer is than proposed to overcome the use of sensors. Using the average model, the author proposes another control technic using fuzzy logic. From a dynamic point of view, this type of control is highly efficient and robust [54]. Always using fuzzy logic, the same author uses the inverse of the harmonic model to design a control law. In [55], the authors propose a hybrid automaton to control the two cell converter. They show that the equilibrium zone is attractive and invariant under the defined invariance set of each operating mode, which means that the control law guarantees a practical attractive to their reference points. This control strategy is then generalized to a 3-cell converter in [56]. Recently, a very interesting control approach has been proposed to control of switched affine linear systems [57]. The control problem is formulated as a desired limit cycle stabilization using a hybrid Poincaré map approach. Indeed, the author proposes a new control automaton scheme by using a hybrid model of the 3-cell converter [3]. The proposed control strategy requires a deep analysis of the 3-cell converter operation for each mode. The control scheme is divided into two-controller blocs, the transitory state controller and the steady-state controller. The first controller guarantees a fast convergence to the steady-state with a minimum number of commutations, whereas the second controller ensures the local asymptotic stability of the predefined limit cycles. Using the hybrid model of the 3-cell converter, the authors in [58] have proposed a control approach based on a state-space partition, by solving a bilinear matrix inequality to guarantee practical stability. The main idea of this control strategy is to assign each discrete mode a quadratic region. The control switching law is then based on the selection of the subsystem that has the highest decrease of Lyapunov function. In [59] the authors propose a method for computing optimal state feedback for continuous switched affine systems exhibiting cyclic behavior in steady-state. They proved that the optimal trajectory synthesis implies to determine singular arcs of the trajectory. The interpolation of the solution through a neural network yields a state feedback control law. The approach is then applied to a 3-cell converter. In [60], a predictive control law is proposed using the hybrid model. The control strategy consists at each switching period, computing the distance between the reference point and the reached point of each configuration. The later, which corresponds to the minimal distance is selected. The approach has been compared to a PWM control strategy,

and it has been experimentally validated. Other approaches have been proposed using sliding mode theory, as in [61], where the proposed sliding surfaces guarantee the attractiveness of the state variables of the 3-cell converter to their references. The authors in [47] propose a sliding direct control law using the Lyapunov theory to show the convergence of the state variables to their references. Furthermore, adjacency constraints are given in order to improve the performance of the system and then minimizing the harmonic content of the load current and the output voltage. A second order super twisting control algorithm has been proposed to regulate the speed of a dc-motor connected to a 3-cell converter in [62]. The authors give away to generate several output voltage levels of the converter that supply the dc-motor. A practical realization of the proposed control algorithm is presented, and the results are very acceptable. Other approaches using the petri-net formalism have been proposed as in [], or the passivity approach based control which has been proposed in [63].

2.3 Necessity of multilevel topologies

Before starting to explore the multicellular converter, it is convenient to give an overview of the common multi-level conversion structures and their properties. The increase of the world energy demand has entailed the appearance of new power converter topologies and new semiconductor technology capable to drive all needed power. However, there is a rough competition between the use of classical power converter topologies (two-level converters) using high voltage semiconductors and new power converter topologies (multi-levels converters) using medium voltage devices [64]. Nowadays, multilevel converters are a good solution for power applications, since they can achieve high power using medium power semiconductor topology. They present great advantages compared with classical topologies. These advantages are fundamentally focussed on improvements of the output signal quality, which can be more improved as the number of levels increases reducing the total harmonic distortion (THD) of the output waveforms. These properties make the multi-levels converters very attractive to industry and researchers all over the world that spend great efforts trying to improve the multi-levels converters performances such as control simplification and performance of different optimization algorithms to enhance the THD of the output signals, the balancing of the dc capacitor voltages, and the ripple of the currents. The multilevel converter is not a new topology, some converters are known since 1960s [65], [1], but they were not used in industry until recently because of certain technical barriers [65]. The first multilevel converter introduced is the series-connected H-Bridge, which is also known as cascaded H-Bridge (CHB) in the late 1960s. In the same year, the low power flying capacitor converter has been introduced [1]. In 1975, The diode clamped converter (DCC) was introduced for the first time [32]. The DCC concept evolved into the three-level neutral point clamped (3L-NPC), and it is considered as the first real multilevel converter for medium voltage application [66]. Around 1995, the clamped H-Bridge would be reintroduced for more relevance in industry application [1]. In the early 1990s, the flying capacitor converter which introduced for low power in the 1960s, developed into the medium-voltage multilevel converter topology and has been reported as the imbricated-cell or multicellular converter [1], [54] [67]. These structures can be considered as the basic structures of multilevel energy conversion, and many of its

properties are common with the new structures of nowadays.

2.4 Multicellular converter : topology, properties and control requirements

Figure (??) depicts the topology of the multi-cell voltage-source converter leg. It is basically composed of p elementary cells associated in series and separated by $(p-1)$ floating voltage sources indicated by capacitors $C_j, (j = 1, ..., p-1)$.

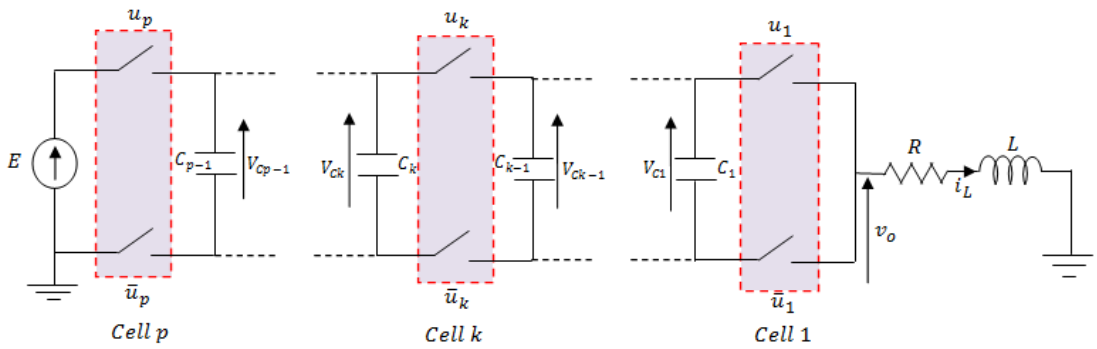

FIGURE 2.1: Multicellular converter

Each elementary cell called also commutation cell (figure (2.2)), consists of a pair of switches. Each of these switches being represented as an IGBT with an antiparallel diode. The two switches of any pair must always be in opposite states, which is obtained by controlling the two IGBT with quasi opposite signals for each commutation. The blocking cell switch has to sustain a voltage equal to $\frac{E}{p}$, where E represents the source voltage which can be chosen accordingly to the desired output voltages. Each commutation cell is controlled by a binary control signal u_k. $u_k = 1$ means that the upper switch of the k^{th} cell is conducting and the lower switch of the same cell is not conducting. $u_k = 0$ means that the upper switch is non conducting and the lower switch is conducting.

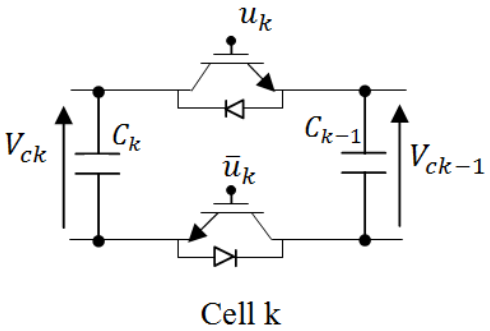

FIGURE 2.2: Elementary commutation cell

The functioning safety of the converter depends directly on a good distribution of the voltage for each cell. This is why, it is necessary to ensure the balancing of the voltage across the floating capacitors. The converter features offer the possibility to ensure this balancing

by acting on the switches control signals. So, a suitable control sequence for switches must be applied. Otherwise, the floating voltages deviate from their references and the converter features are lost.

In order to study the multicellular converter properties, some assumptions should be considered [54] :

- The switches are considered ideals.
- The dead time of the commutation is considered to be zero.
- The voltage sources are considered to be ideals.
- The duty cycle is the same for all switching cell control signals.

The cell index number ($k = 1, ..., p$) starts from the closest cell from the load R-L. Even for the capacitor index number ($j = 1, ..., p-1$) starts from the closest capacitor to the load R-L. The state variables and the input control signals can be chosen as :

- The floating voltages v_{c_j}, ($j = 1, ..., p-1$) across the floating capacitors.
- The load current i_l that flows the load $R - L$.
- The control input signals $u_k \in \{0, 1\}$, with ($k = 1, ..., p$)

In order to share the same constraint in tension over all cells ($v_{cell_k} = \frac{E}{P}$), the floating voltages v_{c_j} should have a difference between two successive cells equal to $v_{c_j} - v_{c_{j-1}} = \frac{E}{p}$, with ($j = 1, ..., p-1$). In this case, the following property is verified.

Property 1 : For a p-cell converter, each floating capacitor must have a voltage equal to $v_{c_j} = j\frac{E}{p}$, ($j = 1, ..., p-1$).

In this case, the output voltage signal has $(p+1)$ voltage levels.

Property 2 : For a p-cell converter, one can have 2^p different topologies and $(p+1)$ voltage levels in the output voltage signal $(0, \frac{E}{p}, ..., \frac{p-1}{p}E, E)$.

Let α be the duty cycle of the cell control signals. By definition, the duty cycle is defined as the average value of the control input signal over the switching period. Noted that the duty cycle is assumed to be the same for all control input signals.

$$\alpha =< u_1 >=< u_2 >= \cdots =< u_p > \tag{2.1}$$

with $< u >$ represents the average value of u. The duty cycle value depends on the desired load current. In the steady state (identical voltages across all switching cell), the average value of the output voltage v_o has the following reference value [3] :

$$< v_o >_{ref} = \alpha \sum_{k=1}^{p} < v_{cell_k} >= \alpha E \tag{2.2}$$

In steady state, using the equation of the current dynamic, we get :

$$\alpha = \frac{I_{ref}}{I_{max}} \tag{2.3}$$

where I_{ref} and I_{max} represent respectively the reference current and the maximal current which can flows the load R-L. This latter is equal to $\frac{E}{R}$.

Property 3 : For a p-cell converter, if the duty cycle $\alpha \in [\frac{k-1}{p}, \frac{k}{p}]$, then the output voltage will be between $(k-1)\frac{E}{p}$ and $k\frac{E}{p}$ over a switching period.

Let ϕ be the phase shift between the control input signals. We have then these properties.

Property 4 : For a p-cell converter, if all control signals have the same duty cycle and are phase shifted by $\frac{2\pi}{p}$, then the output voltage ripple is divided by p.

Property 5 : For a p-cell converter, if we impose the same duty cycle for all control input signals and a regular phase shift equal to $\frac{2\pi}{p}$, then the apparent commutation frequency of the output voltage v_o is multiplied by p.

2.5 Modeling of the multicellular converter

In the literature, researchers have proposed several mathematical models of the converter, instantaneous model, average model, harmonic model and hybrid model. The choice between them depends on its use (analysis, control, observation, diagnosis). In the current section, we focus our attention on the instantaneous and hybrid modeling of the p-cell converter. These two models will be used along of this thesis. However, we just give the definitions for the two other models.

2.5.1 Average model

This model is obtained by replacing each variable (state variables and control inputs) by their average values over the switching period [54], tacking into account that the switching period must be small then the time constant of the system [3]. The obtained model is continuous and offers the possibility to synthesize a certain number of nonlinear control laws. Furthermore, the average model use the duty cycle as the unique information concerning the switching cell. Besides, the phase shift of the control signals is not considering, this implies that the average model does not allow to highlight the harmonic phenomena at the switching times [32]. Consequently, the natural balancing of the floating voltages, which is essential to benefit from all advantages that offers the multi cellular converter, is not respected.

2.5.2 Harmonic model

The harmonic model is based on Fourier series decomposition of different signals as the control inputs, the output voltage and the load current. It allows to obtain a dynamic representation that take into account the harmonic phenomena under some assumptions as :

- The time constant of the load is supposed less than a switching period.

- The current is assumed reaching the steady state.
- The floating voltages are supposed constants over the switching period.
- The dead time between two commutations is supposed zero.
- The switches are considered ideals.
- The load is considered inductive.

More about this model can be found in [54].

2.5.3 Instantaneous model

Instantaneous model called also direct model, represents accurately the state of each commutation cell, i.e., with their real values (0 or 1) over the switching period, and takes into account the instantaneous state of the state variables of the converter [32]. Thus, all harmonic or high frequency related to the switches commutation will be present in this model [54]. Furthermore, the nonlinear phenomena of the converter can be captured using the nonlinear instantaneous model [3].
To describe the dynamic behavior of the $p-$cell converter using the instantaneous model, we have to give $(p-1)$ equations related to the evolution of the floating voltages $v_{c_j}, \quad (j = 1, ..., p-1)$ of each capacitors C_j, and one equation related the current flowing the load R-L.

The voltage evolution across the j^{th} capacitor is related to the current flowing through the capacitor C_j,

$$\frac{dv_{c_j}}{dt} = \frac{1}{C_j} i_{c_j} \tag{2.4}$$

The current flowing the capacitor C_j is related to the state of their adjacent cells and load current, it is given by :

$$i_{c_j} = (u_{j+1} - u_j) i_l, \quad j = 1, ..., p-1. \tag{2.5}$$

Substituting equation (2.5) into equation (2.4), we obtain :

$$\frac{dv_{c_j}}{dt} = \frac{1}{C_j} (u_{j+1} - u_j) i_L, \quad j = 1, ..., p-1, \tag{2.6}$$

which describes the evolution of the floating voltage of each capacitor. Other hand, the output voltage of a p-cell converter, denoted v_o, is given by :

$$v_o = \sum_{k=1}^{p} u_k v_{cell_k}, \tag{2.7}$$

with v_{cell_k} represents the voltage across the k^{th} cell, it is given by :

$$v_{cell_k} = v_{c_k} - v_{c_{k-1}}, \quad k = 1, ..., p. \tag{2.8}$$

Thus, by substituting (2.8) into (2.7), the output voltage across the load is :

$$v_o = \sum_{k=1}^{p} (v_{c_k} - v_{c_{k-1}}) u_k, \tag{2.9}$$

with $v_{c_0} = 0$ and $v_{c_p} = E$.
The dynamic behavior of the load current is :

$$\frac{di_L}{dt} = \frac{v_o}{L} - \frac{R}{L} i_L. \tag{2.10}$$

Substituting equation (2.10) into (2.9), we obtain :

$$\frac{di_L}{dt} = -\frac{R}{L} i_L + \frac{1}{L} \sum_{k=1}^{p} (v_{c_k} - v_{c_{k-1}}) u_k. \tag{2.11}$$

Finally, the instantaneous model of the p-cell converter associated to a load R-L is described by the following equations :

$$\Sigma_{p-cell} : \begin{cases} \frac{dv_{c_k}}{dt} = \frac{1}{C_k}(u_{k+1} - u_k) i_L \\ \frac{di_L}{dt} = -\frac{R}{L} i_L + \frac{1}{L} \sum_{k=1}^{p} (v_{c_k} - v_{c_{k-1}}) u_k \end{cases} \qquad k = 1, ..., p. \tag{2.12}$$

With $v_{c_0} = 0$ and $v_{c_p} = E$. And where $x = [v_{c_1} \quad v_{c_2} \quad ... \quad v_{c_{p-1}} \quad i_L]^T \in R^n$ is the state vector, $u = [u_1 \quad u_2 \quad ... \quad u_p]^T \in \{0, 1\}^p$ is the control input vector. Model (2.12) can be put in a compact form :

$$\dot{x} = A(u)x + B(u), \tag{2.13}$$

where :

$$A(u) = \begin{bmatrix} 0 & \cdots & 0 & \frac{u_2 - u_1}{C_1} \\ \vdots & \ddots & \ddots & \vdots \\ 0 & \cdots & 0 & \frac{u_p - u_{p-1}}{C_{p-1}} \\ -\frac{u_2 - u_1}{L} & \cdots & -\frac{u_p - u_{p-1}}{L} & -\frac{R}{L} \end{bmatrix}, \qquad B(u) = \begin{bmatrix} 0 \\ \ddots \\ 0 \\ \frac{E}{L} u_3 \end{bmatrix}.$$

Moreover, the model (2.12) can be rewritten as a nonlinear affine model of the form :

$$\dot{x} = g_0(x) + \sum_{k=1}^{m} g_k(x) u_k, \tag{2.14}$$

and where $g_0(x)$ and $g_k(x)$, $\quad k = 1, ..., p$, are smooth vector fields. Let $g(x) = [g_1(x) \quad \cdots \quad g_p(x)]$, then :

$$g_0(x) = \begin{bmatrix} 0 \\ \vdots \\ 0 \\ -\frac{R}{L} i_L \end{bmatrix}, g(x) = \begin{bmatrix} -\frac{i_L}{C_1} & \frac{i_L}{C_1} & 0 & 0 & \cdots & 0 & 0 \\ 0 & -\frac{i_L}{C_2} & \frac{i_L}{C_2} & 0 & 0 & \cdots & 0 \\ \vdots & \ddots & \ddots & \ddots & \ddots & \vdots & \vdots \\ 0 & \cdots & \cdots & \cdots & \cdots & -\frac{i_L}{C_{p-1}} & \frac{i_L}{C_{p-1}} \\ \frac{v_{c_1}}{L} & \frac{v_{c_2} - v_{c_1}}{L} & \frac{v_{c_3} - v_{c_2}}{L} & \cdots & \cdots & \frac{v_{c_{p-1}} - v_{c_{p-2}}}{L} & \frac{E - v_{c_{p-1}}}{L} \end{bmatrix}$$

This model will be used for fault detection and isolation of the converter switch faults in

chapter 5.

2.5.4 Hybrid model

It is clear that the multicellular converter is a switching system, since it works on commutation mode. The opening and the closing of the switches by the control signals $u \in \{0, 1\}$, allow to select only one operating mode each commutation. This is why it is judicious to model the multicellular converter as a hybrid system. Many works are presented the hybrid model of the multicellular converter [32], [3], [47],[68],...etc. In this section we propose to model the 3-cell converter, this choice is based on its use along of this thesis. It consists of 3 commutation cells, two floating capacitors C_1 and C_2, a load R-L, a voltage source E. Therefore, $2^3 = 8$ different operating modes, 4 voltage levels $(0, \frac{E}{3}, \frac{2E}{3}, E)$, 3 control inputs u_1, u_2 and u_3. Figure (2.3) depicts the 3-cell converter.

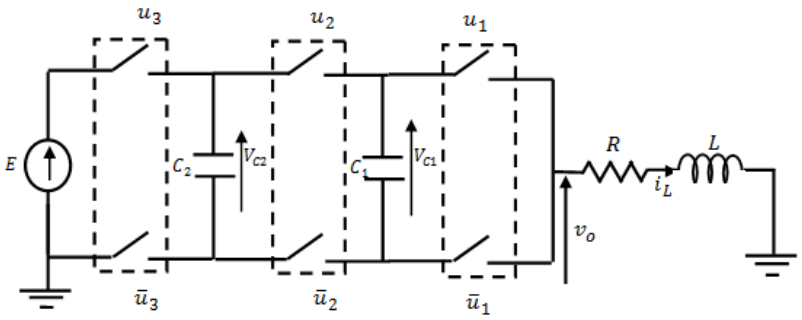

FIGURE 2.3: A three-cell converter

The continuous variables of the 3-cell converter correspond to the capacitor voltages v_{c_1}, v_{c_2}, and the load current i_L. The cells states (u_1, u_2 and u_3 combinations offer eight discrete modes as described by table (2.1).

modes		q_1	q_2	q_3	q_4	q_5	q_6	q_7	q_8
cell states	u_1	0	1	0	1	0	1	0	1
	u_2	0	0	1	1	0	0	1	1
	u_3	0	0	0	0	1	1	1	1
output voltages		0	$\frac{E}{3}$	$\frac{E}{3}$	$\frac{2E}{3}$	$\frac{E}{3}$	$\frac{2E}{3}$	$\frac{E}{3}$	E

TABLE 2.1: Different operating modes associated with the cell states and the output voltage in steady state for the 3-cell converter.

The hybrid model of the 3-cell converter can be described by the following 6-tuple hybrid automaton :

$$H = (Q, X, f_{q_i}, T, G, Init), \tag{2.15}$$

where :

- $Q = \{q_i, i \in 1, \cdots, 8\}$ is a set of discrete states of the converter. For a 3-cell converter, we distinguish eight different discrete modes, each one corresponds to a specific topology of the converter as presented below.
- $X = \{x \in R^3/(0 \leq v_{c_j} \leq E) \wedge (0 \leq i_L \leq I_{max}), j = 1, 2\}$ is the continuous state space of the converter. Where v_{c_k} is the floating voltage of each capacitor, and i_L is the load current.
- $T = \{T_{i,j}, i, j \in 1, \cdots, 8, i \neq j\}$ represent a collection of all possible transition between all operating modes.
- $G : T \to 2^X$ represents the guard conditions.
- $Init \subseteq X \times Q$ gives the initial hybrid states.
- f_{q_i} is a vector field such as $f_{q_i} : Q \times R^3 \to R^3$, that describes the dynamic behavior of the converter for each operating mode, it is defined by the following equation :

$$\dot{x} = f_{q_i}(x, u) = A_{q_i}x + B_{q_i}, i = 1, \cdots, 8 \quad \text{and} \quad q_i \in Q. \tag{2.16}$$

$A_{q_i} \in R^{3\times3}$ and $B_{q_i} \in R^3$ are matrices of appropriate dimension. Different state equations for each operating mode are presented below.

Mode q_1 $(u_1 = 0, \quad u_2 = 0, \quad u_3 = 0)$ **:**

Figure (2.4) shows the 3-cell converter in mode q_1.

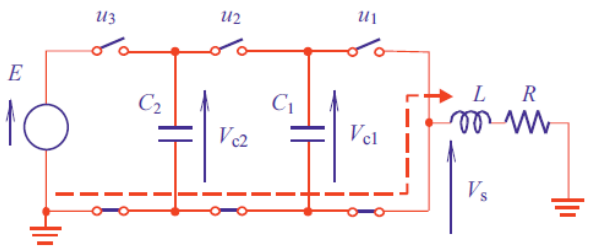

FIGURE 2.4: 3-cell converter in mode q_1

In this situation the dynamic behavior can be represented by the following equations. Note that in the current mode, the output voltage $v_o = 0$.

$$\Sigma_{q_1} : \begin{cases} \dot{x} = \begin{bmatrix} 0 & 0 & 0 \\ 0 & 0 & 0 \\ 0 & 0 & -\frac{R}{L} \end{bmatrix} x \\ v_0 = 0 \end{cases} \tag{2.17}$$

Mode q_2 $(u_1 = 1, \quad u_2 = 0, \quad u_3 = 0)$ **:**

Figure (2.5) shows the 3-cell converter in mode q_2.

The dynamic behavior can be represented by the following equations. Note that the output voltage $v_o = v_{c_1}$.

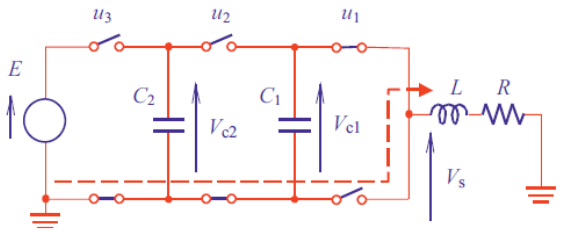

FIGURE 2.5: 3-cell converter in mode q_2

$$\Sigma_{q_2} : \begin{cases} \dot{x} = \begin{bmatrix} 0 & 0 & -\frac{1}{C_1} \\ 0 & 0 & 0 \\ \frac{1}{L} & 0 & -\frac{R}{L} \end{bmatrix} x \\ v_o = v_{c_1} \end{cases} \tag{2.18}$$

Mode q_3 $(u_1 = 0, \quad u_2 = 1, \quad u_3 = 0)$ **:**

Figure (2.6) shows the 3-cell converter in the mode q_3.

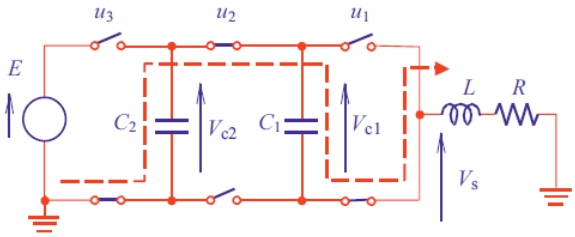

FIGURE 2.6: 3-cell converter in mode q_3

The dynamic behavior can be represented by the following equations. Note that in the current mode, the output voltage $v_0 = v_{c_2} - v_{c_1}$.

$$\Sigma_{q_3} : \begin{cases} \dot{x} = \begin{bmatrix} 0 & 0 & \frac{1}{C_1} \\ 0 & 0 & -\frac{1}{C_2} \\ -\frac{1}{L} & \frac{1}{L} & -\frac{R}{L} \end{bmatrix} x \\ v_0 = v_{c_2} - v_{c_1} \end{cases} \tag{2.19}$$

Mode q_4 $(u_1 = 1, \quad u_2 = 1, \quad u_3 = 0)$ **:**

Figure (2.7) shows the 3-cell converter in mode q_4.

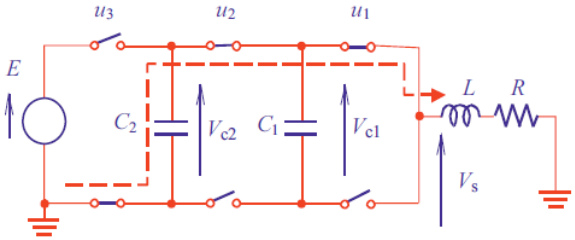

FIGURE 2.7: 3-cell converter in mode q_4

In this situation, the dynamic behavior of the 3-cell converter can be represented by the following equations. Note that in the current mode, the output voltage $v_0 = v_{c_2}$.

$$\Sigma_{q_4} : \begin{cases} \dot{x} = \begin{bmatrix} 0 & 0 & 0 \\ 0 & 0 & -\frac{1}{C_2} \\ 0 & \frac{1}{L} & -\frac{R}{L} \end{bmatrix} x \\ v_0 = v_{c_2} \end{cases} \tag{2.20}$$

Mode q_5 $(u_1 = 0, \quad u_2 = 0, \quad u_3 = 1)$ **:**

Figure (2.8) shows the 3-cell converter in mode q_5.

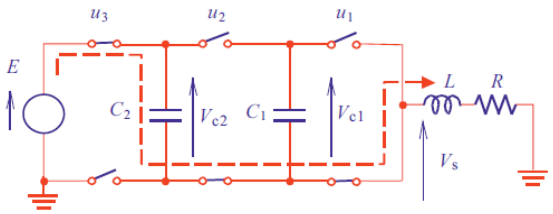

FIGURE 2.8: 3-cell converter in mode q_5

In this situation, the dynamic behavior can be represented by the following equations. Note that in the current mode, the output voltage $v_o = E - v_{c_2}$.

$$\Sigma_{q_5} : \begin{cases} \dot{x} = \begin{bmatrix} 0 & 0 & 0 \\ 0 & 0 & \frac{1}{C_2} \\ 0 & -\frac{1}{L} & -\frac{R}{L} \end{bmatrix} x + \begin{bmatrix} 0 \\ 0 \\ \frac{E}{L} \end{bmatrix} \\ v_o = E - v_{c_2} \end{cases} \tag{2.21}$$

Mode q_6 $(u_1 = 1, \quad u_2 = 0, \quad u_3 = 1)$ **:**

Figure (2.9) shows the 3-cell converter in mode q_6.

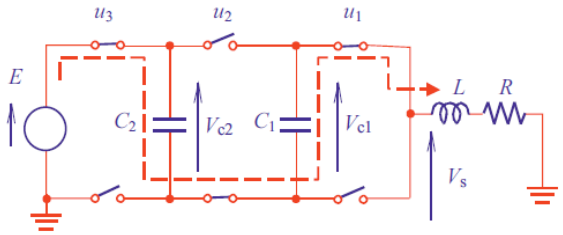

FIGURE 2.9: 3-cell converter in mode q_6

The dynamic behavior of the converter can be represented by the following equations. Note that in the current mode, the output voltage $v_o = E + v_{c_1} - v_{c_2}$.

$$\Sigma_{q_6} : \begin{cases} \dot{x} = \begin{bmatrix} 0 & 0 & -\frac{1}{C_1} \\ 0 & 0 & \frac{1}{C_2} \\ \frac{1}{L} & -\frac{1}{L} & -\frac{R}{L} \end{bmatrix} x + \begin{bmatrix} 0 \\ 0 \\ \frac{E}{L} \end{bmatrix} \\ v_s = E - v_{c_1} - v_{c_2} \end{cases} \tag{2.22}$$

Mode q_7 $(u_1 = 0, \quad u_2 = 1, \quad u_3 = 1)$ **:**

Figure (2.10) shows the 3-cell converter in mode q_7.

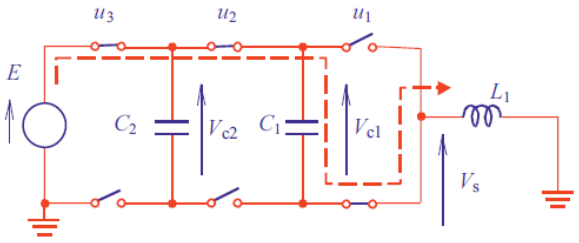

FIGURE 2.10: 3-cell converter in mode q_7

The dynamic behavior can be represented by the following equation. Note that in the current mode, the output voltage $v_o = E - v_{c_1}$.

$$\Sigma_{q_7} : \begin{cases} \dot{x} = \begin{bmatrix} 0 & 0 & \frac{1}{C_1} \\ 0 & 0 & 0 \\ \frac{-1}{L} & \frac{-R}{L} & 0 \end{bmatrix} x + \begin{bmatrix} 0 \\ 0 \\ \frac{E}{L} \end{bmatrix} \\ v_o = E - v_{c_1} \end{cases} \tag{2.23}$$

Mode q_8 $(u_1 = 1, \quad u_2 = 1, \quad u_3 = 1)$ **:**

Figure (2.11) shows the 3-cell converter in mode q_8.

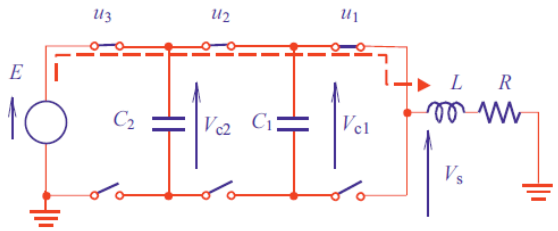

FIGURE 2.11: 3-cell converter in mode q_8

In this situation, the dynamic behavior of the converter can be represented by the following equations. Note that in the current mode, the output voltage $v_s = E$.

$$\Sigma_{q_8} : \begin{cases} \dot{x} = \begin{bmatrix} 0 & 0 & 0 \\ 0 & 0 & 0 \\ 0 & 0 & \frac{-R}{L} \end{bmatrix} x + \begin{bmatrix} 0 \\ 0 \\ \frac{E}{L} \end{bmatrix} \\ v_o = E \end{cases} \tag{2.24}$$

2.6 Control of the 3-cell converter

The main objective of the control is to generate discrete signals $u_k, (k = 1, 2, 3)$ such that :

- The stabilization of the load current i_L around its desired state I_{ref}, i.e., the error $i_L - I_{ref}$ must be close to zero.

- The capacitor floating voltages v_{c_1} and v_{c_2} must be regulated respectively around their references $V_{ref1} = \frac{E}{3}$ and $V_{ref2} = \frac{2E}{3}$.

In what follows, some control strategies of the 3-cell converter that we thought very interesting will be presented.

2.6.1 Hybrid control of 3-cell converter

The presented control strategy in [56] for the 3-cell converter is an extended control strategy for the two cell converter presented in [55]. In fact, for the 3-cell converter, the control scheme is depicted in figure (2.12), and the guard conditions are as follow :

$$
\begin{aligned}
G(T_{1,2}) &= \{x \in X : (v_{c1} > V^{+}_{ref1}) \wedge (i < I^{-}_{ref})\} \\
G(T_{2,1}) &= \{x \in X : (v_{c1} < V^{+}_{ref1}) \wedge (i < I^{+}_{ref})\} \\
G(T_{1,3}) &= \{x \in X : (v_{c1} < V^{-}_{ref1}) \wedge (v_{c2} > V^{+}_{ref2}) \wedge (i < I^{-}_{ref})\} \\
G(T_{3,1}) &= \{x \in X : (v_{c1} > V^{+}_{ref1}) \wedge (v_{c2} > V^{-}_{ref2}) \wedge (i > I^{+}_{ref})\} \\
G(T_{1,5}) &= \{x \in X : (v_{c2} < V^{-}_{ref2}) \wedge (i > I^{-}_{ref})\} \\
G(T_{5,1}) &= \{x \in X : (v_{c2} > V^{+}_{ref2}) \wedge (i > I^{+}_{ref})\} \\
G(T_{2,4}) &= \{x \in X : (v_{c1} < V^{-}_{ref1}) \wedge (v_{c2} > V^{+}_{ref2}) \wedge (i < I^{-}_{ref})\} \\
G(T_{4,2}) &= \{x \in X : (v_{c1} > V^{+}_{ref1}) \wedge (v_{c2} < V^{-}_{ref2}) \wedge (i > I^{+}_{ref})\} \\
G(T_{2,6}) &= \{x \in X : (v_{c1} < V^{-}_{ref1}) \wedge (v_{c2} < V^{-}_{ref2}) \wedge (i < I^{-}_{ref})\} \\
G(T_{6,2}) &= \{x \in X : (v_{c2} < V^{+}_{ref2})\} \\
G(T_{3,4}) &= \{x \in X : (v_{c1} > V^{+}_{ref1})\} \\
G(T_{4,3}) &= \{x \in X : (v_{c1} < V^{-}_{ref1}) \wedge (v_{c2} < V^{-}_{ref2}) \wedge (i > I^{+}_{ref})\} \\
G(T_{3,7}) &= \{x \in X : (v_{c2} < V^{-}_{ref2})\} \\
G(T_{7,3}) &= \{x \in X : (v_{c1} > V^{+}_{ref1}) \wedge (v_{c2} > V^{+}_{ref2}) \wedge (i > I^{+}_{ref})\} \\
G(T_{4,8}) &= \{x \in X : (v_{c2} < V^{-}_{ref2}) \wedge (i < I^{-}_{ref})\} \\
G(T_{8,4}) &= \{x \in X : (v_{c2} > V^{-}_{ref2}) \wedge (i > I^{+}_{ref})\} \\
G(T_{5,6}) &= \{x \in X : (v_{c1} > V^{+}_{ref1}) \wedge (v_{c2} > V^{+}_{ref2}) \wedge (i < I^{-}_{ref})\} \\
G(T_{6,5}) &= \{x \in X : (v_{c1} < V^{-}_{ref2})\} \\
G(T_{5,7}) &= \{x \in X : (v_{c1} < V^{-}_{ref1}) \wedge (v_{c2} > V^{+}_{ref2}) \wedge (i < I^{-}_{ref})\} \\
G(T_{7,5}) &= \{x \in X : (v_{c1} > V^{+}_{ref1}) \wedge (v_{c2} < V^{-}_{ref2}) \wedge (i > I^{+}_{ref})\} \\
G(T_{6,8}) &= \{x \in X : (v_{c1} < V^{-}_{ref1}) \wedge (v_{c2} > V^{+}_{ref2}) \wedge (i < I^{-}_{ref})\} \\
G(T_{8,6}) &= \{x \in X : (v_{c1} > V^{+}_{ref1}) \wedge (v_{c2} < V^{-}_{ref2}) \wedge (i > I^{+}_{ref})\} \\
G(T_{7,8}) &= \{x \in X : (v_{c1} > V^{+}_{ref1}) \wedge (i < I^{-}_{ref})\} \\
G(T_{2,1}) &= \{x \in X : (v_{c1} > V^{-}_{ref1}) \wedge (i > I^{+}_{ref})\}.
\end{aligned}
$$

Where $V^{\pm}_{ref_j} = V_{ref_j} \pm \Delta v_j$ and $I^{\pm}_{ref} = I_{ref} \pm \Delta i$, and where Δv_j and Δi represent respectively the ripples of the floating capacitor voltages and the load current.

2.6.2 Control of 3-cell converter based on stabilization of limit cycles

Recently in [57], [3] proposed a new hybrid control strategy based on stabilization of limit cycles of the 3-cell converter. As depicted in figure (2.13), the authors developed the control strategy using the hybrid automaton formalism. The control scheme is divided into two controller blocs, the transitory state controller and the steady state controller. Indeed, the first controller guarantees a fast convergence to the steady state with minimum number of commutations, whereas the second controller ensures the local asymptotic stability of the predefined limit cycles.

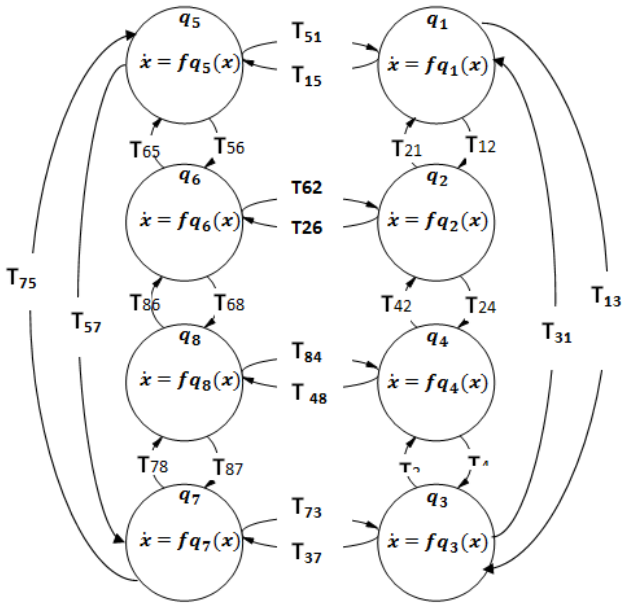

FIGURE 2.12: Hybrid control automaton for a 3-cell converter

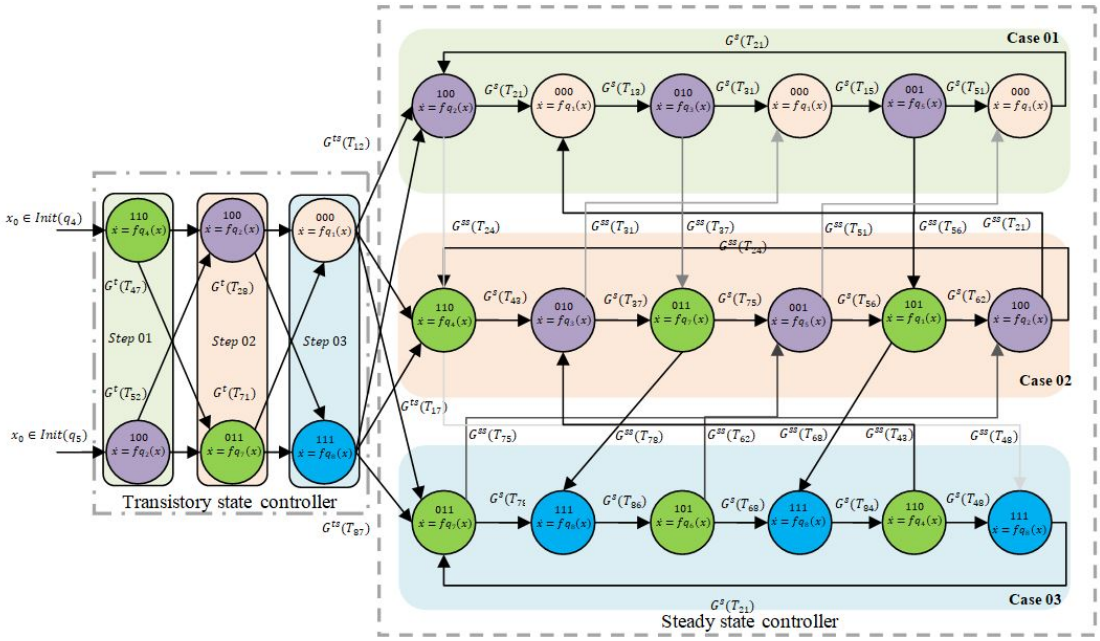

FIGURE 2.13: Hybrid automaton control based on desired limit cycles stabilization of 3-cell converter.

Steady state controller

The authors have seen that it is more suitable to divide the steady state controller hybrid automaton to three stages since the desired limit cycles of the 3-cell converter has 3 main geometric shapes [3]. Let T_i denotes the set of possible transitions in each stages ($i = 1, 2, 3$), and let $G^s(T_{i,j})$, the guard condition between the discrete modes in the same stage. In each stage, the transitions and guards are defined as follow :

Case 1 ($0 < I_{ref} \leq \frac{I_{max}}{3}$) **:** The set of possible transitions in this stage is :

$$T_1 = \{T_{1,2}, T_{2,1}, T_{1,3}, T_{3,1}, T_{1,5}, T_{5,1}\} \tag{2.25}$$

and the guards are :

$$\begin{aligned}
&G^s(T_{1,2}) = G^s(T_{1,2}) = G^s(T_{1,2}) = \{x \in X : i_L < I_{ref} - \Delta i\} \\
&G^s(T_{5,1}) = \{x \in X : v_{c2} \geq V_{ref2} + \Delta v_2\} \\
&G^s(T_{2,1}) = \{x \in X : v_{c1} \leq V_{ref1} - \Delta v_1\} \\
&G^s(T_{3,1}) = \{x \in X : v_{c1} \geq V_{ref1} + \Delta v_1\}
\end{aligned}$$

where $\Delta v_1 = (\frac{I_{ref}}{C_1})\frac{\alpha T}{2}$, $\Delta v_2 = (\frac{I_{ref}}{C_2})\frac{\alpha T}{2}$ and $\Delta i = \alpha(\frac{1}{3} - \alpha)\frac{ET}{2L}$ are respectively the ripples of the capacitor voltages and the load current, with T represents the period of limit cycle and $\alpha = \frac{I_{ref}}{I_{max}}$. The switching points of the desired limit cycle are :

$$x^*_{1,2} = \begin{pmatrix} V^+_{ref1} \\ V^+_{ref2} \\ I^-_{ref} \end{pmatrix}, \quad x^*_{5,1} = \begin{pmatrix} V^+_{ref1} \\ V^+_{ref2} \\ I^+_{ref} \end{pmatrix}, \quad x^*_{1,5} = \begin{pmatrix} V^+_{ref1} \\ V^-_{ref2} \\ I^-_{ref} \end{pmatrix},$$

$$x^*_{3,1} = \begin{pmatrix} V^+_{ref1} \\ V^-_{ref2} \\ I^+_{ref} \end{pmatrix}, \quad x^*_{1,3} = \begin{pmatrix} V^-_{ref1} \\ V^+_{ref2} \\ I^-_{ref} \end{pmatrix}, \quad x^*_{2,1} = \begin{pmatrix} V^-_{ref1} \\ V^+_{ref2} \\ I^+_{ref} \end{pmatrix};$$

where : $V^{\pm}_{refi} = V_{refi} \pm \Delta v_i$ and $I^{\pm}_{ref} = I_{ref} \pm \Delta i$. The dwell time in each discrete mode is given by :

$$\begin{aligned}
&t^*_{1,2} = t^*_{1,3} = t^*_{1,5} = (\tfrac{1}{3} - \alpha)T \\
&t^*_{2,1} = t^*_{3,1} = t^*_{5,1} = \alpha T;
\end{aligned}$$

Case 2 ($\frac{I_{max}}{3} < I_{ref} \leq \frac{2I_{max}}{3}$) : The set of possible transitions in this stage is :

$$T^2 = \{T_{4,3}, T_{3,7}, T_{7,5}, T_{5,6}, T_{6,2}, T_{2,4}\} \tag{2.26}$$

and their corresponding guards conditions are :

$$\begin{aligned}
&G^s(T_{4,3}) = \{x \in X : v_{c2} \leq V_{ref2} + \Delta v^1_2\} \\
&G^s(T_{3,7}) = \{x \in X : v_{c2} \leq V_{ref2} - \Delta v_2\} \\
&G^s(T_{7,5}) = \{x \in X : v_{c1} \geq V_{ref1} - \Delta v_1\} \\
&G^s(T_{5,6}) = \{x \in X : v_{c2} \geq V_{ref2} + \Delta v^1_2\} \\
&G^s(T_{6,2}) = \{x \in X : v_{c2} \geq V_{ref2} + \Delta v_2\} \\
&G^s(T_{2,4}) = \{x \in X : v_{c1} \leq V_{ref1} - \Delta v_1\}
\end{aligned}$$

where $\Delta v_1 = (\frac{I_{ref}}{6C_1})T$, $\Delta v^1_1 = (\frac{I_{ref}}{6C_1})(1 - 2\alpha)$,$\Delta v_2 = (\frac{I_{ref}}{C_2})T$, $\Delta v^1_2 = (\frac{I_{ref}}{C_2})(1 - 2\alpha)$ and $\Delta i = \alpha(\alpha - \frac{1}{3})\frac{ET}{2L}$. The switching points of the limit cycle are :

$$x^*_{2,4} = \begin{pmatrix} V^-_{ref1} \\ V^+_{ref2} \\ I^-_{ref} \end{pmatrix}, \quad x^*_{6,2} = \begin{pmatrix} V_{ref1} + \Delta v^1_1 \\ V^+_{ref2} \\ I^+_{ref} \end{pmatrix}, \quad x^*_{5,6} = \begin{pmatrix} V^+_{ref1} \\ V_{ref2} + \Delta v^1_2 \\ I^-_{ref} \end{pmatrix},$$

$$x^*_{7,5} = \begin{pmatrix} V^+_{ref1} \\ V^-_{ref2} \\ I^+_{ref} \end{pmatrix}, \quad x^*_{3,7} = \begin{pmatrix} V_{ref1} + \delta v^1_1 \\ V^-_{ref2} \\ I^-_{ref} \end{pmatrix}, \quad x^*_{2,1} = \begin{pmatrix} V^-_{ref1} \\ V_{ref2} + \Delta v^1_2 \\ I^+_{ref} \end{pmatrix};$$

The dwell time in each discrete mode is given by :

$$t^*_{4,3} = t^*_{7,5} = t^*_{6,2} = (\alpha - \tfrac{1}{3})T$$
$$t^*_{3,7} = t^*_{5,6} = t^*_{2,4} = (\tfrac{2}{3} - \alpha)T;$$

Case 3 ($\frac{2I_{max}}{3} < I_{ref} \leq I_{max}$) : The set of possible transitions in this stage is :

$$T^3 = \{T_{8,4}, T_{4,8}, T_{8,6}, T_{6,8}, T_{8,7}, T_{7,8}\} \tag{2.27}$$

and their corresponding guard conditions are :

$$G^s(T_{8,4}) = G^s(T_{8,6}) = G^s(T_{8,7}) = \{x \in X : i_L \geq I_{ref} + \Delta i\}$$
$$G^s(T_{4,8}) = \{x \in X : v_{c2} \leq V_{ref2} - \Delta v_2\}$$
$$G^s(T_{6,8}) = \{x \in X : v_{c1} \leq V_{ref1} - \Delta v_1\}$$
$$G^s(T_{7,8}) = \{x \in X : v_{c1} \geq V_{ref1} + \Delta v_1\}$$

where $\Delta v_1 = (\frac{I_{ref}}{C_1})\frac{(1-\alpha)T}{2}$, $\Delta v_2 = (\frac{I_{ref}}{C_2})\frac{(1-\alpha)T}{2}$, and $\Delta i = \alpha(\alpha - \frac{2}{3})(1-\alpha)\frac{ET}{2L}$. The switching points of the limit cycle are :

$$x^*_{8,7} = \begin{pmatrix} V^-_{ref1} \\ V^-_{ref2} \\ I^+_{ref} \end{pmatrix}, \quad x^*_{7,8} = \begin{pmatrix} V^+_{ref1} \\ V^-_{ref2} \\ I^-_{ref} \end{pmatrix}, \quad x^*_{8,6} = \begin{pmatrix} V^+_{ref1} \\ V^-_{ref2} \\ I^+_{ref} \end{pmatrix},$$

$$x^*_{6,8} = \begin{pmatrix} V^-_{ref1} \\ V^+_{ref2} \\ I^-_{ref} \end{pmatrix}, \quad x^*_{3,7} = \begin{pmatrix} V^-_{ref1} \\ V^+_{ref2} \\ I^+_{ref} \end{pmatrix}, \quad x^*_{4,8} = \begin{pmatrix} V^-_{ref1} \\ V^-_{ref2} \\ I^+_{ref} \end{pmatrix};$$

The dwell time in each discrete mode is given by :

$$t^*_{8,7} = t^*_{8,6} = t^*_{8,4} = (\alpha - \tfrac{2}{3})T$$
$$t^*_{2,1} = t^*_{3,1} = t^*_{5,1} = (1 - \alpha)T;$$

Transitions between two successive stages are constrained by the following condition : transition from mode q_i in stage k to mode q_j in stage $k+1$ is possible only if mode q_i is common discrete mode between the two stages and q_j is the successor mode of q_i in the stage $k+1$. The corresponding guard conditions of these transitions, denoted $G^{ss}(T_{i,j})$, depend only on the reference load current value as below :

$$G^{ss}(T_{5,1}) = G^s(T_{2,1}) = G^s(T_{3,1}) = \{I_{ref} \in [0, I_{max}] : i_{ref} \leq \tfrac{I_{max}}{3}\}$$
$$G^{ss}(T_{2,4}) = G^s(T_{3,7}) = G^s(T_{5,6}) = \{I_{ref} \in [0, I_{max}] : i_{ref} > \tfrac{I_{max}}{3}\}$$
$$G^{ss}(T_{4,8}) = G^s(T_{7,8}) = G^s(T_{6,8}) = \{I_{ref} \in [0, I_{max}] : i_{ref} > \tfrac{2I_{max}}{3}\}$$
$$G^{ss}(T_{6,2}) = G^s(T_{4,3}) = G^s(T_{7,5}) = \{I_{ref} \in [0, I_{max}] : i_{ref} \leq \tfrac{2I_{max}}{3}\}$$

Transient state controller

The transitory state controller is based on the following three steps :

Step 1 : We start by charging (discharging) the closest capacitor to the input voltage (v_{c2}) until it reaches its reference value ($v_{ref2} = 2E/3$). Then, we commute to the second step.

These selected discrete modes for this purpose are mode q_4 and mode q_5. This choice allows the convergence of v_{c2} trajectory to v_{ref2} without modifying the other capacitor voltage (v_{c1} trajectory is constant and equal to its initial value). In this step the guards are :

$$\begin{aligned}
G^t(T_{4,2}) &= \{x \in X : (v_{c2} \leq V_{ref2}) \wedge (v_{c1} \geq V_{ref1})\} \\
G^t(T_{4,7}) &= \{x \in X : (v_{c2} \leq V_{ref2}) \wedge (v_{c1} < V_{ref1})\} \\
G^t(T_{4,2}) &= \{x \in X : (v_{c2} \geq V_{ref2}) \wedge (v_{c1} < V_{ref1})\} \\
G^t(T_{4,2}) &= \{x \in X : (v_{c2} \geq V_{ref2}) \wedge (v_{c1} \geq V_{ref1})\}
\end{aligned}$$

where $G^t(T_{i,j})$ corresponds to transitions guard conditions in transient state automaton.

Step 2 : In this second step, we charge (discharge) the voltage across the first capacitor C_1 until it reaches its reference value V_{ref1} keeping the floating voltage v_{c2} constant and equal to its initial value in step one, i.e, $v_{c2} = V_{ref2}$. Hence, the discrete mode used in this case are q_2 and q_7.

$$\begin{aligned}
G^t(T_{2,1}) &= \{x \in X : (v_{c1} \leq V_{ref1}) \wedge (i_L \geq I_{ref})\} \\
G^t(T_{2,8}) &= \{x \in X : (v_{c1} \leq V_{ref1}) \wedge (i_L < I_{ref})\} \\
G^t(T_{7,8}) &= \{x \in X : (v_{c1} \geq V_{ref1}) \wedge (i_L < I_{ref})\} \\
G^t(T_{7,1}) &= \{x \in X : (v_{c1} \geq V_{ref1}) \wedge (i_L \geq I_{ref})\}
\end{aligned}$$

Step 3 : Finally, once the floating capacitor voltages reach their references, this third step concerns the load current. Indeed, to reach the reference current while the floating voltages are keeping constants and equal to their reference, one can use modes q_1 and q_8. Once the trajectories of the states of the converter reach their reference in the transient state, the control strategy needs to commute to the steady state controller.

$$\begin{aligned}
G^{ts}(T_{1,2}) &= \{x \in X : (i_L \leq I_{ref}) \wedge (i_{ref} \leq \tfrac{I_{max}}{3})\} \\
G^{ts}(T_{1,4}) &= \{x \in X : (i_L \leq I_{ref}) \wedge (\tfrac{I_{max}}{3} < I_{ref} \leq \tfrac{2I_{max}}{3})\} \\
G^{ts}(T_{1,7}) &= \{x \in X : (i_L \leq I_{ref}) \wedge (\tfrac{2I_{max}}{3} < I_{ref} \leq I_{max})\} \\
G^{ts}(T_{8,2}) &= \{x \in X : (i_L \geq I_{ref}) \wedge (i_{ref} \leq \tfrac{I_{max}}{3})\} \\
G^{ts}(T_{8,4}) &= \{x \in X : (i_L \geq I_{ref}) \wedge (\tfrac{I_{max}}{3} < I_{ref} \leq \tfrac{2I_{max}}{3})\} \\
G^{ts}(T_{8,7}) &= \{x \in X : (i_L \geq I_{ref}) \wedge (\tfrac{2I_{max}}{3} < I_{ref} \leq I_{max})\}
\end{aligned}$$

where $G^{ts}(T_{i,j})$ corresponds to transition guard conditions from transient state to steady state automaton.

The final element in the construction of the hybrid automaton control is given by :

$$Init = (Init(q_4) \times q_4) \cup (Init(q_5) \times q_5) \tag{2.28}$$

where :

$$\begin{aligned}
Init(q_4) &= \{x \in X : v_{c2} \leq V_{ref2}\} \\
Init(q_5) &= \{x \in X : v_{c2} > V_{ref2}\}
\end{aligned}$$

2.6.3 Binary control of the 3-cell converter

It is proved using Lyapunov function in [47] that under the control law,

$$\begin{array}{l} u_3 = \frac{1-f(i_L-I_{ref})}{2} \\ u_j = \frac{1+g(A_j)}{2}, \quad j = 1, 2. \end{array} \tag{2.29}$$

where

$$f(i_L - I_{ref}) = \begin{cases} 1 & \text{if} \quad i_L - I_{ref} > 0 \\ -1 & \text{if} \quad i_L - I_{ref} < 0 \\ sign(A_2) & \text{if} \quad i_L - I_{ref} = 0 \end{cases} \tag{2.30}$$

and

$$g(A_j) = \begin{cases} 1 & \text{if} \quad A_j > 0 \\ -1 & \text{if} \quad A_j < 0 \\ -sign(A_{j-1}) & \text{if} \quad A_j = 0 \end{cases} \quad j = 1, 2, \tag{2.31}$$

with

$$A_j = -(i_L - I_{ref})v_{c_j} + (v_{c_j} - v_{c_{jref}})i_L, \quad j = 1, 2. \tag{2.32}$$

Applying this control law, the 3-cell converter supplies the load a current i_L that tracks the reference current I_{ref} and ensure an equilibrated distribution of the capacitor floating voltages. Indeed, the author used the following Lyapunov candidate function to prove the convergence of state variables of the converter to their references.

$$V(v_{c_j}, i_L) = \frac{1}{2}(i_L - I_{ref})^2 + \frac{1}{2}\sum_{j=1}^{2} C_j(v_{c_j} - V_{c_{jref}})^2. \tag{2.33}$$

2.6.4 Stabilization of 3-cell converter modes using LMI formalism

An other approach for the control of the 3-cell converter has been proposed in [58]. The authors developed a unified approach to a practical stabilization for piecewise affine systems and then applied respectively to buck-boost converter and 3-cell converter. The approach is based on quadratic stabilization using Lyapunov theory, and the problem is formulated by solving a linear matrix inequality system. The approach assign for each mode i a quadratic region defined as :

$$\Sigma_i = \{z \in R^{n+1}, z^T Q_i z \geq 0\}, \quad i = 1, ..., 8; \tag{2.34}$$

where $Q_i \in R^{(n+1)\times(n+1)}$, $z \in R^{n+1}$ is the augmented state vector. Furthermore, the author proposes a Lyapunov function of the form $V(z) = z^T P z$, with P is a symmetric positive definite matrix of the form

$$P_1 = \begin{bmatrix} 2P & \alpha P \\ \alpha^T P & 0 \end{bmatrix}, \tag{2.35}$$

and where $\alpha \in R^n$ and $P \in R^{n\times n}$. The stabilizing control strategy is based on the maximum

descent control switching strategy, i.e., the activated mode is defined by the sub system that has the highest decrease of Lyapunov function $V(z)$. Then, the subscript of the mode to be activated is given by :

$$\sigma(z) = argmin_{i\in\{1,\dots,8\}}\{\dot{V}_i(z)\} \tag{2.36}$$

and where $\dot{V}_i(z) = z^T(A_i^T P + A_i P)z$.

2.7 Conclusion

This chapter is devoted to a 3-cell converter. We have introduced the advantages that offered by a such structure compared with the classical converter. These advantages are fundamentally focussed on improvement of the output signal quality, in term of reducing the total harmonic distorsion and the ripples of the output signal in one hand, and reducing the constraint in tension across the switches in other hand, which allows the use of medium power semi-conductor instead of high power semi conductor in the classical converter. We have also introduced different model of the 3-cell converter ; mainly, the instantaneous and hybrid models, while fully justifiable since their use along of this thesis. Also, we have given an overview of different control strategy that are presented in different works. Finally, we presented some of control strategies that we thought interesting.

Chapter 3

Observability analysis and sliding mode observer for a 3-cell converter

Contents

3.1 Introduction

This chapter is dedicated to analyzing the observability of the floating capacitor voltages of the 3-cell converter and their reconstruction using an observer. The 3-cell converter is a switching system, it consists of eight modes, each mode is represented by an LTI model. The observability property for each mode is not guaranteed using classical Kalman observability criterion. But it does not imply the unobservability of the system. Indeed, the observability property of hybrid systems is analyzed along the hybrid time trajectory. For that, two approaches are introduced to analyze the observability of the 3-cell converter. In the second part of the current chapter, a sliding mode observer is designed to estimate the observable components of the converter, and the reconstruction of the floating voltages is performed exploiting the properties of the estimations provided by the observer.

3.2 An overview on observer of hybrid systems

Observer design for switched continuous systems has been investigated thoroughly through the two last decades, and different approaches have been proposed to estimate the continuous and discrete state of switching systems. Although, the problem of the reconstruction both continuous and discrete states seems very complex, the imposed assumptions become necessary to simplify the issues. The authors in [46], deal with the estimation of the active mode of switching systems assuming the prior-knowledge of the continuous states, they also assume that the control input is discerning to make the discrete mode observable. While the authors in [69] proposed switched observer to estimate both the continuous and the discrete states of switched linear systems, assuming that all operating modes are detectable. The convergence of the estimation errors is guaranteed if a feasibility solution to a linear matrix inequality is ensured. In [70], the continuous and discrete state estimation is addressed for a class of nonlinear switched systems, where the discrete part is governed by a petri net. The combination of a super twisting second-order sliding mode and discrete unknown input observers based petri net allows the reconstruction of both continuous and discrete states simultaneously. The authors in [71], tackle the problem of observer design for switched systems using a non-smooth optimization approach. They assume neither the continuous states nor the discrete states are known. Then, an observer is designed to estimate the continuous state without requiring estimation of the discrete state. The key idea of the proposed method consists of minimizing a non-smooth ℓ_2-norm based weighted cost function. A high order sliding mode observer for linear autonomous switched systems with unknown input is addressed in [72]and [73]. The authors give first, the necessary conditions for the reconstruction of the switching signal. Indeed, they assume that the system is strongly detectable for each operation mode. A high order sliding mode observer is then designed to estimate the continuous state. After that, a discrete observer is designed to estimate the switching signal, assuming that the weakly unobservable subspace included on the unobservable subspace for each mode. The authors follow with the unknown input identification using the designed continuous state observer. In [74], a robust observer has been proposed capable to estimate the continuous and discrete state in the presence of unknown inputs for linear switched systems with unstable internal dynamics.

In [75], the authors addressed the problem of reconstruction of the switching signal under the availability of free-noise continuous state measurement for a certain class of nonlinear uncertain switched systems. The approach is based on a second-order sliding mode observer. The efficiency of the proposed approach is guaranteed for a small uncertainty term and is applied experimentally to a three tanks system. The authors in [22] give a methodology of designing a hybrid observer to reconstruct the discrete and the continuous states from the knowledge of both continuous and discrete outputs. It consists of two parts ; a location observer that identifies the active plant, while the continuous observer produces an estimate of the evolution of the continuous states. The authors assume that all modes of the hybrid system are observable to guarantee the exponential convergence of the estimation error. A second-order sliding mode observer is proposed for nonlinear switched systems with jumps in [76] and applied to a mechanical system in [77]. In [78], the problem of a switched observer, for linear switched system with jump using multiple Lyapunov functions and dwell time switching, is formulated as a linear matrix inequality problem. It is shown also, that if the dwell time is large enough, the active mode can be reconstructed correctly, hence the estimation continuous error tends to zero. The authors in [79] deal with the designing of a dynamical observer for hybrid system. However, in the case where the hybrid system is not current-location observable, the authors show that the discrete state can be correctly identified, this may be achieved by processing the continuous inputs and output of the hybrid system to obtain more additional informations for the discrete state identification. For this purpose, they introduced an other system called transition detector. It processes the continuous input and output of the system to generate additional signal referred to as complementary discrete output, to be used as an extra input to the discrete observer, and then identify the discrete state. The proposed approach is applied experimentally to the automatic driveline of a car. The authors in [80], address the designing of switched observers for switched linear systems with unknown inputs. After they were proposed a change of coordinates that allows the decoupling of the unknown inputs, a novel Lyapunov function is introduced to analyze the stabilization of continuous estimation switched errors. Under some assumptions based on rank condition on system parameters and the strong detectability of the hybrid system, they show that the estimation continuous error is exponentially stable if a system of linear matrix inequality including the average minimum dwell time constraints is feasible. Asynchronous interval observer for switched LPV systems using multiple ISS [1]-Lyapunov function is addressed in [81]. The switching law is assumed to be uncontrollable but on line available. The authors show that the stability and the positivity conditions of the switched interval error are expressed in terms of Linear Matrix Inequality, which have been established using multiple ISS-Lyapunov function and average dwell time concept. They show that the proposed observer can asymptotically estimate the lower and the upper bounds of the state vector for any switching signal, with a dwell time sufficiently large. The approach is then applied for the robust estimation of the vehicle lateral dynamics using experimental data. In [39], a hybrid observer is designed for the most general case of hybrid systems, assuming the determinability of the system. It is shown that the estimation error decays exponentially even if the individual subsystems may not be observable. The proposed strategy is based upon the idea of accumulating information from individual subsystems. In

1. ISS : Input State Stability

this approach, the minimum dwell time is not required conversely to usual approach as in [78], [80], [82] or [81], but the proposed approach requires persistent switching. The authors in [82] addressed the problem of observer designing and input reconstruction for a class of switched descriptor systems. First, they give away to transform the switched system descriptor to a general switched system, then a reduced observer is designed to estimate the system state without influencing by the unknown input. To reconstruct the unknown inputs, they used a high order sliding mode to estimate the output derivatives. Noted that the minimum dwell time is required for the convergence of the designed observers. In [83], the authors have been proposed a multiple mode-observer for switched positive systems. The existence of multiple observers is related to the feasibility solution of the LMIs system. They show that the estimation error converges exponentially. In the sequel, they have designed multiple output feedback controller based on multiple mode-observers approach, such that the closed-loop system is exponentially stable.

Many works treat the problem of observer design for the multi-cells converter. In [34], a super twisting observer has been proposed to estimate the state variables of the converter. The authors show that there exists a time constant less than the dwell time in each mode, that guarantee the convergence of the observed states to their references. The authors in [2] propose two types of observers to estimate the floating voltages and the dc-motor speed. The first, based on a super twisting observer. It is shown that the fact there exists a constant time less than the dwell time, the observer states tend to their references. However, the second one based on adaptive observer, they use the Lyapunov theory to prove its convergence. In [44] and [45], the super twisting observer is designed for a multi-cell converter that guarantee the finite time convergence. In [5], an adaptive-gain second order sliding mode observer is designed for the 3-cell converter. A comparative study with a Luenberger observer has been presented under uncertainties. The carried out simulation results show the robustness of the sliding mode observer. The authors in [30], propose a super twisting and adaptive observers for the estimation of the floating voltages of the 3-cell converter. They show the convergence of the two observers to their references after a time less than the dwell time for each mode. The carried out simulation results show that the super twisting observer is more robust than the adaptive observer respect to the resistance variation. The authors in [33], used a model consisting of the load current and the output voltage of the 3-cell converter to design a finite time sliding mode observer to reconstruct the floating voltages of the 3-cell converter. The convergence of the estimated floating voltages can be achieved once the finite time stabilization of the estimation error is guaranteed. The proof of the finite time convergence based on Lyapunov theory using Lyapunov function introduced in [84] and [85]. They show that the proposed observer could be seen as an extension of the classical super twisting observer presented in [30]. Comparative simulations are presented in order to highlight the efficiency of the proposed observer. A sliding mode observer based output-feedback for a 3-cell converter is proposed in [31]. The authors design a switching control strategy in closed loop using an observer, i.e., the switching control strategy guarantees the observability of the floating voltages and the convergence of the states to their references. The convergence is proved using Lyapunov theory. In [86], experimental results of the floating voltage estimation of the

3-cell converter using a sliding mode observer are presented. The strategy of the observation is based on the switching between four different observers. The first and the second are used respectively to estimate the floating voltages v_{c_1} and v_{c_2} of the 3-cell converter. The third observer gives the estimation of both of v_{c_1} and v_{c_2}. Where the fourth one, the strategy of observation stops the estimation until the control sequence changes, and other switching observer will be activated. In [87], an interconnected observer is designed to estimate the floating voltages of the 5-cell converter. The authors prove using the Lyapunov theory the exponential convergence of the estimation error. Experimental results illustrate the effectiveness of the proposed observer. A hybrid observer has been proposed in [42]. The provided estimation algorithm is based on the correction vector which can be seen as an approximation of the state estimation error. It is computed using accumulated partial state information provided by a Luenberger observer for the estimation of the observable part. Noticing that the observer strategy do not requires the minimum dwell time condition between two commutations. The authors in [88] deal with the high gain observer for the multi-cell converter. They establish sufficient conditions under which the capacitor voltages can be reconstructed within appropriate specific switching sequence and not necessarily instantaneously. A high gain observer is then designed for the two considered interconnected sub-models. The design of the observer gains is based on the solution of the dynamic Lyapunov equation. Also, the proof of the convergence is based on an appropriate selection of a Lyapunov function, and for a specific switching sequence. Experimental results have been carried out and show the efficiency of the proposed high gain observer to estimate the floating voltages of the 3-cell converter.

3.3 Observability of hybrid systems

The current section is devoted to the observability of the floating voltages of the 3-cell converter. Two approaches are introduced, the $Z\{T_N\}$-observability and the geometric approach. In literature, the $Z\{T_N\}$-observability is widely used to analyze the observability of the 3-cell converter. While the geometric approach which is introduced in 2011 by Tanwani *et* al and has been applied in [40], [41] for a known hybrid time trajectory.

3.3.1 $Z\{T_N\}$-Observability approach

$Z\{T_N\}$-Observability is introduced in [29] and is widely applied to analyze the hybrid observability of the multicellular converter. It checks the observability of a hybrid system for a given hybrid time trajectory. Let us consider the following class of hybrid systems :

$$\begin{cases} \dot{x}(t) = f_{q_i}(t, x(t), u(t)) \\ y(t) = h_{q_i}(t, x(t), u(t)); \end{cases} \tag{3.1}$$

where $x(t) \in R^n$ is the state vector, $u(t) \in R^m$ is the input vector, $Q = \{q_1, ..., q_N\}$ is a finite set of modes such that $q_i \in Q, \quad i = 1, ..., N$ and $f_q : R \times R^n \times R^m \longrightarrow R^n$ is smooth function. All dwell time intervals $[t_{i,0}, \quad t_{i,1}]$ between two commutations satisfying the minimum dwell time $0 < \tau_{min} < t_{i,1} - t_{i,0}$. We assume that some subsystems of (3.1) are not observable in term of classical observability. For switched system, the concept of observability is strongly related

to the dwell time and the switching sequence, thus it is important to recall the following definition of hybrid time trajectory.

Definition 3.1 : A hybrid time trajectory is a finite or infinite sequence of intervals $T_N = \{I_i\}_{i=1}^{N}$, such that

1. $I_i = [t_{i,0}, \quad t_{i,1}]$ for all $1 \leq i < N$
2. For all $i < N$, $t_{i,1} = t_{i+1,0}$
3. $t_{1,0} = t_{initial}$ and $t_{N,1} = t_{end}$

Moreover, we define $< T_N >$ as the ordered list of q_i associated to hybrid time trajectory T_N. In other words it means the ordered mode $\{...q_j...\}$ with q_j the current mode during the interval I_j. Now, we are ready to define the concept of $Z\{T_N\}$-Observability.

Definition 3.2 : Consider the system (3.1) and a variable $z = Z(t, x, u)$. Let $(t, x^1(t), u^1(t))$ be a trajectory in U with a hybrid time trajectory T_N and the ordered list of modes $< T_N >$. Suppose for any trajectory, $(t, x^2(t), u^2(t))$ in U with the same T_N and $< T_N >$, the equality

$$h(t, x^1(t), u^1(t)) = h(t, x^2(t), u^2(t)) \tag{3.2}$$

implies

$$Z(t, x^1(t), u^1(t)) = Z(t, x^2(t), u^2(t)). \tag{3.3}$$

Then we say that $z = Z(t, \xi, u)$ is $Z\{T_N\}$-observable along the trajectory $(t, x^1(t), u^1(t))$.

A straightforward application of the above definition implies the following theorem.

Theorem 3.1 : Consider the system (3.1) and a fixed hybrid time trajectory T_N and $< T_N >$. Let U be an open set in time state-control space. Suppose that $z = Z(t, x(t), u(t))$ is always continuous under any admissible control input. Suppose there exists a sequence of projections $P_i, \quad i = 1, ..., N$, such that

1. given any $1 \leq i \leq N, \quad P_i Z(t, x, u)$ is Z-observable in U on the subinterval $t \in [t_{i,0}, t_{i,1}[$;
2. $Rank[P_1^T ... P_N^T] = dim(Z) = n_z$;
3. $\frac{d\bar{P}_i Z(t,x(t),u(t))}{dt} = 0$ for $t \in [t_{i,0}, \quad t_{i,1}[$ and $(t, x(t), u(t)) \in U$. With $\bar{P}_i$ is the complement of P_i such that $[\bar{P}_i^T, P_i^T]$ has a full rank in $R^{n_z \times n_z}$.

Then $z = Z(t, x(t), u(t))$ is $Z\{T_N\}$-observable in U with respect to the hybrid time trajectory T_N and $< T_N >$.

The first condition means that each element of the state vector is Z-observable within at least one time interval. The second condition means that for an hybrid time trajectory T_N including time intervals, all the components of the Z are observable within it. The last condition means that the unobservable components of the state vector in a time interval I_i, must remain constant during this interval of time when another one is observable.

Application to a three cell converter :

Note that the three cell converter model is a particular case of (3.1), then the application of the previous theorem is possible. Using the theory of linear observability, it can be easily checked that the rank of each observability matrix of each operating mode of the 3-cell converter is less or equal to two, which means that at most two state variables are observable. Table (3.1) shows the observable states in each operating mode. Where it can be seen that the capacitor voltage v_{c_1} is observable in modes q_2 and q_7. Whereas, the floating voltage v_{c_2} is observable in the modes q_4 and q_5. Also, the capacitor voltages v_{c_1} and v_{c_2} are not observable under discrete control $(u_1, u_2, u_3) = (0, 0, 0)$ or $(u_1, u_2, u_3) = (1, 1, 1)$. It is worth noting that if one of the floating voltages is observable in a mode, other floating voltage remains constant. Noting also that the two floating voltages are not simultaneously observable.

q_i	$[u_1 \quad u_2 \quad u_3]$	Evolution of V_{c_1}	Evolution of V_{c_2}	Observable states
q_1	$[0 \quad 0 \quad 0]$	$\rightarrow$	$\rightarrow$	i_l
q_2	$[1 \quad 0 \quad 0]$	$\searrow$	$\rightarrow$	i_l, v_{c_1}
q_3	$[0 \quad 1 \quad 0]$	$\nearrow$	$\searrow$	$i_l, (v_{c_1} - v_{c_2})$
q_4	$[1 \quad 1 \quad 0]$	$\rightarrow$	$\searrow$	i_l, v_{c_2}
q_5	$[0 \quad 0 \quad 1]$	$\rightarrow$	$\nearrow$	i_l, v_{c_2}
q_6	$[1 \quad 0 \quad 1]$	$\searrow$	$\nearrow$	$i_l, (v_{c_2} - v_{c_1})$
q_7	$[1 \quad 1 \quad 1]$	$\nearrow$	$\rightarrow$	i_l, v_{c_1}
q_8	$[0 \quad 1 \quad 1]$	$\rightarrow$	$\rightarrow$	i_l

TABLE 3.1: Capacitor voltages evolution and observable states for each mode in function of $u_i, \quad i = 1, 2, 3$

Let then consider $z = Z(t, x) = [v_{c_1}, v_{c_2}]^T$. In time interval I_1 we apply the the discrete control $(u_1, u_2, u_3) = (1, 0, 0)$ (mode q_2) and the control $(u_1, u_2, u_3) = (1, 1, 0)$ (mode q_4) in the time interval I_2. We can verify easily that $z = Z(t, x) = [v_{c_1}, v_{c_2}]^T$ is $Z\{T_N\}$-observable along such a trajectory. Let us define $P_1 = [1, 0]$ in time interval I_1 and $P_2 = [0, 1]$ in time interval I_2. We have then according to theorem (3.1).

1. $P_1 Z = v_{c_1}$ and $P_2 Z = v_{c_2}$. Which means that v_{c_1} is Z-observable in I_1 and v_{c_2} is Z-observable in I_2 ;
2. $Rank[P_1^T P_2^T] = dim(Z) = 2$;
3. and

$$\begin{cases} \frac{d\bar{P}_1 Z}{dt} = \frac{dv_{c_2}}{dt} = 0, & \text{for} \quad t \in I_1 \\ \frac{d\bar{P}_2 Z}{dt} = \frac{dv_{c_1}}{dt} = 0, & \text{for} \quad t \in I_2 \end{cases}$$

It is clear that as depicted by table (3.1), in the time interval I_1 where the floating voltage v_{c_1} is observable, v_{c_2} remains constant. Inversely, in the time interval I_2, where v_{c_2} is observable v_{c_1} remains constant. Consequently, all conditions of theorem (3.1) are satisfied. Therefore, $Z(t, x) = [v_{c_1}, v_{c_2}]^T$ is $Z\{T_N\}$-observable.

3.3.2 Geometrical approach

This section is devoted to the observability analysis of hybrid systems using the geometrical approach. First, we introduced the approach and applied it to the case of the analyzing the observability of the floating voltages of the 3-cell converter. Let consider a hybrid system given by the following state equations :

$$\Sigma : \begin{cases} \dot{x}(t) = A_{q_i}x(t) + B_{q_i}u(t) \\ y(t) = C_{q_i}x(t), \quad i = 1, ..., m. \end{cases} \tag{3.4}$$

We suppose :

- The switching commutation sequence is well known.
- No jump on states.

A very important characterization for the observability of switching systems, based on the geometrical approach, was introduced by Tanwani *et al* [38]. It consists in finding the unobservable subspace along the hybrid time trajectory. Let N_1^m denotes the unobservability subspace over the time interval $[t_0, t_m)$ that includes switching at $t_0, t_1, ..., t_m$. And let N_i^i denotes the unobservable subspace on the time interval $[t_{i-1}, t_i)$, it is given by :

$$\Gamma_{q_i}^{q_i} = ker\{O_{q_i}\}, i = 1, ..., m. \tag{3.5}$$

where O_{q_i} represents the observability matrix of mode q_i. It is given by

$$O_{q_i} = Col[C_{q_i}, C_{q_i}A_{q_i}, ..., C_{q_i}A_{q_i}^{n-1}], \tag{3.6}$$

over the time interval $[t_{i-1}, t_m)$, if more information can be obtained about the states, then the unobservable subspace along the hybrid time trajectory N_i^m gets smaller as the difference $m - i$ increases. The unobservable subspace can be computed using a recursive algorithm given in [38] as follows :

$$\begin{cases} \Gamma_m^m = ker\{O_m\} \\ \Gamma_{q_i}^m = ker\{O_{q_i}\} \cap e^{-A_{q_i}\tau_{q_i}}\Gamma_{q_i+1}^m, \end{cases} \tag{3.7}$$

where $\tau_{q_i} = t_{q_i} - t_{q_{i-1}}$ is the dwell time.

Theorem 3.2 [38] : The linear hybrid system (3.4) is said to be $[t_0, t_{m-1})-$observable if, and only if the unobservable subspace along the hybrid time trajectory is restricted to zero, i.e.,

$$N_1^m = \{0\}, \tag{3.8}$$

where N_1^m represents the unobservable subspace for $[t_0, t_m)$.

Application to a 3-cell converter :

The parameters of the 3-cell converter model are $C_1 = C_2 = 40\mu F$, $R = 10\Omega$, $L = 0.0005mH$ and $E = 30volts$. The dwell time is taken $\tau_{q_i} = 0.2069$ second for all $i = 1, ..., 8$. Let then

$\tau = \tau_{q_i}$ for $(i = 1, ..., 8)$. Each mode is an LTI system, then the unobservable subspace N_i^i for each mode is :

$$\begin{array}{l} N_1^1 = ker\{O_{q_1}\} = span\{(-1 \quad 0 \quad 0)^T, (0 \quad -1 \quad 0)^T\} \\ N_2^2 = ker\{O_{q_2}\} = span\{(0 \quad 1 \quad 0)^T\} \\ N_3^3 = ker\{O_{q_3}\} = span\{(\frac{\sqrt{2}}{2} \quad \frac{\sqrt{2}}{2} \quad 0)^T\} \\ N_4^4 = ker\{O_{q_4}\} = span\{(1 \quad 0 \quad 0)^T\} \\ N_5^5 = ker\{O_{q_5}\} = span\{(1 \quad 0 \quad 0)^T\} \\ N_6^6 = ker\{O_{q_6}\} = span\{(-\frac{\sqrt{2}}{2} \quad -\frac{\sqrt{2}}{2} \quad 0)^T\} \\ N_7^7 = ker\{O_{q_7}\} = span\{(0 \quad -1 \quad 0)^T\} \\ N_8^8 = ker\{O_{q_8}\} = span\{(-1 \quad 0 \quad 0)^T, (0 \quad -1 \quad 0)^T\} \end{array} \tag{3.9}$$

We know that the observability analysis of the 3-cell converter depends on the control sequence. For this end, we apply the approach for two different switching sequences.

Example 1 : Let the ordered list be $< T_N >= \{q_7, q_5, q_6, q_2, q_4, q_3\}$, which consists of six modes $(N = 6)$. Its corresponding hybrid time trajectory is $T = \{I_i\}_{i=1}^{N}, \quad N = 6$. Before analyzing the observability by the proposed approach, and according to table (3.1), one can note that after one commutation from mode q_7 to mode q_5, i.e., in the time interval I_1 and I_2, we observe all state variables. Since, from mode q_7, we observe v_{c_1}, and from mode q_5 we can observe v_{c_2}. Knowing that v_{c_1} remains constant during the time interval I_1 corresponding to mode q_7. Then after one commutation we observe v_{c1} and v_{c_2}. From this result, we can deduce that the unobservability subspace $N_{q_7}^{q_5}$ is restricted to zero after one commutation. Now, using the proposed approach to obtain the same result. We have

$$N_{q_7}^{q_5} = ker\{O_{q_7}\} \cap e^{-A_7\tau_7} N_{q_5}^{q_5}$$

we obtain

$$N_{q_7}^{q_5} = span\{(0 \quad -1 \quad 0)^T\} \cap e^{-A_7\tau_7} N_{q_5}^{q_5} = \{0\}$$

Then the system becomes observable after one commutation.

Example 2 : Now, the considered ordered list is $T = \{q_2, q_8, q_7, q_5, q_4, q_3\}, \quad \text{with} N = 6.$ According to table (3.1) and by analyzing each mode alone, we can observe all states after 3 commutations. From mode q_2, we observe v_{c_1} only. After the first commutation, the system commute to mode q_8, where v_{c_1} and v_{c_2} are not observable. From mode q_7, we observe for a second time v_{c_1}. The third commutation, the system is brought to mode q_5, where v_{c_2} is observable. Then we can observe v_{c_1} and v_{c_2} after 3 commutations. Using now the geometric approach, we have after the first commutation, the unobservable subspace is

$$N_{q_2}^{q_8} = ker\{O_{q_2}\} \cap e^{-A_2\tau_2} N_{q_8}^{q_8},$$

then we obtain

$$N_{q_2}^{q_8} = span\{(0 \quad 1 \quad 0)^T\} \cap e^{-A_2\tau_2} N_{q_8}^{q_8}$$
$$N_{q_2}^{q_8} = span\{(0 \quad 1 \quad 0)^T\} \neq \{0\}.$$

$N_{q_2}^{q_8}$ is not equal to $\{0\}$. Then the system is not observable after the first commutation. The commutation from q_8 to q_7 gives

$$N_{q_2}^{q_7} = ker\{O_{q_2}\} \cap e^{-A_2\tau_2} N_{q_8}^{q_7},$$

where

$$N_{q_8}^{q_7} = ker\{O_{q_8}\} \cap e^{-A_8\tau_8} N_{q_7}^{q_7}.$$

We have then

$$N_{q_2}^{q_7} = ker\{O_{q_2}\} \cap e^{-A_2\tau_2}(ker\{O_{q_8}\} \cap e^{-A_8\tau_8} N_{q_7}^{q_7}).$$

we obtain

$$N_{q_2}^{q_7} = span\{(0 \quad 1 \quad 0)^T\} \cap span\{(0 \quad -1 \quad 0)^T\}$$
$$N_{q_2}^{q_7} = span\{(0 \quad 1 \quad 0)^T\} \neq \{0\}$$

$N_{q_2}^{q_7} \neq \{0\}$, then the system is not observable. After the third commutation from mode q_7 to q_5 we have :

$$N_{q_2}^{q_5} = ker\{O_{q_2}\} \cap e^{-A_2\tau_2} N_{q_8}^{q_5},$$

where

$$N_{q_8}^{q_5} = ker\{O_{q_8}\} \cap e^{-A_8\tau_8} N_{q_7}^{q_5},$$

and where

$$N_{q_7}^{q_5} = ker\{O_{q_7}\} \cap e^{-A_7\tau_7} N_{q_5}^{q_5},$$

then

$$N_{q_2}^{q_5} = ker\{O_{q_2}\} \cap e^{-A_2\tau_2}\{ker\{O_{q_8}\} \cap e^{-A_8\tau_8}(ker\{O_{q_7}\} \cap e^{-A_7\tau_7} N_{q_5}^{q_5})\}).$$

We obtain then

$$N_{q_7}^{q_5} = span\{(0 \quad -1 \quad 0)^T\} \cap span\{(1 \quad 0 \quad 0)^T\} = \{0\}$$
$$N_{q_8}^{q_5} = span\{(-1 \quad 0 \quad 0)^T, (0 \quad -1 \quad 0)^T\} \cap span\{0\} = \{0\}$$
$$N_{q_2}^{q_5} = span\{(0 \quad 1 \quad 0)^T\} \cap span\{0\} = \{0\}.$$

The unobservable subspace $N_{q_2}^{q_5}$ becomes zero after three commutations. Consequently, the system is observable along the considered hybrid time trajectory.

3.4 Sliding mode observer design

Consider the non linear switched system described by the following equations

$$\begin{cases} \dot{\xi}(t) &= A\xi(t) + f_\sigma(y(t), \delta(t), t) + B_\sigma\delta(t) \\ y(t) &= C\xi(t) \end{cases} \tag{3.10}$$

where $\xi(t) \in R^n$ is the state vector, $\delta(t) \in R^m$ is the control input vector, $y(t) \in R^p$ is the output vector, $\sigma(t)$ is the switching signal. $f_\sigma(y(t), u(t), t)$ is a nonlinear function of the outputs and inputs assumed known over the time t. A, B and C are matrices of appropriate dimensions. Consider the sliding mode observer for the system (3.10) described by the following equations :

$$\begin{cases} \dot{\hat{\xi}}(t) &= A\hat{\xi}(t) + f_\sigma(y(t), \delta(t), t) + B_\sigma\delta(t) + L(y(t) - C\hat{\xi}(t)) + S(\hat{\xi}(t), y(t)) \\ \hat{y}(t) &= C\hat{\xi}(t). \end{cases} \tag{3.11}$$

Where $\hat{\xi}(t) \in R^n$ is the estimated of the state vector $\xi(t)$, $\hat{y}(t) \in R^p$ is the estimated of the output vector $y(t)$, L is the observer gain matrix of appropriate dimension, and $S(\hat{\xi}(t), y(t))$ is a sliding surface given by

$$S(\hat{\xi}, y) = \begin{cases} \frac{P^{-1}C^TC}{\|Ce(t)\|}e(t) & if \quad \|Ce(t)\| > \varepsilon \\ \\ \frac{P^{-1}C^TC}{\varepsilon}e(t) & if \quad \|Ce(t)\| \leq \varepsilon. \end{cases} \tag{3.12}$$

Where $e(t)$ is the estimation error, $\varepsilon > 0$ is a real number, P is a symmetric positive definite matrix and $\|Ce(t)\|$ is the euclidian norm of $Ce(t)$. More about this sliding surface can be found in [89] and [90]. The aim of the design is to determine the observer gain matrix L and the matrix P that defines the sliding surface and guarantee the finite time convergence of the estimation error.

3.4.1 Application to a 3-cell converter

The main objective of this section is to reconstruct the floating voltages v_{c_1} and v_{c_2} of the 3-cell converter assuming that the only available measurement is the load current i_L. The idea is based on the estimation of a certain observable variable of the converter over all operating mode. Then using its interesting properties, we reconstruct the floating voltages v_{c_1} and v_{c_2}. Consider again the model of the 3-cell converter described by equations (2.12). The model can be put in the form (3.10) by considering the following change of coordinates. The time derivative of the load current is.

$$\frac{di_l}{dt} = -\frac{R}{L}i_l - \frac{1}{L}(\delta_1 v_{c1} + \delta_2 v_{c2}) + \frac{E}{L}\delta_3. \tag{3.13}$$

Where $\delta_1 = u_2 - u_1$, $\delta_2 = u_3 - u_2$ and $\delta_3 = u_3$. Knowing that $\delta_i \in \{0, -1, 1\}$, while $u_i \in \{0, 1\}$ for $i = 1, 2, 3$. Let

$$\xi_1 = \delta_1 v_{c_1} + \delta_2 v_{c_2}, \tag{3.14}$$

and

$$\xi_2 = i_l. \tag{3.15}$$

Indeed, ξ_1 and ξ_2 represent the observable states of the converter in each operating mode. Thus, the dynamic of ξ_1 and ξ_2 describe the evolution of the observable subspace of the 3-cell converter. The change of coordinates (3.14) and (3.15) can be justified as follow. The observable sub spaces of each operating mode are given by the orthogonal distribution of each unobservable subspaces of the converter given by equations (3.9). Let then :

$$\begin{array}{l}
(N_1^1)^\perp = span\{(0 \quad 0 \quad 1)^T\} \\
(N_2^2)^\perp = span\{(0 \quad 0 \quad 1)^T, (-1 \quad 0 \quad 0)^T\} \\
(N_3^3)^\perp = span\{(0 \quad 0 \quad 1)^T, (1 \quad -1 \quad 0)^T\} \\
(N_4^4)^\perp = span\{(0 \quad 0 \quad 1)^T, (0 \quad 1 \quad 0)^T\} \\
(N_5^5)^\perp = span\{(0 \quad 0 \quad 1)^T, (0 \quad -1 \quad 0)^T\} \\
(N_6^6)^\perp = span\{(0 \quad 1 \quad 0)^T, (-1 \quad 1 \quad 0)^T\} \\
(N_7^7)^\perp = span\{(0 \quad 0 \quad 1)^T, (1 \quad 0 \quad 0)^T\} \\
(N_8^8)^\perp = span\{(0 \quad 0 \quad 1)^T\}
\end{array} \tag{3.16}$$

It is clear that at most two variables are observable in each mode. The load current is available to measurement, thus, it is observable all times. This is justified by the belonging of the distribution $span\{(0 \quad 0 \quad 1)^T\} = span\{dx_3\}$ in all observable subspaces, which justify equation (3.15). We can also notice that we can write all the second distributions of the observable subspaces as a function of δ_1 and δ_2 as given by equation (3.14). Let then consider the time derivatives of ξ_1 and ξ_2 that allow to obtain the following observable sub model.

$$\begin{cases}
\dot{\xi}_1(t) = (\frac{1}{C_1}\delta_1^2 + \frac{1}{C_2}\delta_2^2)\xi_2(t) \\
\dot{\xi}_2(t) = -\frac{R}{L}\xi_2(t) - \frac{1}{L}\xi_1(t) + \frac{1}{L}\delta_3 E \\
y(t) = \xi_2(t)
\end{cases} \tag{3.17}$$

The model (3.17) can be put in form of (3.10) such that $\xi = [\xi_1 \quad \xi_2]^T$ is the observable state vector of the 3-cell converter. $y = \xi_2$ is the output of the sub model and it represents the load current i_l. The different matrices are then

$$A = \begin{bmatrix} 0 & 0 \\ -\frac{1}{L} & -\frac{R}{L} \end{bmatrix}, B_\sigma = \begin{bmatrix} 0 \\ \frac{1}{L}\delta_3 \end{bmatrix}, C = \begin{bmatrix} 0 & 1 \end{bmatrix},$$

$$f_\sigma(y(t), \delta(t), t) = \begin{bmatrix} (\frac{1}{C_1}\delta_1^2 + \frac{1}{C_2}\delta_2^2)\xi_2(t) \\ 0 \end{bmatrix}.$$

Consider now the sliding mode observer as described by equations (3.11) designed for the observable sub model of the 3-cell converter (3.17). Let $e(t) = [e_1(t) \quad e_2(t)]^T$ the estimation error vector, such that $e_1(t) = \xi_1(t) - \hat{\xi}_1(t)$ and $e_2(t) = \xi_2(t) - \hat{\xi}_2(t)$. Let $\dot{e}(t)$ the dynamic of the estimation error, it is equal to :

$$\dot{e}(t) = (A - LC)e(t) - S(\hat{\xi}, y) \tag{3.18}$$

Proposition 3.1 :

Consider the observable sub model of the 3-cell converter (3.17) and the sliding mode observer (3.11) with the sliding surface (3.12). If there exists observer gain matrix L and a positive definite matrix Q that ensure the existence of a symmetric definite matrix P solution of the following Linear Matrix Inequality

$$(A - LC)^T P + P(A - LC) \leq -Q, \tag{3.19}$$

then the estimation error converge exponentially and the estimated floating voltages $\hat{v}_{c_1}$ and $\hat{v}_{c_2}$ can be reconstructed respectively by :

$$\hat{v}_{c_1} = |\hat{\xi}_1| \quad \text{when} \quad \delta_2 = 0 \quad \text{and} \quad \delta_1 = \{1, -1\} \tag{3.20}$$

$$\hat{v}_{c_2} = |\hat{\xi}_1| \quad \text{when} \quad \delta_1 = 0 \quad \text{and} \quad \delta_2 = \{1, -1\} \tag{3.21}$$

Remark :

It is clear that the pair (A, C) is observable along hybrid time trajectory, this allowing to the existence of a solution to LMI equation (3.19).

The stated proposition consists of two points. First, it gives the necessary and sufficient condition to exponential convergence of the estimation error. The second part of the proposition announces how we can reconstruct the floating voltages $\hat{v}_{c_1}$ and $\hat{v}_{c_2}$ from the observable state $\hat{\xi}$. In the following proof, we treat the exponential convergence of the estimation error. Whereas, the reconstruction of the voltages will be treated in the next section.

3.4.2 Proof of the exponential convergence

Consider the Lyapunov candidate function $V(e(t)) = e(t)^T P e(t)$. To guarantee the exponential convergence of the estimation error, the sufficient condition to ensure is $\dot{V} \leq -\mu V$, where $\mu > 0$. The time derivative of V is

$$\dot{V} = e^T[(A - LC)^T P + P(A - LC)]e - 2e^T P S(\hat{\xi}, y) \tag{3.22}$$

Two cases to be considered, $\|Ce\| > \varepsilon$ and $\|Ce\| \leq \varepsilon$ according to the sliding surface (3.12).

1^{st} **case** $\|Ce\| > \varepsilon$ **:** Since $\varepsilon > 0$, the selected sliding surface from (3.12) is

$$S(\hat{x}, y) = \frac{P^{-1}C^T(y - C\hat{x})}{\|Ce(t)\|} = \frac{P^{-1}C^T(y - C\hat{x})}{\|Ce\|}. \tag{3.23}$$

by replacing the sliding surface (3.23) into equation (3.22), $\dot{V}$ becomes

$$\dot{V} = e^T[(A - LC)^T P + P(A - LC)]e - 2\|Ce\| \tag{3.24}$$

The last equation is obtained by taking into account $e^T C^T Ce = (Ce)^T(Ce) = \|Ce\|^2$. And since $\|Ce\| > \varepsilon > 0$ and if the equation (3.19) holds for $P > 0$, we obtain

$$\dot{V} < -e^T Qe - 2\varepsilon < -e^T Qe < -\lambda_{min}\{Q\}e^T e \tag{3.25}$$

where $\lambda_{min}\{Q\}$ is the minimum eigenvalue of the symmetric positive definite matrix Q. Also we have

$$V = e^T Pe \Rightarrow V \leq \lambda_{max}\{P\}e^T e \Rightarrow e^T e \geq \frac{1}{\lambda_{max}\{P\}}V, \tag{3.26}$$

with $\lambda_{max}\{P\}$ is the maximum eigenvalue of the symmetric positive definite matrix P. And since $\lambda_i\{P\} > 0$ and $\lambda_i\{Q\} > 0$ $(P > 0, Q > 0)$, then we have

$$\dot{V} \leq -\mu_1 V, \tag{3.27}$$

with $\mu_1 = \frac{\lambda_{min}\{Q\}}{\lambda_{max}\{P\}} > 0$ Hence, the exponential convergence is guaranteed.

2^{nd} **case** $\|Ce\| \leq \varepsilon$ **:** In this case, the sliding surface is

$$S(\hat{x}, y) = \frac{P^{-1}C^T(y - C\hat{x})}{\varepsilon}. \tag{3.28}$$

We obtain

$$\dot{V} = e^T[(A - LC)^T P + P(A - LC)]e - \frac{2}{\varepsilon}e^T C^T Ce. \tag{3.29}$$

If (3.19) holds for $P > 0$, then we can write

$$\dot{V} \leq -e^T Qe - \frac{2}{\varepsilon}e^T C^T Ce = e^T[Q + \frac{2}{\varepsilon}C^T C]e, \tag{3.30}$$

Then

$$\dot{V} \leq -\lambda_{min}\{Q + \frac{2}{\varepsilon}C^T C\}e^T e, \tag{3.31}$$

where $\lambda_{min}\{Q + \frac{2}{\varepsilon}C^T C\}$ is the minimum eigenvalue of the matrix $Q + \frac{2}{\varepsilon}C^T C$. By using equation (3.26), we then obtain

$$\dot{V} \leq \frac{-\lambda_{min}\{Q + \frac{2}{\varepsilon}C^T C\}}{\lambda_{max}\{P\}}V. \tag{3.32}$$

Since $\lambda_{min}\{Q + \frac{2}{\varepsilon}C^T C\} > 0$ and $\lambda_{max}\{P\} > 0$, then

$$\dot{V} \leq -\mu_2 V, \tag{3.33}$$

with $\mu_2 = \frac{\lambda_{min}\{Q + \frac{2}{\varepsilon}C^T C\}}{\lambda_{max}\{P\}} > 0$

Consequently, the exponential convergence is demonstrated for the two cases.

3.4.3 Reconstruction of vc1 and vc2

Now, the main question is how to reconstruct v_{c_1} and v_{c_2} from $\hat{\xi}_1$ and $\hat{\xi}_2$? Table (3.2) summarizes the evolution of v_{c_1} and v_{c_2} and the observable states of the converter in each mode.

q_i	δ_1	δ_2	δ_3	Evolution of V_{c_1}	Evolution of V_{c_2}	Observable states
q_1	0	0	0	$\rightarrow$	$\rightarrow$	i_l
q_2	-1	0	0	$\rightarrow$	$\nearrow$	i_l, v_{c_1}
q_3	1	-1	0	$\nearrow$	$\searrow$	$i_l, (v_{c_1} - v_{c_2})$
q_4	0	-1	0	$\nearrow$	$\rightarrow$	i_l, v_{c_2}
q_5	0	1	1	$\searrow$	$\rightarrow$	i_l, v_{c_2}
q_6	-1	1	1	$\searrow$	$\nearrow$	$i_l, (v_{c_2} - v_{c_1})$
q_7	1	0	1	$\rightarrow$	$\searrow$	i_l, v_{c_1}
q_8	0	0	1	$\rightarrow$	$\rightarrow$	i_l

TABLE 3.2: Capacitor voltages evolution and observable states for each mode in function of δ_i, $i = 1, 2, 3$.

We can notice from table (3.2), that v_{c_1} is observable when $\delta_2 = 0$ and $\delta_1 \neq 0$. This situation is indicated by modes q_2 and q_7. In a same way, v_{c_2} is observable when $\delta_1 = 0$ and $\delta_2 \neq 0$, and it is indicated by modes q_4 and q_5. Now, according to equation (3.14) and if ξ_1 is well estimated by the sliding mode observer (3.11), then we can write :

$$\hat{\xi}_1 = \delta_1 \hat{v}_{c_1} + \delta_2 \hat{v}_{c_2} \tag{3.34}$$

Knowing that $\hat{\xi}_1 > 0$ for $(\delta_1, \delta_2) = (1, 0)$ or $(\delta_1, \delta_2) = (0, 1)$ and $\hat{\xi}_1 < 0$ for $(\delta_1, \delta_2) = (-1, 0)$ or $(\delta_1, \delta_2) = (0, -1)$. Then we can reconstruct the floating voltages $\hat{v}_{c_1}$ and $\hat{v}_{c_2}$ respectively by equations (3.20) and (3.21), knowing also that the state ξ is observable at any time.

3.4.4 Simulation results

In this section, simulation results have been carried out in order to highlight the performances of the proposed sliding mode observer for a 3-cell converter model. The parameters are kept as given in section (3.3.2). The control sequence is taken as considered in example 1 of section (3.3.2). Thus, it satisfies the observability condition (3.8). Also, the control signals are phase shifted by $2\pi/3$. After linearization of equation (3.19) by considering $Y = PL$, and let $Q = I_2$, the obtaining solution using Matlab LMI control toolbox is :

$$P = \begin{bmatrix} 811.3153 & 40.3142 \\ 40.3142 & 811.3153 \end{bmatrix} \Rightarrow P^{-1} = \begin{bmatrix} 0.0012 & -0.0001 \\ -0.0001 & 0.0012 \end{bmatrix}$$

$$Y = 10^4 \begin{bmatrix} -1.2145 \\ -8.0726 \end{bmatrix} \Rightarrow L = P^{-1}Y \begin{bmatrix} -10.04 \\ -99.0013 \end{bmatrix}$$

The obtained simulation results are shown in figures (3.1)-(3.6). Note that $\varepsilon = 0.01$ has an effect only in the simulation results and not in the resolution of equation (3.19). Figure (3.1) depicts the real $\xi_1 = \delta_1 v_{c_1} + \delta_2 v_{c_2}$ and its estimation $\hat{\xi}_1$ given by the observer (3.11), where it is shown the convergence of $\hat{\xi}_1$ to ξ_1.

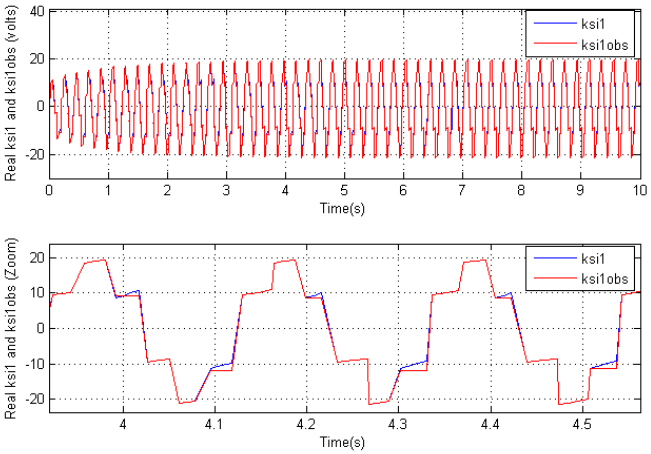

FIGURE 3.1: Evolution of ξ_1 and its estimate $\hat{\xi}_1$

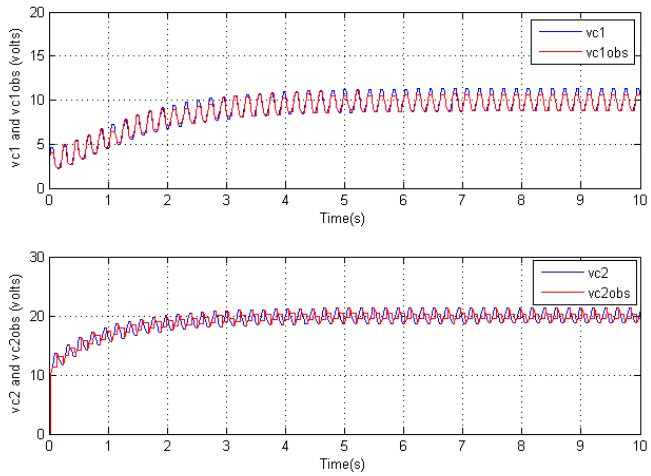

FIGURE 3.2: Evolution of a-v_{c_1} and its estimation $\hat{v}_{c_1}$, b- v_{c_2} and its estimation $\hat{v}_{c_2}$

The reconstructed floating voltages $\hat{v}_{c_1}$ and $\hat{v}_{c_2}$ are depicted respectively by figures (3.2.a) and (3.2.b). Where the two floating voltages converge to their references v_{c_1} and v_{c_2} respectively. Figure (3.3) represents a zoom of the estimated voltages in steady state, where we can show the origin of estimation errors $e_1 = v_{c_1} - \hat{v}_{c_1}$ and $e_2 = v_{c_2} - \hat{v}_{c_2}$ depicted by figure (3.4.a) and (3.4.b) respectively, where we can observe their convergence around zero.

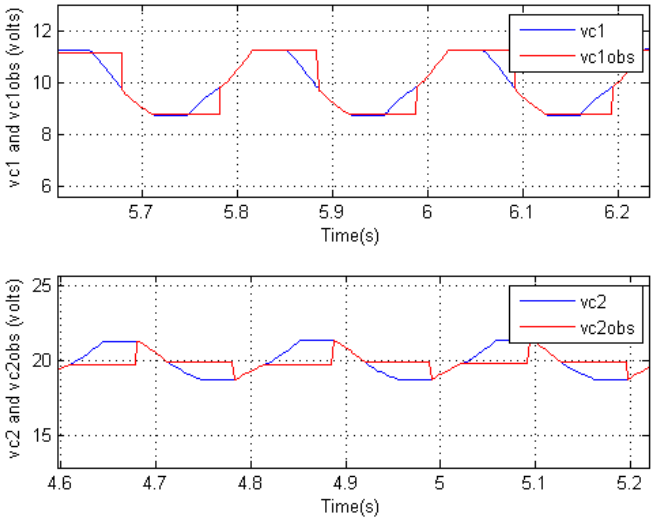

FIGURE 3.3: Zoom of evolution of a-v_{c_1} and its estimation $\hat{v}_{c_1}$, b-v_{c_2} and its estimation $\hat{v}_{c_2}$ in steady state

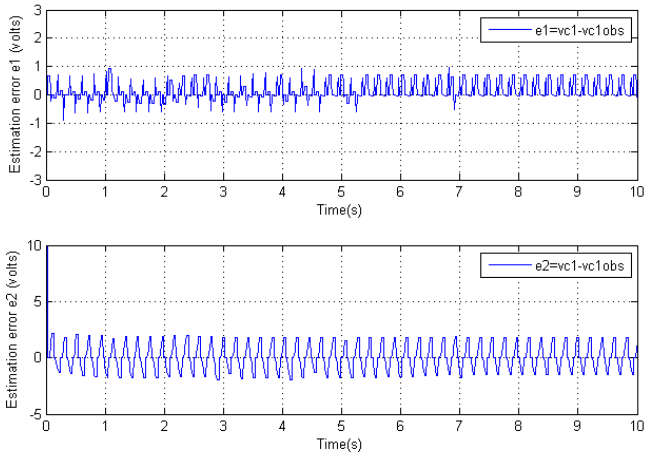

FIGURE 3.4: Estimation errors $e_1 = v_{c_1} - \hat{v}_{c_1}$ and $e_2 = v_{c_2} - \hat{v}_{c_2}$

Indeed, figures (3.5) and (3.6) show respectively the reconstruction strategy of the floating voltages $\hat{v}_{c_1}$ and $\hat{v}_{c_2}$. Figure (3.5) depicts the estimated $\hat{\xi}_1$, the reconstructed floating voltage $\hat{v}_{c_1}$ and the control signal u_2 in steady state. As enounced by the proposition (3.1) above, the floating voltage v_{c_1} can be reconstructed as $\hat{v}_{c_1} = |\hat{\xi}_1|$ at the time interval where $u_2 = 0$. This is well represented by the figure (3.5), where we can see after reconstructing the voltage, $\hat{v}_{c_1}$ remains constant in time intervals where $u_2 = 1$ or $u_2 = -1$. While the real v_{c_1} evolves (increases or decreases) over the time, which explain the estimation errors depicted by figure (3.4.a).

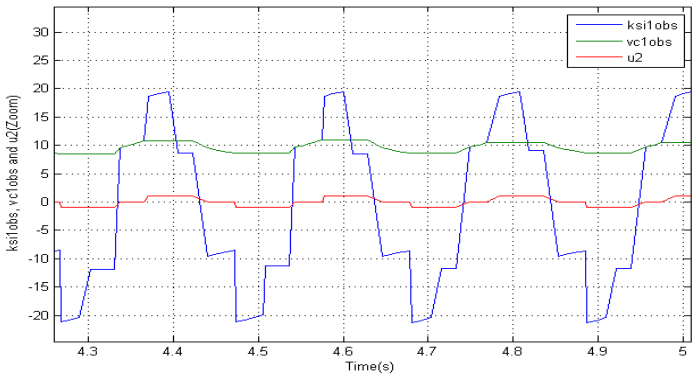

FIGURE 3.5: Zoom of $\hat{\xi}_1$, $\hat{v}_{c_1}$ and u_2 in steady state clarifying the reconstruction strategy of $\hat{v}_{c_2}$.

In the same way, figure (3.6) depicts the estimated $\hat{\xi}_1$, the reconstructed floating voltage $\hat{v}_{c_2}$ and the control signal u_1 in steady state. The floating voltage v_{c_2} can be reconstructed as $\hat{v}_{c_2} = |\hat{\xi}_1|$ at the time interval where $u_1 = 0$. This is well represented by the figure (3.6), where we can see after reconstructing the voltage, $\hat{v}_{c_2}$ remains constant in time intervals where $u_1 = 1$ or $u_1 = -1$. While the real v_{c_1} evolves (increases or decreases) over the time, which explain another time the estimation errors depicted by figure (3.4.b).

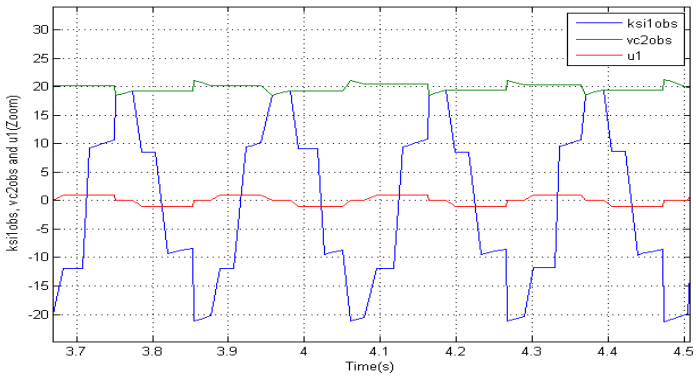

FIGURE 3.6: Zoom of $\hat{\xi}_1$, $\hat{v}_{c_2}$ and u_1 in steady state clarifying the reconstruction strategy of $\hat{v}_{c_2}$

3.5 Conclusion

This chapter is devoted to the observability analysis and the observation of the floating voltages of the 3-cell converter, assuming that the load current is the only available measurement. The analysis of the observability of each mode in a classical sense amounts to computing the rank of the observability matrix, this indicates that at most two variables can be observed in each mode. But this does not imply the unobservability of the system. Indeed, the observability of a switching system is analyzed along a hybrid time trajectory. therefore, we have presented two approaches for observability analysis. The $Z\{T_N\}$-observability, which is widely used in the analysis of the observability of the floating voltages of the converter since its introduction. The second is based on the calculation of the unobservable subspace. The latter

was calculated for a well-chosen control sequence so that the floating voltages can be estimated by an observer. The second part of this chapter is devoted to reconstructing the floating voltages of the 3-cell converter. The idea is based on the designing of a sliding mode observer for the observable subspace of the converter, then reconstructing the floating voltages from an estimated variable provided by the observer. For that, a mathematical model describing the dynamics of the observable subspace of the converter is determined. The model is written then in a special form of switching nonlinear systems. The nonlinear part is described by a function of the inputs and output of the system, that are assumed to be known. The second step consists in designing a sliding mode observer to estimate the observable subspace. The convergence of the estimation error is based using the Lyapunov theory. Indeed, the exponential stabilization of the estimation error has been shown, and the observer parameters are deduced from a LMI equation, where a solution is obvious. The reconstruction of the floating voltages as announced by proposition 1 is then possible by exploiting the interesting properties offered by the estimation variable. The carried out simulation results show the efficiency of the proposed strategy to reconstruct the floating voltages of the converter.

Chapter 4

Nonlinear Geometric Approach to Fault Detection and Isolation

Contents

4.1 Introduction

The first part of this chapter is devoted to a bibliographical study of different diagnosis methods, namely, the methods based on physical redundancy and those based on analytical redundancy. For each method, we present the carried out works as well as their advantages and their drawbacks. While the second part of this chapter is devoted to the geometric approach to fault diagnosis of non-linear systems to apply it for fault diagnosis of a three-cell converter along of the next chapter. This approach was introduced by M. A. Masooumnia in 1986 [91] for linear systems, then generalized for nonlinear systems by C. De. Persis and A. Isidori in 2000 [92]. This geometric approach is based on the computation of observable and unobservable subspaces whose main objective is to decouple the system to dissociate the faults between them. Indeed, the generation of a subspace sensitive to a set of faults and insensitive to another set is constrained by sufficient and necessary geometric conditions related to the observability co-distribution. If these conditions are checked, a residual generator can be designed, thus solving the fundamental problem of residual generation. During this chapter, we will expose the steps of this diagnosis approach, as well as for each step an illustrative example is presented to better adapt to the relatively heavy calculations.

4.2 State of the art

The fault diagnosis domain has attracted the attention of several researchers over the world in recent years due to its importance in industrial installations, hence several researches have been developed over the years. Basically, the are two main methods for fault detection and isolation, physical redundancy and analytical redundancy. The first is based on the unavailability of mathematical model describing the behavior of the system. While the second is based on the availability of mathematical model of the system.

4.2.1 Physical redundancy methods

In physical redundancy FDI methods, the sensitivity of sensors are set, adjusted or additional sensors are installed, such that they are able to detect and isolate the faults.

Limit checking sensors for FDI : The most simple and frequently used for fault diagnosis is the limit checking measured variable. In practice, plant measurements are compared to preset limits that are called also thresholds. Exceeding the threshold indicates a fault situation [51], [48]. Normally, there will be two levels of preset limits [53], exceeding the first one will issue a warning, while exceeding the second triggers an alarm and an emergency reaction should be taken. The thresholds are mostly selected based on experiences in the case of limit checking of absolute values while it represent a compromise. This approach suffers from two serious drawbacks [51]. 1- since the system variables may vary widely, the test thresholds need to be set quite conservatively. 2- The effect of a single component fault may propagate to many plant variables, triggering multitude of alarms and making isolation extremely difficult. To overcome to these drawbacks, an approach based on trend checking is proposed. Indeed, the first derivative of the monitoring variable is computed. If relatively, small thresholds are

selected, an alarm can be obtained earlier than for the limit checking of absolute values. Noted that the two strategies can be combined. Figure (4.1) shows an example of the two strategies.

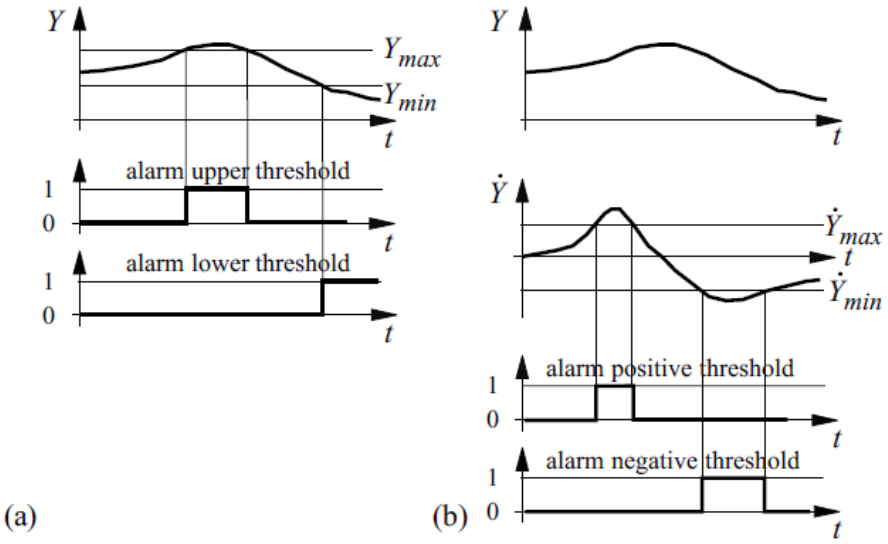

FIGURE 4.1: a- Limit checking method, b- Trend Limit checking method

Installing special sensor for FDI : Unlike the previous method, where measurements are compared to their threshold limits, this method uses sensors with built-in limits (integrated limits) checking ability to determine anomalies or any other unusual values while measurements are being taken [53]. Special sensors may measure some fault indicating the physical quantity, such as sound, vibration, elongation, or heat, and this is extremely useful for FDI if the type of faults that occur on the system are known or expected. In [93] and [94], a comparative study between accelerometer and laser vibrometer measurement carried out on universal motor of washing machines that exhibit faults localized mainly in the bearing, is presented. The authors in [95] present an experimental study to early detection of the presence of misalignment on support bearing of a motor by measuring the temperature of the shaft coupling using a thermal imaging camera.

FDI using multiple sensors : In this approach, multiple sensors are installed onto the system so that there will be more than one sensor to make the same measurement. Any serious deviation between the measurements indicates a sensor fault. With only two parallel sensors, fault isolation is not possible. The fault isolation needs at least three sensors. FDI using multiple sensors approach involves extra hardware cost and extra weight, the latter represents a serious drawback in aeronautic space applications [51]. The method has been applied to a mechanical system as in [96]. More about sensor faults diagnosis advanced techniques can be found in [97].

Other methods that do not use either hardware redundancy or analytical redundancy and which are very interesting in the case where the system does not have a model, based only on the input-output data of the system, we can cite :

Principal Component Analysis (PCA) approach : PCA is a linear orthogonal projection technique that projects multidimensional observations represented in a space of dimension onto a subspace of lower dimension while maximizing the variance of the projections [98]. The main purpose of the transformation is to study the relationships between the data set. It allows the identification of a structure of dependence between multivariate observations to obtain a compact description of the information. Linear PCA is a tool for modeling linear relationships between a set of variables representing the behavior of a studied process, where only linear or quasi-linear dependencies between variables can be revealed. The identification of the model is based on two stages : the first consists in estimating its parameters while the second consists in determining its structure. Once the PCA model has been identified, residuals can be generated by comparing the observed behavior to that given by the reference PCA model. These residuals make it possible to detect and then locate all of the variables at fault. The goal of the PCA is, therefore, to find a set of factors (components) that is smaller than the original data set, and that can correctly describe the main trends. Since most of the real processes are nonlinear, the application of classical PCA is not suitable. More advanced PCA approaches can be found in [99] for Joint PCA or in [83] for Structured Joint PCA or in [98].

Stochastic and statistical FDI : It is also called the generalized likelihood ratio approach, as mentioned by [53]. This method tests the residual for its statistical properties, such as zero-mean gaussian white noise and covariance. When a fault occurs, the statistical properties of residuals deviate from their nominal operation. Several works have applied this approach to fault diagnosis of different systems one can cite [100], and [101]. Over the year, various improvements have been made to this approach and are combined with other approaches as in [102], where the authors combine the statistical approach with neural networks.

Spectrum Analysis : Spectrum analysis of measurements may also be used for fault detection and isolation. Most systems operate at a specified frequency spectrum under normal operating conditions. However, any detected frequencies spectrum that does not correspond to the operating frequency spectrum is an indication of the occurrence of faults. Moreover, certain types of faults may have their own unique frequencies characteristics signature in the spectrum, which facilitating fault isolation. The most popular signal processing algorithms that have been widely used for FDI purposes are the Fourier Transform (FT) and the Wavelet Transform (WT), which extract the frequency and time-frequency features from time-series data [103]. The method has been applied to fault diagnosis of machinery components such as gearbox [96], or for fault diagnosis of rolling element bearings [104], or as in [105] for diagnosis of broken bar fault in induction machine, or for diagnosis of permanent synchronous motor [106].

4.2.2 Analytical redundancy method

The major drawbacks of physical redundancy methods which use multiple sensors and actuators are extra equipment that induces extra weight, maintenance cost, and more additional space to accommodate the equipment, or for some constraints where the measurement is dif-

ficult or almost infeasible. These drawbacks are overcome by analytical redundancy methods. All that we need for FDI based analytical redundancy is a mathematical model that describes the evolution of the system variables accurately, under observation. Generally, the analytical redundancy methods are based on residual generators that generate a set of signals called "residual signals". These residuals should be zero under fault-free conditions and it should be nonzero if and only if there are faults that affect the system. Several approaches are proposed in the literature using an analytical model, some of them are presented below :

Fault detection filter : Filters are used in a stochastic context for fault detection and isolation of systems. Faults sensitive filters can be considered as particular observers, where for each fault situation, their gains are set so that the residual vectors take a particular direction. The first results concerning filters sensitive to faults are due to Beard (1971) and Johns (1973), known also as Bear-Jones fault detection filter. It is considered one of the pioneering methods that have inspired the directional residual concept [103]. The Bear-Jones approach has inspired the geometrical approach to fault detection and isolation filter, introduced for linear systems by M. A. Massoumnia 1986 [91] using the concept of unobservability subspace, and has proved that the basic necessary and sufficient condition to a fundamental problem of residual generation is the existence of an unobservability subspace. Later in 2000, C. De Persis and A. Isidori [92], extended the Massoumia's geometric approach to nonlinear systems by introducing necessary and sufficient conditions for solving the problem of nonlinear FDI. This approach will be detailed in current chapter and applied to fault detection and isolation of the switch's faults of the three cell converter in chapter five. Kalman Filter is another type of filter that has been widely used for estimation and in fault diagnosis, especially in noisy systems. Because of its simplicity and its effectiveness results, several applications for fault diagnosis have been carried out using Kalman Filter and its derivatives. In [107], the authors used a Kalman Filter (KF) fault detection and isolation to improve the security of the cyber-physical system. In [108], Extended Kalman Filter (EKF) is designed to sensor incipient fault detection and isolation of nuclear power plants. A Cubature Kalman Filter (CKF) has been used to fault diagnosis of a railway suspension system in [109]. The authors in [110] have proposed an algorithm to compute the optimal observer gains based fault detection using the Zonotopic Kalman Filter(ZKF), and the approach has been applied to a quadruple tank system. In [111], an Adaptive Unscented Kalman Filter (AUKF) has been used to fault diagnosis of a nonlinear system and applied to a low earth orbit space vehicle planer model, the obtained results have been compared to those obtained using respectively the UKF and EKF. In [112], the nonlinear Kalman Filter is used for fault diagnosis of gas-turbine power units.

Parameter estimation for FDI : This approach is based on the parameter estimation under the assumption that the faults are reflected in the physical parameters of the system. Hence, to identify the faults, the system parameters are estimated using well-known parameter estimation techniques. The residuals in this approach are essentially the difference between the online estimates of the system parameters and their corresponding values under free-fault conditions. The parameter estimation approach was initially developed for linear systems due to the availability of the linear parameter estimation techniques. The most known techniques

are the least-squares and its multiple extensions. However, recent advances in nonlinear parameter estimation using Extended Kalman Filter (EKF) [113], or the Unscented Kalman Filter (UKF) [114], or neural networks [115], have made it possible to use a parameter estimation approach for FDI of nonlinear dynamic systems.

Parity space approach for FDI : This technique is based on the projection of the model's equations in a particular space, called the parity space. Indeed, this technique is initially based on the left multiplication of the output equation by a matrix W [1]. The interpretation of this multiplication is to eliminate the unknown states by a projection on W. Initially, this method originates from the hardware redundancy used for fault detection and isolation of fault sensors, then it was extended to diagnose the complete system (generalized parity space). Some early contributions on parity space equation strategies can be found in [116], [117] and [118]. Some authors have linked between the generation of residuals by parity space and by state observer, and demonstrate a certain degree of equivalence. Massoumnia in [91] was the first to speak of a correspondence between the two strategies. A comparison study between the parity space and observer based-approaches is given in [48]. Recently, extensive works of parity space approach for FDI are presented as in [119], where parity equation is combined with support vector machine (SVM) classification algorithm to minimize the noise effect on the generated residual signals, or as in [120], where the authors used the nonlinear parameter varying (NLPV) parity equation for fault detection and isolation of wind farm. For hybrid systems, the parity space approach is not yet well investigated sufficiently, the work of [121] treats this issue. However, it should be noted that the parity space method is more sensitive to measurement noise and process noise (or disturbance) compared to observer-based methods, which are more robust to noise and disturbances due to their closed-loop structure [103].

Observer based-approach for FDI : This approach consists of the reconstruction of the system outputs from a subset of system measurements and defining residual as the difference between the actual measurements and the output estimations provided by the observer. Since the pioneering work of Kalman 1971, the observer's theory has been improved increasingly, and this for both linear and nonlinear systems [122], [123],[124]. Several types of observers are proposed in the literature to fault diagnosis of different systems as sliding mode observer [125], [126], adaptive observer [127], [128], or high gain observer [129].

Faults reconstruction : Besides detecting and isolating the faults, sometimes it is important to estimate their occurrences. Hence, further analysis can be provided as the nature and the magnitude that can measure the severity of faults. So, appropriate corrective actions can be taken. This approach is very useful for incipient faults with slow drifts, which are known to be very difficult to detect. Generally, fault reconstruction approach is based on using an observer as in [130], [131], [132]. However, several other methods have been proposed to faults reconstruction as in [133], where the authors used an improved PCA to reconstruct sensor

1. W is made up of vectors of $Ker(C^T)$, hence it has the property of orthogonality with the output matrix C

faults in nuclear power plant, or in [134] where the authors proposed the use a statistical based approach to fault reconstruction.

4.3 Geometric Approach to Fault Detection and Isolation

The most delicate task of a diagnostic procedure is to locate the origin of the fault, in another way this indicates the fault isolation procedure. For the nonlinear systems, this task becomes more and more delicate because of the nonlinearities as well as the strong coupling of the state variables. The use of linearization methods around an operating point can lead to information losses, and consequently false alarms that can be caused by the diagnostic procedure based on the linear model. Thereby, the use of non-linear diagnostic methods becomes necessary and essential. Among the robust diagnostic approaches, we can cite those which are based on faults decoupling. This means partitioning the state space such that a subspace will be sensitive to one fault and insensitive to other faults and disturbances in the ideal case, or will be sensitive to a set of faults and insensitive to another set of faults, consequently this will decrease the performances of the diagnostic procedure, especially in the case of simultaneous faults. During the two last decades, the geometric approach proposed by C. De. Persis and A. Isidori in [92], [135], has arisen from other methods, not only by its robustness but also by its power that resides in its application for nonlinear systems. If necessary and sufficient conditions are verified, then the decoupling of the system is systematic, so a solution to the FPRG problem exists, i.e., the existence of a residual generator filter that allows the detection and isolation of the fault. In this section, a geometric approach to fault detection and isolation of both linear and nonlinear systems is presented (our attention will be focused on the nonlinear system). The necessary and sufficient conditions for the existence of a solution to a Fundamental Problem of Residual Generation (FPRG) that provided by this power approach is related to the unobservability co-distribution (the dual of the observability co-distribution). The computation of the observability co-distribution is given by a non-decreasing sequence that will be presented. This observability co-distribution has several interesting properties that allow the determination of a state and output diffeomorphisms which finalize a detection and isolation filter synthesis, therefore solving the FPRG. We are particularly interested in the work of M. A. Massoumnia [91], who was the first to introduce the geometric approach for the diagnosis of linear systems, and also we are mainly interested in the work of C. De. Persis and A. Isidori [92], [135] who generalized the linear approach of M. A. Massoumnia for nonlinear systems. This later will be applied to fault detection and isolation of 3-cell converter presented in next chapter. This approach is based on the observability codistribution that allows to construct a change of coordinates resulting in a subspace decoupled from a set of faults. A simple construction of an observer for the obtained subsystem can be considered as a residual generator. In literature, several works have been presented applying this approach. In [136], the authors designed a Luenberger observer to estimate the states of the obtained system and generate residual signals, the method was applied to a VTOL air craft system. In [137] a nonlinear adaptive observer was designed to accomplish the diagnosis procedure for a ship propulsion system. A nonlinear observer designed for a class of nonlinear system was proposed in [138] to detect and isolate actuator faults for induction motor drive. In [139],

combination between sliding mode and high gain observers to generate residual signals was applied to current sensor fault diagnosis in induction motor drives. In [50], the geometric approach has been extended for nonlinear systems using a generalized output injection. This approach has been applied to the fault diagnosis of stator short-circuit faults [140]. Recently, a very interesting geometric approach has been proposed and applied to both discrete and parametric fault diagnosis in a grid-connected inverter in [141].

4.3.1 Fondamental problem of residual generation for LTI system

Let the Linear Time Invariant (LTI) system described by the following equations :

$$\begin{cases} \dot{x}(t) = Ax(t) + Bu(t) + Pw(t) + Ld(t) \\ y(t) = Cx(t), \end{cases} \tag{4.1}$$

where $x(t) \in R^n$ is the state vector, $u(t) \in R^m$ is the input vector, $y(t) \in R^p$ is the output vector, $w(t) \in R^q$ is the fault vector that their occurrence should be detected and isolated from other faults and disturbances $d(t) \in R^d$. A, B and C are matrices of appropriate dimension. P and L are respectively the effects of the fault $w(t)$, and the disturbances and other faults $d(t)$. The Fondamental Problem of Residual Generation (FPRG) for the system (4.1) consists on finding a residual generator of the form [137], [91], [92], [135] :

$$\begin{cases} \dot{z}(t) = Fz(t) + Ku(t) + Ey(t) \\ r(t) = Jz(t) + Hy(t), \end{cases} \tag{4.2}$$

where $z(t) \in R^{\tilde{n}}$ is the state vector of the residual generator, and $r(t) \in R^{\tilde{p}}$ is the residual vector. F, K, E, J and H are matrices of appropriate dimensions. The augmented system obtained from the composition of (4.1) and (4.2) is described by :

$$\begin{cases} \dot{x^e}(t) = A^e x^e(t) + B^e u^e(t) + P^e w(t) \\ r(t) = C^e x^e(t) \end{cases} \tag{4.3}$$

with

$$x^e(t) = \begin{pmatrix} x(t) \\ z(t) \end{pmatrix}, \quad u^e(t) = \begin{pmatrix} u(t) \\ d(t) \end{pmatrix}, \quad A^e = \begin{pmatrix} A & 0 \\ EC & F \end{pmatrix}, \quad B^e = \begin{pmatrix} B & L \\ K & 0 \end{pmatrix},$$

$$P^e = \begin{pmatrix} P \\ 0 \end{pmatrix}, \quad C^e = \begin{pmatrix} HC & J \end{pmatrix}$$

Then the FPRG consists in synthesizing a residual generator of the form (4.2), and whose the unknown matrices F, K, E, J and H will satisfy the following properties :

1- The transfer function matrix between $u^e(t)$ and $r(t)$ given by $C^e(sI_{n+\tilde{n}} - A^e)^{-1}B^e$ is identically zero.

2- The transfer function matrix between the fault $w(t)$ and the residual $r(t)$ must not be zero.

3- The poles of $C^e(sI_{n+\tilde{n}} - A^e)^{-1}$ must be in negative real parts.

The first condition ensures the robustness of the residual signal with respect to the disturbances and other faults $d(t)$and control input $u(t)$, which is the most delicate task to satisfy, and which makes it possible to avoid false alarms. While the second condition ensures the detectability of the faults by the residual. The third condition ensures the stability of the observable space of the augmented system (4.3) , i.e., ensure that the effect of the initial conditions is not durable on the residuals. It is shown in [91] that the existence of a solution to FPRG depends on a simple relation between the subspace containing the effect of fault that we would like to detect and isolate and the minimal unobservability co-distribution which contains the effect of other faults and disturbances. For linear LTI systems, the computation of the unobservability co-distribution passes by two steps :

1- Consider the sequence of sub-spaces of R^n given by :

$$\begin{cases} D_0 = span\{L\} \\ D_{i+1} = D_0 + A(D_i \cap ker\{C\}), \quad i = 0, ..., n-1 \end{cases} \tag{4.4}$$

with the stop condition

$$D_*^p = D_{n-1} \tag{4.5}$$

2- Let the non decreasing sequence of dual sub-spaces of R^n :

$$\begin{cases} Q_0 = (D_*^p)^\perp \cap span\{C\} \\ Q_{i+1} = (D_*^p)^\perp + (Q_i A + span\{C\}), \quad i = 0, ..., n \end{cases} \tag{4.6}$$

with the stop condition

$$Q_*^p = Q_{n-1} \tag{4.7}$$

Thus, the minimal unobservability subspace that contains the disturbance and other faults is given by

$$Q_{unob} = (Q_*^p)^\perp \tag{4.8}$$

Note that $(\bullet)^\perp$ represent the orthogonal distribution of $(\bullet)$. Based on this generated co-distribution, the existence of a solution to fundamental problem of residual generation can be checked using the following theorem.

Theorem 4.1 [91] : Let consider the system (4.1). There exists a solution to fundamental problem of residual generation if and only if

$$L \cap Q_{unob} = 0 \tag{4.9}$$

The above condition of the previous theorem is valid for the residual generator given by (4.2). If this condition is verified, it is possible to determine a state transformation so as to decompose the overall system into two subsystems, one of which is decoupled from the effect of disturbances and other faults. It has been shown that this transformation is related to the observability subspace (the observability distribution). This subsystem is defined as follows [92] :

$$\begin{cases} \dot{x}_1(t) = A_{11}x_1(t) + A_{12}x_2(t) + B_1u(t) + Pw(t) \\ y_1(t) = C_1x_1(t) \end{cases} \tag{4.10}$$

and where the pair (A_{11}, C_1) is observable. Hence the design of a detection and isolation filter for fault $w(t)$ is immediate. Let consider the Luenberger observer for the system (4.10) described by the following equations :

$$\begin{cases} \dot{z} = A_{11}z(t) + A_{12}y_2(t) + B_1u(t) + G(C_1z(t) - y_1(t)) \\ r(t) = C_1z(t) - y_1(t) \end{cases} \tag{4.11}$$

The matrix G is such that the eigenvalues of $(A_{11} + GC_1)$ are of negative real part. The dynamic error is :

$$\dot{e}(t) = (A_{11} + GC_1)e(t) + pw(t) \tag{4.12}$$

and the residual signal can be considered as

$$r(t) = Ce(t) \tag{4.13}$$

From (4.12), we can notice that if the system is in free fault situation and the eigenvalues of $(A_{11} + GC_1)$ have negative real parts, then the error $e(t)$ tends asymptotically to zero, consequently $r(t)$ tends to zero. However, if the system is affected by the fault $w(t)$, the error $e(t)$ deviate from zero, consequently, also $r(t)$ deviate from zero indicating the occurrence of the fault. Thus, the filter (4.11) resolve the fundamental problem of residual generation for LTI systems.

4.3.2 Fondamental problem of residual generation for nonlinear systems

The geometric approach to fault detection and isolation for nonlinear systems is recalled in this section. This approach is introduced in [92], [135]. Consider the following faulty nonlinear system

$$\begin{cases} \dot{x}(t) = g_0(x) + \sum_{i=1}^{m} g_i(x)u_i + p_j(x)m_j + \sum_{k=1,k\neq j}^{d} p_k(x)m_k \\ y(t) = h(x) \end{cases} \tag{4.14}$$

where $x \in \mathbb{R}^n$ is the state, $u \in \mathbb{R}^m$ is the input control and $y \in \mathbb{R}^p$ is the output. $m_j \in \mathbb{R}$ is the fault whose occurrence will be detected and isolated from other faults and unknown inputs m_k, $(k = 1, ..., d$ with $k \neq j)$ and $g_i(x)$, $p_j(x)$, $(i = 0, ..., m)$, are smooth vector fields. It is assumed that the fault m_k is bounded, i.e., $||m_k||_p < \infty$($||.||_p$ denotes the p-norm). The Local Nonlinear Fundamental Problem of Residual Generation (l-NLFPRG) consists on designing a filter of the form

$$\begin{cases} \dot{\tilde{z}}(t) = \tilde{g}_0(\tilde{z}, y) + \sum_{i=1}^{m} \tilde{g}_i(\tilde{z}, y)u_i \\ r_j(t) = \tilde{h}_j(\tilde{z}, y) \end{cases} \tag{4.15}$$

where $\tilde{z} \in \mathbb{R}^{\tilde{n}}$ is the state of the filter, u and y are respectively the input and the output of the original system, $r_j \in \mathbb{R}$ is the residual of the fault m_j, and $\tilde{g}_j(\tilde{z}, y)$ $(j = 0, ..., m)$ and $\tilde{h}_j(\tilde{z}, y)$ are smooth vector fields such that the extended system obtained from the composition of

(4.14) and (4.15) written in a compact form as

$$\begin{cases} \dot{x^e} = g_0^e(x^e) + \sum_{i=1}^{m} g_i^e(x^e)u_i + p^e(x^e)m_j + \sum_{k=1,k\neq j}^{d} p_k^e(x^e)m_k, \\ r_j = h^e(x^e), \end{cases} \tag{4.16}$$

with $x^e = \begin{pmatrix} x \\ \tilde{z} \end{pmatrix}$, $g_0^e(x^e) = \begin{pmatrix} g_0(x) \\ \tilde{g}_0(\tilde{z}, y) \end{pmatrix}$, $g_i^e(x^e) = \begin{pmatrix} g_i(x) \\ \tilde{g}_i(\tilde{z}, y) \end{pmatrix}$, $p^e(x^e) = \begin{pmatrix} p_j(x) \\ 0 \end{pmatrix}$, $p_k^e(x^e) = \begin{pmatrix} p_k(x) \\ 0 \end{pmatrix}$, $h^e(x^e) = \tilde{h}(z, h(x))$,
satisfied the following properties :

1. the residual r_j is not affected by $m_k \ \forall \ k \neq j$ but only affected by the fault m_j.
2. $lim\|r_j(t, x^0, z^0, u_1, ..., u_m, m_j = 0, m_1, ..., m_k)\| = 0$, for any initial condition x^0, z^0 and any set of admissible inputs u_i, with $k = 1, ..., d$ and $k \neq j$.

The first condition ensures the sensitivity of the residual r_j to m_j and its insensitivity to the other faults, while the second condition ensures the stability of the residual.
From the model of the system (4.14), the first condition can be written geometrically as follows :

$$span\{p_1, ..., p_{j-1}, p_{j+1}, ..., p_d\} \subset Q_{unob}, \tag{4.17}$$

and

$$span\{p_j\} \nsubseteq Q_{unob}, \tag{4.18}$$

where Q_{unob} represents the unobservability distribution, which contains $\ker(dh)$ and invariant under $g_i, (i = 0, ..., m)$ and $p_k, (k = 1, ..., j-1, j+1, ..., d)$. It represents the minimal unobservability distribution containing $span\{p_1, ..., p_{j-1}, p_{j+1}, ..., p_d\}$. Its characterization plays an important role in the filter design for the fault m_j. The two following algorithms are used to compute this distribution.

4.3.3 Conditioned invariant distribution

Consider system (4.14) with the distributions $P_j = span\{p_1, ..., p_{j-1}, p_{j+1}, ..., p_d\}$ and $L = span\{p_j\}$. We consider the non-decreasing sequence of distributions defined as follows :

$$\begin{aligned} D_0^{P_j} &= \bar{P}_j \\ D_{i+1}^{P_j} &= \bar{D}_i^{P_j} + \sum_{k=0}^{m} \left[g_k(x), \bar{D}_i^{P_j} \cap \ker(dh) \right], \end{aligned} \tag{4.19}$$

where $\bar{D}_i^{p_j}$ denotes the involutive closure of $D_i^{p_j}$, and $ker(dh)$ is the distribution annihilating the differentials of the rows of the mapping $h(x)$, and $[,]$ denotes the Lie brackets. Suppose that there exists an integer $k^* \leq n-1$ such that

$$D_{k^*+1} = \bar{D}_{k^*}. \tag{4.20}$$

We set $\Sigma^{P_j} = \bar{D}_{k^*}$. Then, Σ^{P_j} is involutive, contains P_j and is conditioned invariant.

Remark : The stop condition (4.20), which is related to the existence of an integer k^*, may not be satisfied. In this case, the progress of the algorithm is stopped as soon as the number

of performed iterations is greater than the dimension of the system. Thus, the continuity condition of this algorithm is related to the existence of an integer k^* which can satisfy the condition (4.20).
The conditioned invariant distribution Σ^{P_j} has some interesting properties summarized as follow :

- Σ^{P_j} is involutive and it is conditioned invariant.
- Σ^{P_j} contains the effect of other faults and disturbances $P_j(x) = span\{p_1, ..., p_{j-1}, p_{j+1}, ..., p_d\}$.
- Any involutive distribution Δ contains $P_j(x)$ is conditioned invariant and satisfy $\Sigma^{P_j} \subset \Delta$.
- If the stop condition (4.20) is satisfied, then the distribution Σ^{P_j} is the minimal element of the family of all involutive distributions which contains $P(x)$.
- The stopped condition (4.20) will be satisfied if all generated distribution by the algorithm (4.19) are nonsingular.

Academic example : Let consider the academic nonlinear system :

$$\begin{cases} \dot{x}_1 = x_2 \\ \dot{x}_2 = x_1 x_4^2 - a_1 \frac{1}{x_1}^2 + a_2 u_1 + m_2 \\ \dot{x}_3 = x_4 \\ \dot{x}_4 = -\frac{2x_2 x_4}{x_1} + a_2 \frac{u_2}{x_1} + a_2 \frac{m_1}{x_1} \end{cases} \tag{4.21}$$

with $x \in R^4$ is the state vector, $u \in R^2$ is the control input vector, a_1 and a_2 are known parameters. Assume that the system is affected by a fault m_1 on the second actuator and by a disturbance m_2. The aim objective is to design a filter that detect and isolate the fault m_1 from the disturbance m_2. A long of this section we follow the presented methodology step by step until the design of the filter. First, we compute the conditioned invariant distribution. The system (4.21) can be put in the nonlinear form as in (4.14) with :

$$g_0(x) = \begin{pmatrix} x_1 \\ x_1 x_4^2 - a_1 \frac{1}{x_1^2} \\ x_4 \\ -\frac{2x_2 x_4}{x_1} \end{pmatrix}, \quad G(x) = \begin{pmatrix} g_1(x) & g_2(x) \end{pmatrix} = \begin{pmatrix} 0 & 0 \\ a_2 & 0 \\ 0 & 0 \\ 0 & a_2 \end{pmatrix},$$

$$p_1(x) = \begin{pmatrix} 0 \\ 0 \\ 0 \\ \frac{a_2}{x_1} \end{pmatrix}, \quad p_2(x) = \begin{pmatrix} 0 \\ 1 \\ 0 \\ 0 \end{pmatrix}.$$

Assume that the output vector is :

$$y(t) = \begin{pmatrix} x_1 \\ x_3 \\ x_4 \end{pmatrix}.$$

Let P a distribution spanned by the effect of the disturbance, i.e., $P = span\{p_2(x)\} = span\{(0 \quad 1 \quad 0 \quad 0)^T\}$, its involutive closure is $\overline{P} = span\{p_2(x)\} = span\{(0 \quad 1 \quad 0 \quad 0)^T\}$.

The algorithm (4.19) is initialized then by the distribution $D_0 = \overline{P}$. Applying the algorithm (4.19) for first iteration, we have :

$$D_1 = \overline{D_0} + \sum_{i=0}^{2} [g_i, \overline{D_0} \cap ker\{dh\}] \tag{4.22}$$

we have : $ker\{dh(x)\} = span\{(0 \quad -1 \quad 0 \quad 0)^T\}$, then

$$\overline{D_0} \cap ker\{dh\} = span\{(0 \quad 1 \quad 0 \quad 0)^T\}, \tag{4.23}$$

thus

$$\begin{aligned}
\left[\; g_0(x), \quad \overline{D_0} \cap ker\{dh\} \; \right] &= \frac{\partial(\overline{D_0} \cap ker\{dh\})}{\partial x} g_0(x) - \frac{\partial g_0(x)}{\partial x} (\overline{D_0} \cap ker\{dh\}) \\
&= - \begin{bmatrix} 0 & 1 & 0 & 0 \\ x_4^2 + \frac{a_1}{x_1^4} & 0 & 0 & 2x_1x_4 \\ 0 & 0 & 0 & 1 \\ \frac{2x_2x_4}{x_1^2} & -\frac{2x_4}{x_1} & 0 & -\frac{2x_2}{x_1} \end{bmatrix} \begin{bmatrix} 0 \\ -1 \\ 0 \\ 0 \end{bmatrix} \\
&= \begin{bmatrix} 1 \\ 0 \\ 0 \\ -\frac{2x_4}{x_1} \end{bmatrix},
\end{aligned}$$

also :

$$\begin{aligned}
\left[\; g_1(x), \quad \overline{D_0} \cap ker\{dh\} \; \right] &= \frac{\partial(\overline{D_0} \cap ker\{dh\})}{\partial x} g_1(x) - \frac{\partial g_1(x)}{\partial x} (\overline{D_0} \cap ker\{dh\}) \\
&= \begin{pmatrix} 0 & 0 & 0 & 0 \end{pmatrix}^T,
\end{aligned} \tag{4.24}$$

and

$$\begin{aligned}
\left[\; g_2(x), \quad \overline{D_0} \cap ker\{dh\} \; \right] &= \frac{\partial(\overline{D_0} \cap ker\{dh\})}{\partial x} g_2(x) - \frac{\partial g_2(x)}{\partial x} (\overline{D_0} \cap ker\{dh\}) \\
&= \begin{pmatrix} 0 & 0 & 0 & 0 \end{pmatrix}^T,
\end{aligned} \tag{4.25}$$

we obtain then

$$D_1 = span\{(0 \quad 1 \quad 0 \quad 0)^T, (1 \quad 0 \quad 0 \quad -\frac{2x_4}{x_1})^T\}. \tag{4.26}$$

Notice that D_1 is not singular and the stopped condition is not yet satisfied since $D_1 \neq D_0$. Applying the algorithm (4.19) for second iteration. We have

$$D_2 = \overline{D_1} + \sum_{i=0}^{2} [g_i, \overline{D_1} \cap ker\{dh\}], \tag{4.27}$$

where $\overline{D_1}$ is the involutive closure of the distribution D_1, it is equal to

$$\overline{D_1} = D_1 = span\{(0 \quad 1 \quad 0 \quad 0)^T, (1 \quad 0 \quad 0 \quad -\frac{2x_4}{x_1})^T\}, \tag{4.28}$$

thus

$$\overline{D_1} \cap ker\{dh\} = span\{(0 \quad 1 \quad 0 \quad 0)^T\} \tag{4.29}$$

Noticing that equation (4.29) is the same equation as in (4.23). Therefore, the rest of calculation is the same, consequently :

$$D_2 = \overline{D_1} = span\{(0 \quad 1 \quad 0 \quad 0)^T, (1 \quad 0 \quad 0 \quad -\frac{2x_4}{x_1})^T\}. \tag{4.30}$$

Thus, the stop condition (4.20) is verified. Set then :

$$\Sigma_*^p = D_2 = span\{(0 \quad 1 \quad 0 \quad 0)^T, (1 \quad 0 \quad 0 \quad -\frac{2x_4}{x_1})^T\}. \tag{4.31}$$

Which represents the minimal conditioned invariant distribution containing the effect of the disturbance. Note that Σ_*^p is nonsingular and involutive for any $x_1 \neq 0$. Then its orthogonal codistribution is spanned by exact differentials and it can expressed as follow :

$$(\Sigma_*^p)^\perp = span\{(0 \quad 0 \quad 1 \quad 0)^T, (2x_1x_4 \quad 0 \quad 0 \quad x_1^2)^T\} = span\{dx_3, \quad d(x_1^2x_4)\}. \tag{4.32}$$

Once the conditioned invariant distribution is computed, the next step is the computation of the observability distribution, which is the subject of the next section.

4.3.4 Observability codistribution

The following algorithm determines the maximal observability distribution contained in ${P_j}^\perp$ and the minimal unobservability codistribution that contains P_j. For this end, consider the non-decreasing sequence of codistributions given as follow :

$$\begin{aligned} Q_0 &= (\Sigma^{P_j})^\perp \cap span\{dh\} \\ Q_{k+1} &= (\Sigma^{P_j})^\perp \cap (\sum_{i=0}^{m} L_{g_i} Q_k + span\{dh\}). \end{aligned} \tag{4.33}$$

If there exists an integer, $k^* \leq n-1$, such that $Q_{k^*+1} = Q_{k^*}$, $\forall k > k^*$. We set $Q_{k^*} = \Omega$ and we denote this codistribution by

$$\Omega = o.c.a((\Sigma^{P_j})^\perp), \tag{4.34}$$

where *o.c.a* refers to the observability codistribution algorithm. The codistribution $\Omega = o.c.a((\Sigma^{P_j})^\perp)$ represents the maximal observability codistribution contained in $P^\perp$, i.e $o.c.a((\Sigma^{P_j})^\perp) \subset P^\perp$. Its orthogonal distribution $\Omega^\perp = Q_{unob}$ represents the minimal unobservability distribution. In nonlinear geometric approach, the residual $r_j(t)$ can be generated if the unobservability distribution Q_{unob} satisfies the following necessary condition :

$$L = span\{p_j(x)\} \nsubseteq Q_{unob}. \tag{4.35}$$

Properties of the observability codistribution : The observability codistribution has some properties where are summarized as follow :

1- Suppose that all generated codistribution by the algorithm (4.33) are nonsingular, and let $\Omega^* = o.c.a((\Sigma^{P_j})^\perp)$, therefore :

$$\begin{aligned} Q_0 &= \Omega^* \cap span\{dh\} \\ Q_{k+1} &= \Omega^* \cap (\sum_{i=0}^{m} L_{g_i} Q_k + span\{dh\}), \end{aligned} \tag{4.36}$$

consequently.

2- Let θ be any distribution. If θ is conditioned invariant, then $\Omega^* = o.c.a(\theta)$ it is.

3- A distribution Δ is an unobservability distribution if its orthogonal codistribution is an observability distribution.

4- For simplicity of computation, the following property can be used [92]

$$Q_{k+1} = \theta \cap (Q_k + \sum_{i=0}^{m} Lg_i Q_k + span\{dh\}), \tag{4.37}$$

where $Lg_i Q_k$ represents the derivative of the codistribution Q_k along of the vector field g_i, it is given by

$$Lg_i Q_k = (\frac{\partial Q_k^T}{\partial x} g_i)^T + Q_k \frac{\partial g_i}{\partial x} \tag{4.38}$$

5- If Σ^{P_j} is well defined and nonsingular, then $o.c.a((\Sigma^{P_j})^\perp)$ represents the maximal observability codistribution (in sense of codistribution inclusion) which is spanned by exact differentials and contained in $P_j^\perp$. Its orthogonal distribution represents the minimal unobservability distribution. Let Q be :

$$Q = (o.c.a(\Sigma^{P_j})^\perp)^\perp \tag{4.39}$$

6- Q represents the minimal involutive unobservability conditioned invariant and contains the effect of the other faults and disturbance.

Example : Consider again the academic example introduced above. We have computed its minimal involutive conditioned invariant distribution Σ_*^p given by the equation (4.31), and its orthogonal codistribution given by equation (4.32). Compute then the observability codistribution using algorithm (4.33). At the first step, the algorithm is initialized by :

$$Q_0 = (\Sigma_*^p)^\perp \cap span\{dh\} = span\{(0 \quad 0 \quad 1 \quad 0)^T, (2x_1x_4 \quad 0 \quad 0 \quad x_1^2)^T\} \tag{4.40}$$

thus

$$Q_1 = (\Sigma_*^p)^\perp \cap \sum_{i=0}^{2} Lg_i Q_0 + span\{dh\} \tag{4.41}$$

using the property (4.37), we can write

$$Q_1 = (\Sigma_*^p)^\perp \cap (Q_0 + \sum_{i=0}^{2} Lg_i Q_0 + span\{dh\}) \tag{4.42}$$

we have

$$Q_0+\sum_{i=0}^{2} Lg_iQ_0+span\{dh\} = span\{w_{01}, \quad w_{02}, \quad Lg_0w_{01}, \quad Lg_0w_{02}, \quad Lg_1w_{01}, \quad Lg_1w_{02}, \quad Lg_2w_{01}, \quad Lg_2w_{02}\}, \tag{4.43}$$

with $w_{01} = (0 \quad 0 \quad 1 \quad 0)^T$ and $w_{02} = (2x_1x_4 \quad 0 \quad 1 \quad x_1^2)^T$. Using equation (4.38), we obtain :

$$\begin{array}{rcl} Lg_0w_{01} & = & (0 \quad 0 \quad 0 \quad 1)^T, \\ Lg_0w_{02} & = & (0 \quad 0 \quad 0 \quad 0)^T, \\ Lg_1w_{01} & = & (0 \quad 0 \quad 0 \quad 0)^T, \\ Lg_1w_{02} & = & (0 \quad 0 \quad 0 \quad 0)^T, \\ Lg_2w_{01} & = & (0 \quad 0 \quad 0 \quad 0)^T, \\ Lg_2w_{02} & = & (2a_2x_1 \quad 0 \quad 0 \quad 0)^T, \end{array} \tag{4.44}$$

we obtain then

$$Q_0+\sum_{i=0}^{2} Lg_iQ_0 = span\{(0 \quad 0 \quad 1 \quad 0)^T, (2x_1x_4 \quad 0 \quad 0 \quad x_1^2)^T, (0 \quad 0 \quad 0 \quad 1)^T, (2a_2x_1 \quad 0 \quad 0 \quad 0)^T\}, \tag{4.45}$$

thus,

$$(Q_0+\sum_{i=0}^{2} Lg_iQ_0)+span\{dh\} = span\{(0 \quad 0 \quad 1 \quad 0)^T, (2x_1x_4 \quad 0 \quad 0 \quad x_1^2)^T, (0 \quad 0 \quad 0 \quad 1)^T, (1 \quad 0 \quad 0 \quad 0)^T\}. \tag{4.46}$$

Finally, we obtain

$$Q_1 = span\left\{\begin{pmatrix}0\\0\\1\\0\end{pmatrix}, \begin{pmatrix}2x_1x_4\\0\\0\\x_1^2\end{pmatrix}\right\} \cap span\left\{\begin{pmatrix}0\\0\\1\\0\end{pmatrix}, \begin{pmatrix}2x_1x_4\\0\\0\\x_1^2\end{pmatrix}, \begin{pmatrix}0\\0\\0\\1\end{pmatrix}, \begin{pmatrix}1\\0\\0\\0\end{pmatrix}\right\},$$

$$\Rightarrow Q_1 = span\left\{\begin{pmatrix}0\\0\\1\\0\end{pmatrix}, \begin{pmatrix}2x_1x_4\\0\\0\\x_1^2\end{pmatrix}\right\}.$$

Noticing that $Q_1 = Q_0 = (\Sigma_*^p)^\perp$, then the stop condition is verified. Hence, we can write :

$$\Omega = o.c.a((\Sigma_*^p)^\perp) = span\{(0 \quad 0 \quad 1 \quad 0)^T, (2x_1x_4 \quad 0 \quad 0 \quad x_1^2)^T\}, \tag{4.47}$$

which represents the observability codistribution. Its orthogonal distribution represents the unobservability distribution, it is given as follow :

$$Q_{unob} = (o.c.a((\Sigma_*^p)^\perp))^\perp = span\{(0 \quad 1 \quad 0 \quad 0)^T, (1 \quad 0 \quad 0 \quad 0)^T\} \tag{4.48}$$

4.3.5 Fault detection and isolation filter design

The last step of this diagnosis approach consists on the designing of a residual generator which allows the detection and isolation of fault p_j from other faults and disturbances $p_k, (k \neq j)$. The method is based on the observability co-distribution Ω. Indeed, state and output diffeomorphisms can be determined, whose objective is to decouple a part of the state space from the faults $p_k, (k \neq j)$, using an output injection computed from the output diffeomorphism. The obtained sub-space is affected by the fault that we want to detect and isolate p_j and completely decoupled from other faults and disturbances $p_k, (k \neq j)$. In what follows the methodology to be followed to obtain this subsystem [92], [136], [137].

Consider system (4.14) and its observability codistribution Ω satisfying (4.35). Let n_1 denotes the dimension of Ω and suppose that $span\{dh\}$ is nonsingular. Let $p-n_2$ (where p represents the number of outputs) denotes the dimension of $\Omega \cap span\{dh\}$ and suppose that there exists a surjection $\psi_1 : \mathbb{R}^p \to \mathbb{R}^{p-n_2}$, such that

$$\Omega \cap span\{dh\} = span\{d(\psi_1 oh)\}. \tag{4.49}$$

If we fix $x^0 \in X$ and $y^0 = h(x^0)$. Then, there exists a selection matrix, H_2 (i.e., a matrix in which any row has all 0 entries but one, which is equal to 1), such that

$$\psi(y) = \begin{pmatrix} \tilde{y}_1 \\ \tilde{y}_2 \end{pmatrix} = \begin{pmatrix} \psi_1(y) \\ H_2 y \end{pmatrix} \tag{4.50}$$

is a local diffeomorphism at y^0 in $\mathbb{R}^p$. Choose a neighborhood U^0 of x^0 and a function $\phi_1 : U^0 \to \mathbb{R}^{n_1}$ such that

$$\Omega = span\{d\phi_1\} \tag{4.51}$$

at any point of U^0. Then, there exists a function $\phi_3 : U^0 \to \mathbb{R}^{n-n_1-n_2}$ such that

$$\phi(x) = \begin{pmatrix} \tilde{x}_1 \\ \tilde{x}_2 \\ \tilde{x}_3 \end{pmatrix} = \begin{pmatrix} \phi_1(x) \\ H_2 h(x) \\ \phi_3(x) \end{pmatrix} \tag{4.52}$$

is a local diffeomorphism at x^0 in X. In the new local coordinates defined by (4.50) and (4.52), system (4.14) is described by equations of the form ([137])

$$\begin{aligned} \dot{\tilde{x}}_1 &= f_{10}(\tilde{x}_1, \tilde{x}_2) + \sum_{i=1}^{m} g_{1i}(\tilde{x}_1, \tilde{x}_2)u_i + l_{1,1}(\tilde{x}_1, \tilde{x}_2, \tilde{x}_3)m_j \\ \dot{\tilde{x}}_2 &= f_{20}(\tilde{x}_1, \tilde{x}_2) + \sum_{i=1}^{m} g_{2i}(\tilde{x}_1, \tilde{x}_2)u_i + \sum_{i=1}^{d} l_{2,i}(\tilde{x}_1, \tilde{x}_2, \tilde{x}_3)m_j \\ \dot{\tilde{x}}_3 &= f_{30}(\tilde{x}_1, \tilde{x}_2) + \sum_{i=1}^{m} g_{3i}(\tilde{x}_1, \tilde{x}_2)u_i + \sum_{i=1}^{d} l_{3,i}(\tilde{x}_1, \tilde{x}_2, \tilde{x}_3)m_j \end{aligned} \tag{4.53}$$

It is clear that the subsystem $\tilde{x}_1$ is affected by the fault m_j but decoupled from others. Thus, the fault detection and isolation filter for the fault m_j is reduced to a simple construction of an observer for the subsystem $\tilde{x}_1$. By doing the same procedure to isolate each fault m_j, $(j = 1, ..., d)$, we construct d filters that detect and isolate each one.

Example : Follow with the previous example in order to design a residual generator that detect and isolate the fault m_1 from the disturbance m_2 following the steps announced above. The dimension of the observability codistribution is $n_1 = 2$. We have :

$$\begin{aligned} \Omega \cap span\{dh\} &= span\left\{\begin{pmatrix}0\\0\\1\\0\end{pmatrix}, \begin{pmatrix}2x_1x_4\\0\\0\\x_1^2\end{pmatrix}\right\} \cap span\left\{\begin{pmatrix}1\\0\\0\\0\end{pmatrix}, \begin{pmatrix}0\\0\\1\\0\end{pmatrix}, \begin{pmatrix}0\\0\\0\\1\end{pmatrix}\right\}, \\ &= span\left\{\begin{pmatrix}0\\0\\1\\0\end{pmatrix}, \begin{pmatrix}2x_1x_4\\0\\0\\x_1^2\end{pmatrix}\right\}, \end{aligned} \tag{4.54}$$

thus, $dim(\Omega \cap span\{dh\} = 2 = p - n_2$. Let $\Psi_1 : R^4 \to R^2$ such that the solution :

$$\Omega \cap span\{dh\} = span\{d(\Psi_1 \circ h)\}, \tag{4.55}$$

gives :

$$\Psi_1(h(x)) = \begin{pmatrix} y_2 \\ y_1^2 y_3 \end{pmatrix}, \tag{4.56}$$

and from equation (4.51), we obtain :

$$\Phi(x) = \begin{pmatrix} x_3 \\ x_1^2 x_4 \end{pmatrix}. \tag{4.57}$$

Choose the selection matrix $H_2 = (1 \quad 0 \quad 0)^T$. Thus, the state diffeomorphism is :

$$\begin{aligned} \tilde{x}_1 &= \begin{pmatrix} x_3 \\ x_1^2 x_4 \end{pmatrix} \\ \tilde{x}_2 &= x_1 \\ \tilde{x}_3 &= x_2 \end{aligned} \tag{4.58}$$

and the output diffeomorphism

$$\begin{aligned} \tilde{y}_1 &= \begin{pmatrix} y_2 \\ y_1^2 y_3 \end{pmatrix} \\ \tilde{y}_2 &= y_1. \end{aligned} \tag{4.59}$$

In the new coordinates defined by the state and the output diffeomorphism, the system can be written as :

$$\begin{aligned}\dot{\tilde{x}}_1 &= \begin{pmatrix} \dot{\tilde{x}}_{11} \\ \dot{\tilde{x}}_{12} \end{pmatrix} = \begin{pmatrix} \frac{\tilde{x}_{12}}{\tilde{x}_2^2} \\ a_2\tilde{x}_2u_2 + a_2\tilde{x}_2m_1 \end{pmatrix} \\ \dot{\tilde{x}}_2 &= \tilde{x}_3 \\ \dot{\tilde{x}}_3 &= \frac{a_2^2}{\tilde{x}_2^3} - \frac{a_1}{\tilde{x}_2^2} + a_2u_1 + m_2,\end{aligned} \tag{4.60}$$

and the output in the new coordinates :

$$\begin{aligned}\tilde{y}_1 &= \begin{pmatrix} \tilde{y}_{11} \\ \tilde{y}_{12} \end{pmatrix} = \begin{pmatrix} \tilde{x}_{11} \\ \tilde{x}_{12} \end{pmatrix} \\ \tilde{y}_2 &= \tilde{x}_2.\end{aligned} \tag{4.61}$$

Let the sub-system defined by the state $\tilde{x}_{12}$

$$\begin{cases} \dot{\tilde{x}}_{12} = a_2\tilde{x}_2u_2 + a_2\tilde{x}_2m_1 \\ \tilde{y}_2 = \tilde{x}_2. \end{cases} \tag{4.62}$$

The sub-system defined by the equations (4.62) is affected by the fault m_1 and completely decoupled from the disturbance m_2. As discussed above, a simple construction of an observer can be used as a residual generator. In this case, consider a Luenberger observer as cited in [92].

$$\begin{cases} \dot{z} = a_2y_2u_2 + k(y_2 - z) \\ r = y_2 - z, \end{cases} \tag{4.63}$$

with $k > 0$ is the observer gain. Let $e(t) = \tilde{x}_{12} - z$ be the estimation error. Its time derivative is :

$$\dot{e} = -ke + a_2y_2m_2, \tag{4.64}$$

The residual signal can be defined as $r(t) = e(t)$. In the absence of the fault and after the initialization error vanished, the residual tends to zero. But once the fault m_1 affects the system, the residual deviate from zero, indicating the presence of fault. Noticed that the residual is never affected by the disturbance.

4.4 Conclusion

In this chapter, a state of art of different diagnosis methods is presented. There are two main methods for fault detection and isolation in physical systems ; hardware redundancy and analytical redundancy. This later is based on the availability of an accurate mathematical model that describes the behavior of the system in a healthy situation as well as in a faulty situation to avoid false alarms. For this, an appropriate choice of approach is essential for the success of the diagnosis procedure. The choice is made on the geometrical approach which is based on partitioning the state space on several sub-spaces according to the faults scenario. This power approach has been the subject of the second part of this chapter. Where necessary

and sufficient conditions to a fundamental problem of residual generation are presented, which is related to a simple relation linked the distribution containing the fault effects that we want to detect and isolate and the minimal unobservability distribution containing the disturbance and other fault effects. To compute the observability co-distribution an algorithm is provided and due to its interesting properties, a methodology to construct a residual generator for fault detection and isolation is also presented. The next chapter is devoted to the application of the geometrical approach to carry out fault detection and isolation procedure for the 3-cell converter.

Chapter 5

Application to switch faults detection and isolation of 3-cell converter

Contents

5.1 Introduction

Safety and reliability are crucial for the operation of power electronics converters. Indeed, the continuous increase in the use of power converters in complex and sensitive industrial plants and the emergence of complex control techniques make it necessary to ensure its safety and reliability. Therefore, it becomes necessary to detect and isolate the faults in the power converters to prevent the system from unacceptable abnormal behaviors before any unexpected event, which can cause a lot of damage. In power electronics, we distinguish two types of faults, parameter faults, and discrete faults. Parameter faults depend mainly on the variation of certain parameters of the converter from their nominal values. Such faults are of low dynamics and can often be detected before the breakdown of the converter. Capacitance degradation of the 3-cell converter, due to multiple causes, such as high ambient temperature, high humidity [8], and aging of the capacitance are some examples of parameters faults. Discrete faults which include short and open-circuit of the converter cells are considered as hard faults and lead to a breakdown of the component if the fault is not detected on time. These faults are of high dynamics and are often difficult to handle to save the entire component [9]. In this chapter, the geometric approach to nonlinear fault detection and isolation is investigated to detect and isolate the discrete faults of the 3-cell converter. The approach is based on the computational of the observability co-distribution for each situation of faults, which leads to decoupling the system from a set of faults. An observer is then designed to complete the fault diagnosis of the considered faults.

5.2 An overview on fault diagnosis of power converter

Model-based diagnosis methods require a faulty model of the power converters in order to establish the detection and isolation procedure. Some works that treat this issues can be find in [142], where the authors proposed a uniform modeling method for open-circuit faults in the 3-NPC converter and was validated experimentally. Or as in [141] where the faulty model of the grid-connected converter is modeled as a nonlinear affine system. Using the recent theory of switched systems, the authors in [143] and [6] proposed a model-inversion-based approach for both linear and nonlinear switched systems, and provided conditions to uniquely recover the faults. The method was applied to the detection and isolation of both continuous and discrete faults of different switched electrical networks. Many approaches have been proposed to fault diagnosis of such parameter and discrete faults of different types of converters. In [144], a Luenberger observer is used for the detection and isolation of both parametric and discrete faults in a buck converter. The faults are identified by an appropriate choice of the filter gains. The same method was applied in [145] to AC-DC power converters. In [146], the authors proposed an approach to estimate the unmeasurable states and the switching signal of a networked switched systems by designing an event driven communication system and constructing an event driven asynchronous filter. The estimation of the switching signal can be used for the detection and isolation of the discrete faults. In [141], a very interesting geometric approach has been proposed and applied to both discrete and parametric fault diagnosis in a grid-connected inverter.

The p-cell converter consists of a series of p elementary cells of semiconductor devices that operate in a switched mode. It is considered as a switched system composed by 2^p discrete modes generated by the state of the cells. For control purposes, the control sequence is designed to ensure the voltage balancing and track the output current reference. In the healthy situation, the control sequence and the states of the switches are equal, whereas in discrete faulty mode, the expected control sequence and the state of the switches are different. Consequently, the control objectives are not achieved and can damage the semiconductor devices. Therefore, it is necessary to have reliable diagnosis tools to ensure good functioning of the converter and to protect not only the electrical devices that are connected to it and avoid the shutdown of the production, but also to protect the human operators around. In literature the diagnosis of the 3-cell converter is not yet well investigated, some works are appeared during the last decade. The diagnosis method proposed in [7] is based on comparison between the measured and the estimated state using a robust second-order sliding mode observer. Another approach based on the hybrid bond graph for each healthy and faulty situations has been proposed by [147]. The Signal Signature Study localization (SSS) procedure is based on analyzing the output voltage and the load current of the 3-cell converter for each considered faulty situation. In [148], the author propose a centralized approach to fault detection and isolation of the 3-cell converter. The authors in [149], proposed a decentralized approach for both discrete and parameter faults of the 3-cell converter using several local hybrid diagnosers. Recently, a scheme based on the use of unsupervised machine learning approach has been proposed in [150] to fault detection and isolation of both simple and multiple stuck opened and stuck closed of the switches of 3-cell converter.
In this chapter, we investigate the geometric approach presented in chapter four to detect and isolate switch faults of the three-cell converter. These type of faults are considered as discrete faults. Model-based fault detection and isolation approaches need a mathematical model to describe the effect of the discrete faults on the system. To this end, we develop a switched faulty model for the three-cell converter. By assuming measured state variables and non-simultaneous appearance of faults, an observability co-distribution is computed for the discrete faults subset. Based on this co-distribution and the corresponding subsystems, a residual generator based on Luenberger observer is then designed for each faulty situation. In the case where the load current is the unique available measurement, we provide a robust sliding mode observer to estimate the other state variables in finite-time. Sliding-mode-based residual generators are then proposed. Several simulation results are carried out to show the effectiveness of the proposed sliding-mode-based residual generators. Furthermore, the robustness is further illustrated against measurement noise, resistance uncertainty, and capacitor's degradation. A comparison between the two proposed types of residual generators is then carried out to distinguish which of the two residual generators is suitable for a reliable diagnostic procedure for the 3-cell converter.

5.3 Modeling discrete faults in the three-cell converter

Let consider the 3-cell converter depicted by figure (2.3). It consists of three elementary cells connected in series. Each elementary cell consists of a pair of two switches. The two switches

are always in opposite states, i.e., if the upper switch is opened (or closed) then the lower switch is closed (or opened). Since the switches work in commutation mode, then they are subject to the occurrence of faults. In this study, we are interesting on asymmetric faults that can affect a cell of the converter. Figures (5.1) and (5.2) depicts these situations of faults.

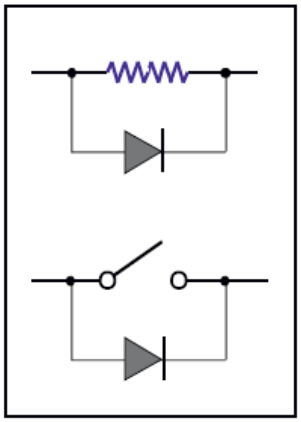

FIGURE 5.1: Asymmetric fault in switched cell $u_j = 1$

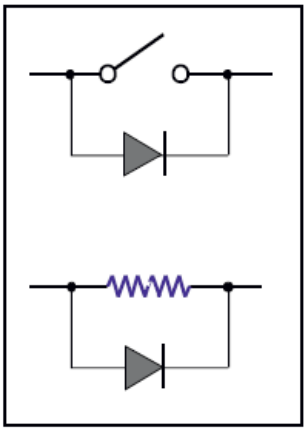

FIGURE 5.2: Asymmetric fault in switched cell $u_j = 0$

Thus, two types of faults can occur in each cell. The first situation as depicted by figure (5.1), the upper switch of j^{th} cell remains closed, while the lower switch of the same cell remains opened. We refer to this situation of fault as *"u_j stuck closed"*, $j = 1, 2, 3$. The occurrence of this type of fault in the cell means that the value of $u_j = 1$ permanently. Consequently, the upper switch of the j^{th} cell is permanently conducting, while the lower switch is non-conducting. The second situation which is depicted by figure (5.2) and that we refer to *"u_j stuck opened"*, the upper switch of j^{th} cell remains opened, while the lower switch of the same cell remains closed. In this case $u_j = 0$ permanently after the occurrence of the fault. And hence, the upper switch of the j^{th} cell is permanently non-conducting, while the lower switch is permanently conducting. In what follows, we will give a faulty model of the 3-cell converter that takes into account the considered faults. Let consider the instantaneous nonlinear affine model of 3-cell converter as described for p-cell converter given by equations (2.15), in absence of faults and disturbances the model can be written :

$$g_0(x) = \begin{pmatrix} 0 \\ 0 \\ -\frac{R}{L}x_3 \end{pmatrix}, g(x) = \begin{pmatrix} -\frac{x_3}{C_1} & \frac{x_3}{C_1} & 0 \\ 0 & -\frac{x_3}{C_2} & \frac{x_3}{C_2} \\ \frac{x_1}{L} & \frac{x_2-x_1}{L} & \frac{E-x_2}{L} \end{pmatrix}, \tag{5.1}$$

where $g(x) = [g_1(x), g_2(x), g_3(x)]$ and $x \in \mathbb{R}^3$ is the state vector such that $x_1 = v_{c1}$, $x_2 = v_{c2}$ and $x_3 = i_l$ are, the voltage across the capacitors C_1 and C_2, and the load current, respectively, $u = [u_1, u_2, u_3]^T$ is the binary control input and E is the voltage source . For fault diagnosis purposes, we suppose that all states are available for measurement or estimated in finite time by a robust observer against the faults if some states are not measurable. In the case where all states are measured, the output equation is

$$h(x) = \begin{pmatrix} y_1 \\ y_2 \\ y_3 \end{pmatrix} = \begin{pmatrix} x_1 \\ x_2 \\ x_3 \end{pmatrix} \tag{5.2}$$

In the healthy situation, the control sequence and the states of the switches are equal, whereas in discrete faulty mode, the expected control sequence and the state of the switches are different. Denote by u_j^f as the faulty value of the switch states for $j = 1, 2, 3$, and by m_j the fault that can affect u_j. Then, the faulty model of three-cell converter becomes :

$$\begin{cases} \dot{x} = g_0(x) + \sum_{i=1}^{3} g_i(x) u_i^f \\ y = h(x), \end{cases} \tag{5.3}$$

with

$$u_j^f = 1 \Rightarrow m_j = \begin{cases} 0 & \text{if } u_j = 1 \\ 1 & \text{if } u_j = 0 \end{cases} \qquad j = 1, 2, 3, \tag{5.4}$$

$$u_j^f = 0 \Rightarrow m_j = \begin{cases} 0 & \text{if } u_j = 0 \\ -1 & \text{if } u_j = 1 \end{cases} \qquad j = 1, 2, 3, \tag{5.5}$$

From (5.4) and (5.5), the faulty value of each cell can be expressed as

$$u_j^f = u_j + m_j, \qquad j = 1, 2, 3, \tag{5.6}$$

where $m_j \in \{0, 1, -1\}$ represents the discrete fault of the cell j. If $m_j = 0$, then $u_j^f = u_j$ which correspond to $u_j^f = u_j$ and no fault occur in the cell j. However, if $m_j = 1$ or $m_j = -1$ this correspond to the occurrence of a fault in the cell j. For instance, if the control sequence $u_j = 1, 1, 0, 1, 0$ and $u_j^f = 1$, i.e., the cell j^{th} stuck opened all the time, then $m_j = 0, 0, 1, 0, 1$. Moreover, if $u_j^f = 0$, i.e., the j^{th} cell stuck closed, then $m_j = -1, -1, 0, -1, 0$. From this analysis, the detection and the isolation of real fault u_j^f, $(j = 1, 2, 3)$ is equivalent to the detection and the isolation of m_j, $(j = 1, 3)$. The latter is given by

$$m_j = u_j^f - u_j, \tag{5.7}$$

Using (5.3) and (5.6), the faulty model of the three-cell converter can be described as :

$$\begin{cases} \dot{x} = g_0(x) + \sum_{i=1}^{3} g_i(x) u_i + \sum_{i=1}^{3} g_i(x) m_i \\ y = h(x), \end{cases} \tag{5.8}$$

In the following section by using the model (5.8) in simulation environment, we analyze the evolution of the floating voltages of the converter for all fault situations.

5.4 Functional analysis of the 3-cell converter in failure mode

Table (5.1) depicts the evolution of the floating voltages v_{c_1} and v_{c_2} and the load current i_L of the 3-cell converter in a healthy mode. This will be useful when analyzing the floating voltages evolution in failure mode.

operating modes		q_1	q_2	q_3	q_4	q_5	q_6	q_7	q_8
cell states	u_1	0	1	0	1	0	1	0	1
	u_2	0	0	1	1	0	0	1	1
	u_3	0	0	0	0	1	1	1	1
state evolution	v_{c_1}	→	↘	↗	→	→	↘	↗	→
	v_{c_2}	→	→	↘	↘	↗	↗	→	→
	i_L	↘	↗↘	↗↘	↗↘	↗↘	↗↘	↗↘	↗

TABLE 5.1: Evolution of state variables of 3-cell converter in each operating mode in healthy mode. → : constant, ↗ : increase and ↘ : decrease.

u_1 stuck closed : When a fault occurs causing the first cell stuck closed, the number of operating modes in failure mode will be reduced to a four modes despite of eight. According to table (5.2), the set of operating modes and as depicted by hybrid automaton in figure (5.3) is $Q_{u_1=1} = \{q_2, q_4, q_6, q_8\}$.

healthy mode		q_1	q_2	q_3	q_4	q_5	q_6	q_7	q_8
cell states	u_1	1	1	1	1	1	1	1	1
	u_2	0	0	1	1	0	0	1	1
	u_3	0	0	0	0	1	1	1	1
failure mode		q_2	q_2	q_4	q_4	q_6	q_6	q_8	q_8

TABLE 5.2: Operating modes when u_1 stuck closed.

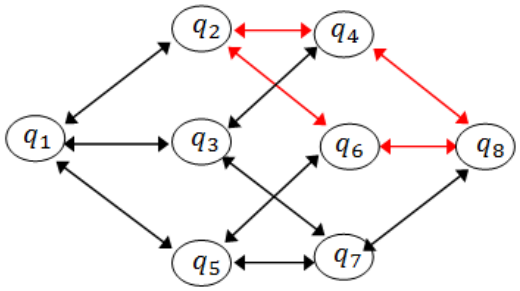

FIGURE 5.3: Hybrid trajectory in failure mode u_1 stuck closed (in red color)

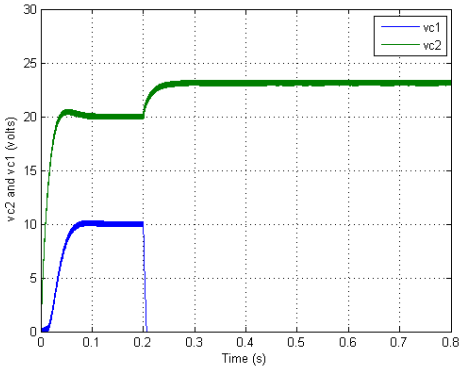

FIGURE 5.4: v_{c_1} and v_{c_2} in failure mode u_1 stuck closed

According to table (5.1), by analyzing the evolution of the floating voltage v_{c_1} over the operating modes in failure situation, we can notice that v_{c_1} is either it remains constant, either it decreases over time. Thus, The floating voltage v_{c_1} has a trend to decrease in this faulty mode. Furthermore, the dynamic equation of the v_{c_1} in this faulty situation is $\dot{v}_{c_1} = \frac{1}{C_1}(u_2 - 1)i_L$

The load current evolves on the interval $[I_{min}, I_{max}]$, and assuming that $I_{min} \geq 0$, therefore, $i_L > 0$ over the time. Thus, $\forall u_2 \in \{0, 1\}, \dot{v}_{c_1} \leq 0$, which explains the gradually decreasing

of v_{c_1} as depicted by figure (5.4) . However, the dynamic equation of the floating voltage v_{c_2} is $\dot{v}_{c_2} = \frac{1}{C_2}(u_3 - u_2)i_L$. $\dot{v}_{c_2}$ can be less or greater than zero according to u_2 and u_3, then it depends on the applied control law. Figure (5.4) shows the evolution of v_{c_2}, where it increase until it reaches a certain value without reaching E.

u_2 stuck closed : The appearance of fault causing the cell two remains closed, reduced the number of operating modes to $Q = \{q_3, q_4, q_7, q_8\}$ as reported in table (5.3).

healthy mode		q_1	q_2	q_3	q_4	q_5	q_6	q_7	q_8
cell states	u_1	0	1	0	1	0	1	0	1
	u_2	1	1	1	1	1	1	1	1
	u_3	0	0	0	0	1	1	1	1
failure mode		q_3	q_4	q_3	q_4	q_7	q_8	q_7	q_8

TABLE 5.3: Operating modes in failure mode of the first switching cell (u_2 stuck closed).

The hybrid automaton in this faulty case is depicted by figure (5.5). The dynamic equation of v_{c_1} in this situation is $\dot{v}_{c_1} = \frac{1}{C_1}(1 - u_1)i_L$, and since $i_L \geq 0$, $\forall u_1 \in \{0, 1\}$, $\dot{v}_{c_1} \geq 0$, i.e., v_{c_1} is increasing over the times to stabilize to an other value greater than $V_{c_{ref1}} = 10volts$. From a practical point of view, this can be explained by the presence of modes q_3 and q_7 that offer the possibility to increase the voltage v_{c_1}, and the total absence of modes that decrease the voltage.

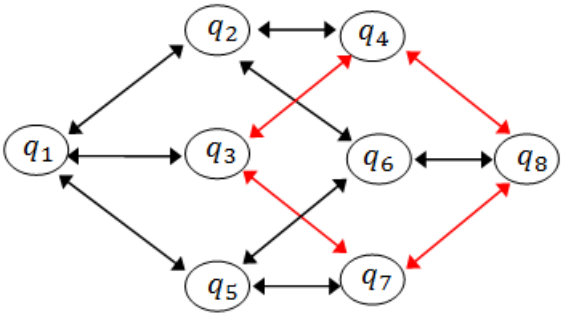

FIGURE 5.5: Hybrid trajectory in failure mode u_2 stuck closed (in red color)

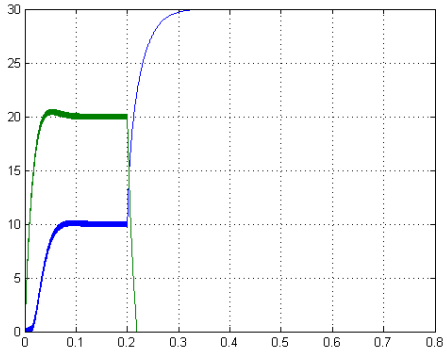

FIGURE 5.6: v_{c_1} and v_{c_2} in failure mode u_2 stuck closed

Whereas, the dynamic equation of v_{c_2} is $\dot{v}_{c_2} = \frac{1}{C_2}(u_3 - 1)i_L$. And $\forall \quad u_3 \in \{0, 1\}$, $\dot{v}_{c_2} \leq 0$, which it means that v_{c_2} decrease until it reaches the origin. This decreasing can be explained by the presence of modes q_3 and q_4 that have trends to decrease the floating voltage v_{c_2}. Simulation results depicted in figure (5.6) show the evolution of the two floating voltages.

u_3 stuck closed : In this case of fault, the operating set is reduced to $Q_{u_3=1} = \{q_5, q_6, q_7, q_8\}$ as reported by table (5.4), and depicted by the hybrid automaton given by figure (5.7). The source voltage is abundantly connected to the floating capacitor C_2. Consequently, C_2 will be charged until it reaches $E = 30volts$. This is explained by the presence of operating modes

q_5 and q_6 that are trends to increase the voltage v_{c_2}. The dynamic evolution of v_{c_2} is given as $\dot{v}_{c_2} = \frac{1}{C_2}(1-u_2)i_L$. Hence, $\forall \quad u_2 \in \{0,1\}$, $\dot{v}_{c_2} \geq 0$ over the time, hence, v_{c_2} increase. Figure (5.8) shows the evolution of the voltage v_{c_2} in this case of fault.

healthy mode		q_1	q_2	q_3	q_4	q_5	q_6	q_7	q_8
	u_1	0	1	0	1	0	1	0	1
cell states	u_2	0	0	1	1	0	0	1	1
	u_3	1	1	1	1	1	1	1	1
failure mode		q_5	q_6	q_7	q_8	q_5	q_6	q_7	q_8

TABLE 5.4: Operating modes in failure mode of the third switching cell (u_3 stuck closed).

Whereas, the dynamic equation of v_{c_1} is $\dot{v}_{c_1} = \frac{1}{C_1}(u_2-u_1)i_L$, its sign depends on u_1 and u_2. Indeed, the floating voltage v_{c_1} increases if the remaining modes containing on the hybrid trajectory after the appearance of the fault, have the trends to elevate it. Otherwise, v_{c_1} decreases. Simulation results depicted in figure (5.8) show the evolution of the floating voltages v_{c_1}.

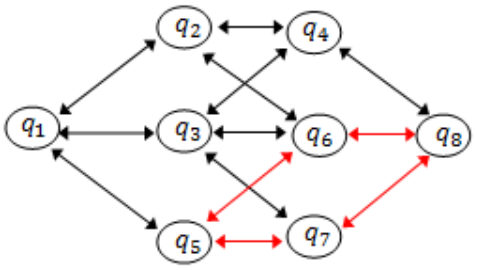

FIGURE 5.7: Hybrid trajectory in failure mode u_3 stuck closed (in red color)

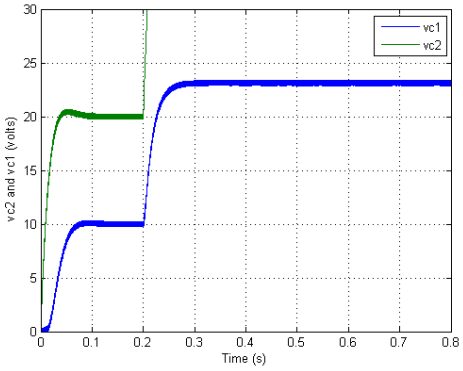

FIGURE 5.8: v_{c_1} and v_{c_2} in failure mode u_3 stuck closed

u_1 stuck opened : The occurrence of a fault causing the cell one to remain opened (u_1 stuck opened) leads to the following set of operating modes $Q_{u_1=0} = \{q_1, q_3, q_5, q_7\}$ as indicated by the table (5.5).

healthy mode		q_1	q_2	q_3	q_4	q_5	q_6	q_7	q_8
	u_1	0	0	0	0	0	0	0	0
cell states	u_2	0	0	1	1	0	0	1	1
	u_3	0	0	0	0	1	1	1	1
failure mode		q_1	q_1	q_3	q_3	q_5	q_5	q_7	q_7

TABLE 5.5: Operating modes in failure mode of the first switching cell (u_1 stuck opened).

From a practical point of view, the capacitor C_1 is charging over the times and it can never

discharging. The dynamic equation of its floating voltage is $\dot{v}_{c_1} = \frac{1}{C_1} u_2 i_L$. Therefore, $\forall u_2 \in \{0,1\}, \quad \dot{v}_{c_1} \geq 0$, which implies that v_{c_1} increases until reaches the source voltage $E = 30volts$. This is explained by the presence of modes q_3 and q_7 that offer the possibility to increase the voltage v_{c_1}. Whereas, the dynamic equation of the floating voltage v_{c_2} is $\dot{v}_{c_2} = \frac{1}{C_2}(u_3 - u_2) i_L$, its sign depends on u_2 and u_3, it increases if the remaining modes in faulty situation have trends to increase the voltage, otherwise it decreases. The simulation results shown in figure (5.10) depicts the evolution of the floating voltages v_{c_1} and v_{c_2}.

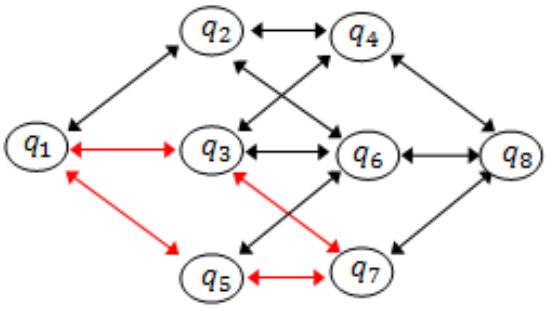

FIGURE 5.9: Hybrid trajectory in failure mode u_1 stuck opened (in red color)

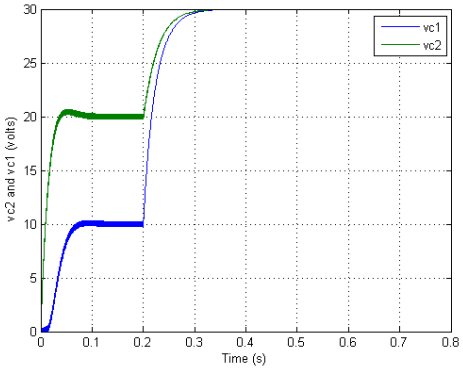

FIGURE 5.10: v_{c_1} and v_{c_2} in failure mode u_1 stuck opened

u_2 stuck opened : Table (5.6) gives the operating modes in the case of occurrence of fault causing the cell two to remain opened. The set of operating modes in this case is $Q = \{q_1, q_2, q_5, q_6\}$. The hybrid automaton in this failure situation is given by figure (5.11).

healthy mode		q_1	q_2	q_3	q_4	q_5	q_6	q_7	q_8
cell states	u_1	0	1	0	1	0	1	0	1
	u_2	1	1	1	1	1	1	1	1
	u_3	0	0	0	0	1	1	1	1
failure mode		q_1	q_2	q_1	q_2	q_5	q_6	q_5	q_6

TABLE 5.6: Operating modes in failure mode of the second switching cell (u_2 stuck opened).

Practically, in this failure mode, the capacitor C_1 is discharging across the load R-L and never it can be charged. Thus, v_{c_1} decreases until it reaches zero. Its dynamic equation is $\dot{v}_{c_1} = -\frac{1}{C_1} u_1 i_L$. And it is clear that $\dot{v}_{c_1} \leq 0, \quad \forall u_1 \in \{0,1\}$, which explains the decreasing of v_{c_1}. This is due essentially to the operation of the converter in modes q_2 and q_6 that offer the possibility to decrease the voltage v_{c_1}, and while q_1 and q_5 keep it constant. Figure (5.12) shows effectively the decreasing of v_{c_1}.
Whereas, the dynamic equation of v_{c_2} is $\dot{v}_{c_2} = \frac{1}{C_2} u_3 i_L$. Thus, $\dot{v}_{c_2} \geq 0, \quad \forall u_3 \in \{0,1\}$. Which explains its increasing until reaching the value of the source voltage E, as shown in figure (5.12). This is can be explained by the presence of modes q_5 and q_6 that increase the voltage v_{c_2}.

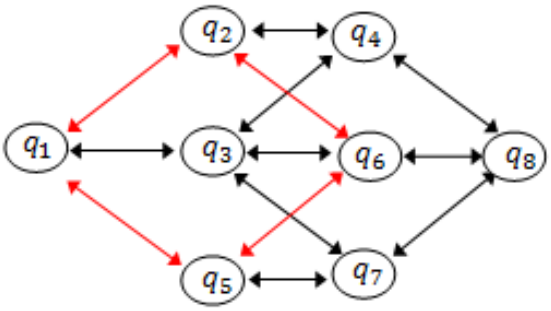

FIGURE 5.11: Hybrid trajectory in failure mode u_2 stuck opened (in red color)

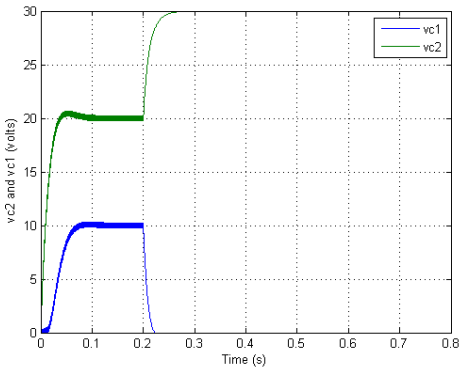

FIGURE 5.12: v_{c_1} and v_{c_2} in failure mode u_2 stuck opened

u_3 stuck opened : Table (5.7) gives the operating modes in the case of occurrence of fault causing the cell three to remain opened. The set of operating modes is reduced to $Q_{u_3=0} = \{q_1, q_2, q_3, q_4\}$. The hybrid automaton in this failure situation is given in figure (5.13).

healthy mode		q_1	q_2	q_3	q_4	q_5	q_6	q_7	q_8
	u_1	0	1	0	1	0	1	0	1
cell states	u_2	0	0	1	1	0	0	1	1
	u_3	0	0	0	0	0	0	0	0
failure mode		q_1	q_2	q_3	q_4	q_1	q_2	q_3	q_4

TABLE 5.7: Operating modes in failure mode of the third switching cell (u_3 stuck opened).

From point of view, once the cell three stuck opened, which means that the source energy E is disconnected from the converter and no energy is provided to the converter. The stored energy in capacitors C_1 and C_2 will be consumed by the load. Hence, v_{c_1} and v_{c_2} are discharging over the time until reaching the origin.

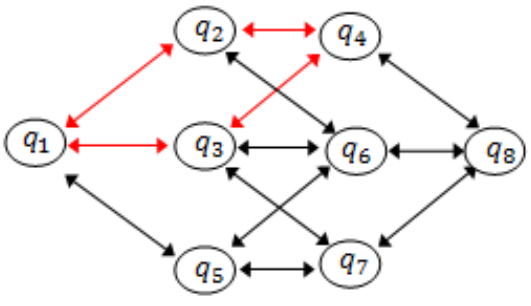

FIGURE 5.13: Hybrid trajectory in failure mode u_3 stuck opened (in red color)

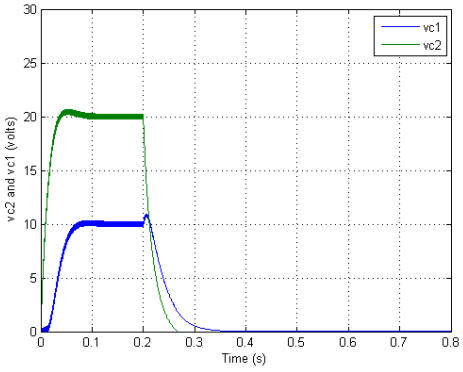

FIGURE 5.14: v_{c_1} and v_{c_2} in failure mode u_3 stuck opened

The dynamic equation of v_{c_2} is $\dot{v}_{c_2} = -\frac{1}{C_2} u_2 i_L$. This later is less than zero $\forall u_2 \in \{0, 1\}$, which explains the decreasing of the voltage v_{c_2}. Simulation results depicted in figure (5.14)

show the decreasing of the floating voltages v_{c_1} and v_{c_2} in this failure mode.

5.5 Application of the geometric approach to FDI of switched faults of the three-cell converter

The ideal case to faults detection and isolation procedure is that each generated residual signal is only affected by one fault, and each fault affects only one residual. Unfortunately, in most diagnosis applications, this is not always possible due to the coupling of the model. In the 3-cell converter, the ideal case is the isolation of one fault from two others, and generate 3 residuals, each one is sensitive only to one fault. Consequently, the isolation of instantaneous faults can be possible. For that, the application of the geometrical approach does not give a solution to a fundamental problem of residual generation, which means the non-existence of an output injection that decouple a part of the system sensitive only to one fault and insensitive to two others, and this is due to the non-satisfaction of the condition (4.35). Later, the idea that we have suggested is the isolation of two faults from one, i.e., generating residuals such that each residual is sensitive to two faults and insensitive to one fault. The isolation conditions, in this case, are fulfilled, but the isolation of the instantaneous occurrence of faults is not possible. For that, we proceed by decoupling a set of two faults from one. More precisely, for the proposed application we generate three scalar residuals, each one detects any faults from the set of faults whose the residual is sensitive. The isolation is ensured by analyzing residuals vector (The three generated residuals) but assuming the occurrence of only one fault. To this end, and to have decoupled structure from a set of faults, we define three sets of faults : $\Delta_1 = \{m_1(t), m_3(t)\}$, $\Delta_2 = \{m_2(t), m_3(t)\}$ and $\Delta_3 = \{m_1(t), m_2(t)\}$. We will generate three residuals $r_1(t)$, $r_2(t)$ and $r_3(t)$, each one is affected only by a single set of faults. The isolation of each discrete fault is carried out by analyzing the three residuals.

5.5.1 Decoupling faults

a- Isolation of $m_1(t), m_3(t)$ from $m_2(t)$: In order to obtain a sub-system sensitive to set of faults $\Delta_1 = \{m_1(t), m_3(t)\}$ and insensitive to fault $m_2(t)$, as a first step, we compute using (4.19), the minimal conditioned invariant distribution $\sum_*^{p_2}$ containing $P = span\{p_2(x)\}$. Let :

$$P_{13} = span\{g_2(x)\} = span\{(\tfrac{1}{C_1}x_3 \quad -\tfrac{1}{C_2}x_3 \quad \tfrac{1}{L}(x_2 - x_1)^T\} \ , \tag{5.9}$$

$$L = span\{g_1(x), g_3(x)\} = span\left\{\begin{pmatrix} -\frac{1}{C_1}x_3 \\ 0 \\ \frac{1}{L}x_1 \end{pmatrix}, \begin{pmatrix} 0 \\ \frac{1}{C_2}x_3 \\ \frac{1}{L}(E - x_2) \end{pmatrix}\right\} \tag{5.10}$$

and we have

$$span\{dh\} = span\{(1 \quad 0 \quad 0)^T, (0 \quad 1 \quad 0)^T, (0 \quad 0 \quad 1)^T\} \tag{5.11}$$

$\Rightarrow ker\{dh\} = \{0\}$. Hence, $\bar{D_i^P} \cap ker\{dh\} = 0 \Rightarrow [g_k(x), \bar{D}_i \cap ker\{dh\}] = \{0\}, \forall i, k$. Consequently, the algorithm (4.19) stop for $k = 0$, yielding

$$\Sigma^{P_{13}} = span\{g_2(x)\} = span\{(\tfrac{1}{C_1}x_3 \quad -\tfrac{1}{C_2}x_3 \quad \tfrac{1}{L}(x_2 - x_1))^T\}. \tag{5.12}$$

which is trivially involutive. Applying (4.33) to compute the observability codistribution. The orthogonal codistribution of $\Sigma^{P_{13}}$ is :

$$\left(\Sigma^{P_{13}}\right)^{\perp} = span\left\{\begin{pmatrix} \frac{C_1}{C_2} \\ 1 \\ 0 \end{pmatrix}, \begin{pmatrix} \frac{1}{LC_2}x_1 \\ \frac{1}{LC_1}x_2 \\ \frac{1}{C_1C_2}x_3 \end{pmatrix}\right\}. \tag{5.13}$$

Notice that $\left(\Sigma^{P_{13}}\right)^{\perp} \subset span\{dh\}$. At the first step Q_0 is given by

$$\begin{aligned} Q_0 &= \left(\Sigma^{P_{13}}\right)^{\perp} \cap span\{dh\} = \left(\Sigma^{P_{13}}\right)^{\perp} \\ &= span\{w_{01}, w_{02}\}. \end{aligned} \tag{5.14}$$

Then,

$$\begin{aligned} Q_1 &= \left(\Sigma^{P_{13}}\right)^{\perp} \cap \left(\sum_{i=0}^{3} L_{g_i}Q_0 + span\{dh\}\right) \\ &= \left(\Sigma^{P_{13}}\right)^{\perp} \cap \left(Q_0 + \sum_{i=0}^{3} L_{g_i}Q_0 + span\{dh\}\right). \end{aligned} \tag{5.15}$$

We have $Q_0 + L_{g_i}Q_0 = span\{w_{01}, w_{02}, L_{g_i}w_{01}, L_{g_i}w_{02}\}, \quad i = 1, 2, 3$, such that :

$$\begin{aligned} &L_{g_0}w_{01} = L_{g_2}w_{01} = L_{g_1}w_{02} = L_{g_2}w_{02} = 0, \\ &L_{g_1}w_{01} = \begin{pmatrix} 0 & 0 & -\frac{1}{C_2} \end{pmatrix}, \\ &L_{g_3}w_{01} = \begin{pmatrix} 0 & 0 & \frac{1}{C_2} \end{pmatrix}, \\ &L_{g_0}w_{02} = \begin{pmatrix} 0 & 0 & -\frac{2R}{LC_1C_2} \end{pmatrix}, \\ &L_{g_3}w_{02} = \begin{pmatrix} 0 & 0 & \frac{E}{LC_1C_2} \end{pmatrix}. \end{aligned}$$

Notice that all $L_{g_i}w_{0j} \in span\{dh\}$, for $i = 1, ..., 3$ and $j = 1, 2$. We conclude that $Q_1 = Q_0$. Thus,

$$o.c.a\left(\left(\Sigma^{P_{13}}\right)^{\perp}\right) = span\left\{\begin{pmatrix} \frac{C_1}{C_2} \\ 1 \\ 0 \end{pmatrix}, \begin{pmatrix} \frac{1}{LC_2}x_1 \\ \frac{1}{LC_1}x_2 \\ \frac{1}{C_1C_2}x_3 \end{pmatrix}\right\}, \tag{5.16}$$

which represents the observability codistribution. The fulfillment of the condition (4.35) can be easily verified.

$$L = span\{g_1(x), g_3(x)\} \nsubseteq \left(oca\left(\left(\Sigma^{P_{13}}\right)^{\perp}\right)\right)^{\perp}. \tag{5.17}$$

Therefore, A filter for the fault diagnosis exists. Let $n_1 = dim(oca((\Sigma^{P_{13}})^{\perp})) = 2$ and $(oca((\Sigma^{P_{13}}))^{\perp}) \cap span\{dh\} = (oca((\Sigma^{P_{13}})^{\perp}))$. Hence, $p - n_2 = 2$, where $p = 3$ represents the number of outputs, yielding $n_2 = 1$. Let $\psi_1 : \mathbb{R}^3 \to \mathbb{R}^2$ be a surjection that satisfies (4.49) defined as follow

$$\psi_1(y) = \begin{pmatrix} \frac{C_1}{C_2}y_1 + y_2 \\ \frac{1}{2LC_2}y_1^2 + \frac{1}{2LC_1}y_2^2 + \frac{1}{2C_1C_2}y_3^2 \end{pmatrix} \tag{5.18}$$

and, to satisfy (4.51), ϕ_1 can be chosen such that

$$\phi_1(x) = \begin{pmatrix} \frac{C_1}{C_2}x_1 + x_2 \\ \frac{1}{2LC_2}x_1^2 + \frac{1}{2LC_1}x_2^2 + \frac{1}{2C_1C_2}x_3^2 \end{pmatrix}, \tag{5.19}$$

and the selection matrix $H_2(1 \times 3)$ is

$$H_2 = \begin{pmatrix} 1 & 0 & 0 \end{pmatrix}. \tag{5.20}$$

The output diffeomorphism and the state diffeomorphism are then, respectively,

$$\begin{aligned} \psi(y) &= \begin{pmatrix} \tilde{y_1} \\ \tilde{y_2} \\ \tilde{y_3} \end{pmatrix} = \begin{pmatrix} \psi_1(y) \\ H_2 y \end{pmatrix} \\ &= \begin{pmatrix} \frac{C_1}{C_2}y_1 + y_2 \\ \frac{1}{2LC_2}y_1^2 + \frac{1}{2LC_1}y_2^2 + \frac{1}{2C_1C_2}y_3^2 \\ y_1 \end{pmatrix} \end{aligned} \tag{5.21}$$

and

$$\begin{aligned} \phi(x) &= \begin{pmatrix} \tilde{x}_1 \\ \tilde{x}_2 \\ \tilde{x}_3 \end{pmatrix} = \begin{pmatrix} \phi_1(x) \\ H_2 h(x) \end{pmatrix} \\ &= \begin{pmatrix} \frac{C_1}{C_2}x_1 + x_2 \\ \frac{1}{2LC_2}x_1^2 + \frac{1}{2LC_1}x_2^2 + \frac{1}{2C_1C_2}x_3^2 \\ x_1 \end{pmatrix}. \end{aligned} \tag{5.22}$$

Since $rank(\frac{d\phi}{dt}) = 3$, ϕ_3 is not needed to be added. Let then

$$z_1 = \frac{C_1}{C_2}x_1 + x_2. \tag{5.23}$$

The time derivative of z_1 gives

$$\dot{z}_1 = \frac{x_3}{C_2}(u_3 - u_1) + \frac{x_3}{C_2}(m_3 - m_1). \tag{5.24}$$

As expected, the above system is affected by the faults m_1 and m_3 and unaffected by the fault m_2. We therefore focus on it to design a residual generator that should be sensitive to faults m_1 and m_3 and insensitive to fault m_2.

b- Isolation of m_2 and m_3 from m_1 : Using the same procedure as above to obtain a sub-system sensitive to a set faults $\Delta_2 = \{m_2(t), m_3(t)\}$, and insensitive to a fault $m_1(t)$. Let

$$P_{23} = span\{g_1(x)\} = span\{(-\tfrac{1}{C_1}x_3 \quad 0 \quad \tfrac{1}{L}x_1)^T\} \tag{5.25}$$

and

$$L = span\left\{\begin{pmatrix} \frac{1}{C_1}x_3 \\ -\frac{1}{C_2}x_3 \\ \frac{1}{L}(x_2 - x_1)) \end{pmatrix}, \begin{pmatrix} 0 \\ \frac{1}{C_2}x_3 \\ \frac{1}{L}(E - x_2) \end{pmatrix}\right\}. \tag{5.26}$$

The corresponding conditioned invariant distribution is given by

$$\Sigma^{P_{23}} = span\{(-\tfrac{1}{C_1}x_3 \quad 0 \quad \tfrac{1}{L}x_1)^T\}\ , \tag{5.27}$$

and its orthogonal distribution is

$$\left(\Sigma^{P_{23}}\right)^{\perp} = span\left\{\begin{pmatrix} 0 \\ 1 \\ 0 \end{pmatrix}, \begin{pmatrix} \frac{1}{L}x_1 \\ 0 \\ \frac{1}{C_1}x_3 \end{pmatrix}\right\}. \tag{5.28}$$

Hence

$$\begin{aligned} Q_0 &= \left(\Sigma^{P_{23}}\right)^{\perp} \cap\ span\{dh\} = \left(\Sigma^{P_{23}}\right)^{\perp} \\ &= span\{w_{11}, w_{12}\}. \end{aligned} \tag{5.29}$$

The obtained vector fields for $i = 0, 1, 2, 3$ are

$$\begin{aligned} &L_{g_0}w_{11} = L_{g_1}w_{11} = L_{g_1}w_{12} = 0, \\ &L_{g_2}w_{11} = \begin{pmatrix} 0 & 0 & -\frac{1}{C_2} \end{pmatrix}, \\ &L_{g_3}w_{11} = \begin{pmatrix} 0 & 0 & \frac{1}{C_2} \end{pmatrix}, \\ &L_{g_0}w_{12} = \begin{pmatrix} 0 & 0 & -\frac{2R}{LC_1}x_3 \end{pmatrix}, \\ &L_{g_2}w_{12} = \begin{pmatrix} 0 & \frac{1}{LC_1}x_3 & \frac{1}{LC_1}x_2 \end{pmatrix}, \\ &L_{g_3}w_{12} = \begin{pmatrix} 0 & -\frac{1}{LC_1}x_3 & \frac{1}{LC_1}(E - x_2) \end{pmatrix}. \end{aligned}$$

Finally the observability codistribution is given by

$$\Omega = oca\left(\left(\Sigma^{P_{23}}\right)^{\perp}\right) = span\left\{\begin{pmatrix} 0 \\ 1 \\ 0 \end{pmatrix}, \begin{pmatrix} \frac{1}{L}x_1 \\ 0 \\ \frac{1}{C_1}x_3 \end{pmatrix}\right\}. \tag{5.30}$$

The condition (4.35) is satisfied, i.e.,

$$L = span\left\{g_2(x), g_3(x)\right\} \nsubseteq \left(oca\left(\left(\Sigma^{P_{23}}\right)^{\perp}\right)\right)^{\perp}. \tag{5.31}$$

As before, let $n_1 = dim(oca((\Sigma_*^{p_{23}})^{\perp})) = 2$ and $(oca((\Sigma^{P_{23}}))^{\perp}) \cap span\{dh\} = (oca((\Sigma^{P_{23}})^{\perp}))$. Hence $p - n_2 = 2$. Let $\psi_1 : \mathbb{R}^3 \to \mathbb{R}^2$ be a surjection that satisfies the condition (4.49) such as

$$\psi_1(y) = \begin{pmatrix} y_2 \\ \frac{1}{2L}y_1^2 + \frac{1}{2C_1}y_3^2 \end{pmatrix}. \tag{5.32}$$

To satisfy condition (4.51), let the function ϕ_1 be

$$\phi_1(x) = \begin{pmatrix} x_2 \\ \frac{1}{2L}x_1^2 + \frac{1}{2C_1}x_3^2 \end{pmatrix}. \tag{5.33}$$

We can choose

$$H_2 = \begin{pmatrix} 0 & 0 & 1 \end{pmatrix}. \tag{5.34}$$

The output and the state diffeomorphisms are respectively

$$\psi(y) = \begin{pmatrix} \tilde{y}_1 \\ \tilde{y}_2 \\ \tilde{y}_3 \end{pmatrix} = \begin{pmatrix} \psi_1(y) \\ H_2 y \end{pmatrix} = \begin{pmatrix} y_2 \\ \frac{1}{2L}y_1^2 + \frac{1}{2C_1}y_3^2 \\ y_3 \end{pmatrix}, \tag{5.35}$$

and

$$\phi(x) = \begin{pmatrix} \tilde{x}_1 \\ \tilde{x}_2 \\ \tilde{x}_3 \end{pmatrix} = \begin{pmatrix} \phi_1(x) \\ H_2 h(x) \end{pmatrix} = \begin{pmatrix} x_2 \\ \frac{1}{2L}x_1^2 + \frac{1}{2C_1}x_3^2 \\ x_3 \end{pmatrix}. \tag{5.36}$$

Let

$$z_2 = x_2. \tag{5.37}$$

Then,

$$\dot{z}_2 = \frac{x_3}{C_2}(u_3 - u_2) + \frac{x_3}{C_2}(m_3 - m_2). \tag{5.38}$$

As expected, the above system is affected by faults $m_2(t)$ and $m_3(t)$ and unaffected by fault $m_1(t)$. Starting from this sub system to construct a residual generator affected by faults $m_2(t)$ and $m_3(t)$ and completely decoupled from the effect of the fault $m_1(t)$.

c- Isolation of m_1 and m_2 from m_3 : We follow the same steps as before and is briefly given below to obtain a sub-system sensitive to set faults $\Delta_3 = \{m_1(t), m_2(t)\}$ and insensitive to $m_3(t)$. Let

$$P_{12} = span\{g_3(x)\} = span\{(-\tfrac{1}{C_1}x_3 \quad 0 \quad \tfrac{1}{L}x_1)^T\} \tag{5.39}$$

and

$$L = span\left\{ \begin{pmatrix} -\frac{1}{C_1}x_3 \\ 0 \\ \frac{1}{L}x_1 \end{pmatrix}, \begin{pmatrix} \frac{1}{C_1}x_3 \\ -\frac{1}{C_2}x_3 \\ \frac{1}{L}(x_2 - x_1) \end{pmatrix} \right\}. \tag{5.40}$$

Then

$$\Sigma^{P_{12}} = span\{(0 \quad -\tfrac{1}{C_2}x_3 \quad \tfrac{1}{L}(E - x_2))^T\}\ , \tag{5.41}$$

its orthogonal distribution is

$$\left(\Sigma^{P_{12}}\right)^{\perp} = span\left\{ \begin{pmatrix} 1 \\ 0 \\ 0 \end{pmatrix}, \begin{pmatrix} 0 \\ \frac{1}{L}(x_2 - E) \\ \frac{1}{C_2}x_3 \end{pmatrix} \right\}. \tag{5.42}$$

Applying algorithm (4.33), at the first step Q_0 is

$$\begin{aligned} Q_0 &= \left(\Sigma^{P_{12}}\right)^{\perp} \cap \ span\{dh\} = \left(\Sigma^{P_{12}}\right)^{\perp} \\ &= span\{w_{21}, w_{22}\}, \end{aligned} \tag{5.43}$$

then

$$\begin{aligned} Q_1 &= \left(\Sigma^{P_{12}}\right)^{\perp} \cap \left(\sum_{i=0}^{3} L_{g_i} Q_0 + span\{dh\}\right) \\ &= \left(\Sigma^{P_{12}}\right)^{\perp} \cap \left(Q_0 + \sum_{i=0}^{3} L_{g_i} Q_0 + span\{dh\}\right). \end{aligned} \tag{5.44}$$

We have $Q_0 + L_{g_i} Q_0 = span\{w_{21}, w_{22}, L_{g_i} w_{21}, L_{g_i} w_{22}\}, \quad i = 1, 2, 3$, such that :

$$\begin{aligned} &L_{g_0} w_{21} = L_{g_3} w_{21} = L_{g_3} w_{22} = 0, \\ &L_{g_1} w_{21} = \begin{pmatrix} 0 & 0 & -\frac{1}{C_1} \end{pmatrix}, \\ &L_{g_2} w_{21} = \begin{pmatrix} 0 & 0 & \frac{1}{C_1} \end{pmatrix}, \\ &L_{g_0} w_{22} = \begin{pmatrix} 0 & 0 & -\frac{2R}{LC_2} x_3 \end{pmatrix}, \\ &L_{g_1} w_{22} = \begin{pmatrix} \frac{1}{LC_2} x_3 & 0 & \frac{1}{LC_1} x_1 \end{pmatrix}, \\ &L_{g_2} w_{22} = \begin{pmatrix} -\frac{1}{LC_2} x_3 & 0 & \frac{1}{LC_2}(E - x_1) \end{pmatrix}. \end{aligned}$$

Finally, the obtained observability codistribution is

$$\Omega = oca\left(\left(\Sigma^{P_{12}}\right)^{\perp}\right) = span\left\{\begin{pmatrix} 1 \\ 0 \\ 0 \end{pmatrix}, \begin{pmatrix} 0 \\ \frac{1}{L}(x_2 - E) \\ \frac{1}{C_2} x_3 \end{pmatrix}\right\}. \tag{5.45}$$

Its orthogonal distribution is the unobservability distribution. The fulfillment of the condition (4.35) is satisfied and can be checked easily.

$$L = span\left\{g_1(x), g_2(x)\right\} \nsubseteq \left(oca\left((\Sigma_*^{p_{12}})^{\perp}\right)\right)^{\perp}. \tag{5.46}$$

Thus, ψ_1 and ϕ_1 are respectively

$$\psi_1(y) = \begin{pmatrix} y_1 \\ \frac{1}{2L} y_2^2 - \frac{E}{L} y_2 + \frac{1}{2C_2} y_3^2 \end{pmatrix}, \tag{5.47}$$

and

$$\phi_1(x) = \begin{pmatrix} x_1 \\ \frac{1}{2L} x_2^2 - \frac{E}{L} x_2 + \frac{1}{2C_2} x_3^2 \end{pmatrix}. \tag{5.48}$$

We choose $H_2 = \begin{pmatrix} 0 & 0 & 1 \end{pmatrix}$. Then, the output and the state diffeomorphisms are respectively given by :

$$\psi(y) = \begin{pmatrix} \tilde{y_1} \\ \tilde{y_2} \\ \tilde{y_3} \end{pmatrix} = \begin{pmatrix} \psi_1(y) \\ H_2 y \end{pmatrix} = \begin{pmatrix} y_1 \\ \frac{1}{2L} y_2^2 - \frac{E}{L} y_2 + \frac{1}{2C_2} y_3^2 \\ y_3 \end{pmatrix}, \tag{5.49}$$

and

$$\phi(x) = \begin{pmatrix} \phi_1(x) \\ H_2 h(x) \end{pmatrix} = \begin{pmatrix} x_1 \\ \frac{1}{2L}x_2^2 - \frac{E}{L}x_2 + \frac{1}{2C_2}x_3^2 \\ x_3 \end{pmatrix}. \tag{5.50}$$

Let

$$z_3 = x_1, \tag{5.51}$$

its time derivative is then,

$$\dot{z}_3 = \frac{x_3}{C_1}(u_2 - u_1) + \frac{x_3}{C_1}(m_2 - m_1). \tag{5.52}$$

As expected, the above system is affected by faults $m1(t)$ and $m2(t)$ and unaffected by fault $m3(t)$. Then it is a good departure point to construct a residual generator to detect and isolate the faults $m1(t)$ and $m2(t)$.

5.5.2 Residual generator based Luenberger observer

a- Residual generator design sensitive to $\Delta_1 = \{m_1(t), m_3(t)\}$ and insensitive to $m_2(t)$:

In the current section, we assume that all state variables of the three-cell converter are available to measurement. Consider the following Luenberger observer as given by equation (4.11) to estimate the state z_1 of the decoupled subsystem (5.24).

$$RG_1 : \begin{cases} \dot{\tilde{z}}_1 = \frac{1}{C_2}(u_3 - u_1)y_3 + k_1(\frac{C_1}{C_2}y_1 + y_2 - \tilde{z}_1) \\ \tilde{r}_1 = \frac{C_1}{C_2}y_1 + y_2 - \tilde{z}_1. \end{cases} \tag{5.53}$$

The filter (5.53) is a residual generator sensitive to set of faults $\Delta_1 = \{m_1(t), m_3(t)\}$ and insensitive to $m_2(t)$, where k_1 is the observer's gain. Hence, the following properties can be stated :

- The residual $\tilde{r}_1(t)$ is sensitive to faults $m_1(t)$ and $m_3(t)$ and is insensitive to fault $m_2(t)$.
- The residual signal $\tilde{r}_1(t)$ converges exponentially to zero in the absence of the faults.

The proof of these two properties is as follow. The time derivative of the residual signal $\tilde{r}_1$ is

$$\dot{\tilde{r}}_1(t) = \dot{z}_1 - \dot{\tilde{z}}_1. \tag{5.54}$$

From (5.24) and (5.53), we obtain

$$\dot{\tilde{r}}_1 = -k_1\tilde{r}_1 - \frac{1}{C_2}y_3 m_1 + \frac{1}{C_2}y_3 m_3, \quad k_1 \in R^+. \tag{5.55}$$

It is clear that the dynamic of $\tilde{r}_1$ is sensitive to the set of faults $\Delta_1 = \{m_1(t), m_3(t)\}$ and insensitive to $m_2(t)$. in the presence of the error initialization and in the absence of faults, if $k_1 > 0$ then the residual $\tilde{r}_1$ tends exponentially to zero.

b- Residual generator design sensitive to $\Delta_2 = \{m_2(t), m_3(t)\}$ and insensitive to $m_1(t)$:

Consider again the following Luenberger observer to estimate the state variable z_2 of the decoupled subsystem (5.38).

$$RG_2 : \begin{cases} \dot{\tilde{z}}_2 = \frac{1}{C_2}(u_3 - u_2)y_3 + k_2(y_2 - \tilde{z}_2) \\ \tilde{r}_2 = y_2 - \tilde{z}_2 \end{cases} \tag{5.56}$$

The filter (5.56) is a residual generator sensitive to faults $\Delta_2 = \{m_2(t), m_3(t)\}$ and insensitive to $m_1(t)$ where k_2 is the observer's gain.The following properties can be stated.

- The residual $\tilde{r}_2(t)$ is sensitive to set of faults $\Delta_2 = \{m_2(t), m_3(t)\}$ and it is insensitive to fault $m_1(t)$.
- The residual signal $\tilde{r}_2(t)$ converges exponentially to zero in the absence of faults.

Indeed, the time derivative of the residual signal $\tilde{r}_2$ is

$$\dot{\tilde{r}}_2 = -k_2\tilde{r}_2 - \frac{1}{C_2}y_3m_2 + \frac{1}{C_2}y_3m_3, \quad k_2 \in R^+. \tag{5.57}$$

It is clear from the above equation that the residual $\tilde{r}_2$ is only sensitive to the set of faults $\Delta_2 = \{m_2(t), m_3(t)\}$ and insensitive to m_1. In the absence of the faults, this residual converges exponentially to zero independently from the initial conditions since $k_2 > 0$.

c- Residual generator design sensitive to $\Delta_3 = \{m_1(t), m_2(t)\}$ and insensitive to $m_3(t)$:

Consider again the following Luenberger observer to estimate the state variable z_3 of the decoupled subsystem (5.52).

$$RG_3 : \begin{cases} \dot{\tilde{z}}_3 = \frac{1}{C_1}(u_2 - u_1)y_3 + k_3(y_1 - \tilde{z}_3) \\ \tilde{r}_3 = y_1 - \tilde{z}_3 \end{cases} \tag{5.58}$$

The filter (5.58) is the residual generator sensitive to the set of faults $\Delta_3 = \{m_1(t), m_2(t)\}$ and insensitive to $m_3(t)$ where $k_3 > 0$ is the observer's gain. The two following properties hold.

- The residual $\tilde{r}_3(t)$ is sensitive to fault m_1 and m_2 and is insensitive to fault m_3.
- The residual signal $\tilde{r}_3(t)$ converges exponentially to zero in the absence of the faults.

The time derivative of the residual signal $\tilde{r}_3$ is

$$\dot{\tilde{r}}_3 = -k_3\tilde{r}_3 - \frac{1}{C_1}y_3m_1 + \frac{1}{C_1}y_3m_2, k_3 > 0. \tag{5.59}$$

The dynamic of the residual $\tilde{r}_3$ is affected by the faults m_1 and m_2 and it is completely decoupled from the fault m_3. In the absence of the faults and with $k_3 > 0$, this residual converges exponentially to zero independently from the initial conditions.

5.5.3 Simulation results

In this section, simulation results of the studied system will be presented in order to validate the proposed fault detection and isolation filters. Figure (5.15) depicts a synoptic diagram of the diagnosis procedure based on Luenberger residual generator. Recalling that we have assumed that all states of the converter are available to measurement. The parameters of the model are $C_1 = C_2 = 40\mu F$, $R = 131\Omega$ and $L = 1mH$, the source voltage $E = 30volts$. The residual generator gains are $k_1 = k_2 = k_3 = 150$.

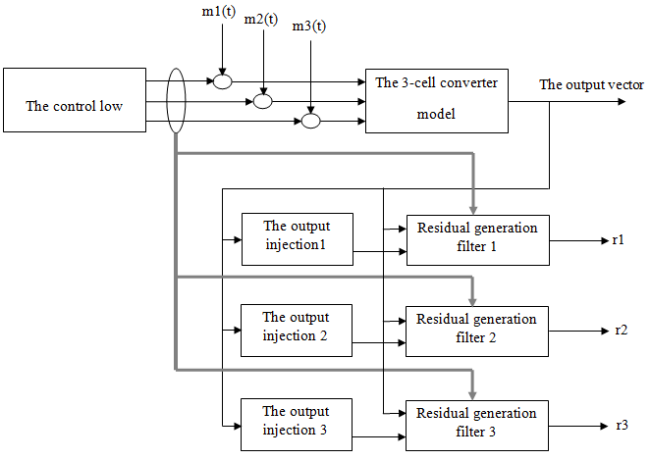

FIGURE 5.15: Synoptic diagram of the diagnostic procedure without observer

Figure (5.16) shows the applied control signals u_1, u_2 and u_3 which are periodic with a period of $T = 5.10^{-4}$ second, the dwell time is then $\tau = \frac{T}{6}$. This sequence of control is chosen to satisfy the observability condition of the three-cell converter.

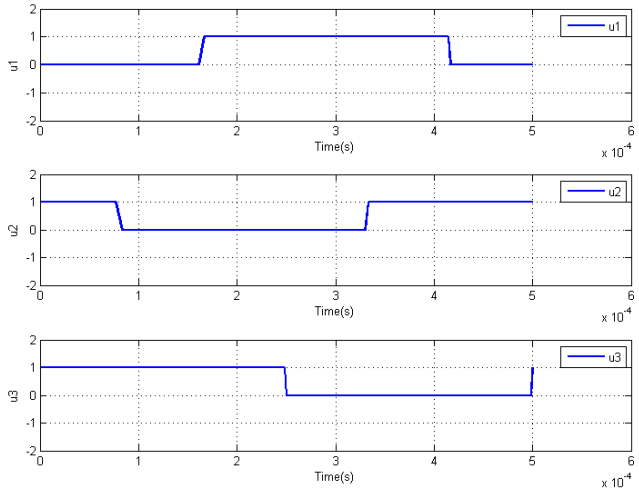

FIGURE 5.16: Control signals u_1, u_2 and u_3

Figures (5.17), (5.18) and (5.19) depict respectively the evolution of the load current i_L and the floating voltages v_{c_1} and v_{c_2}. Where we can see the convergence of floating voltages to their references $v_{c_{1ref}} = \frac{E}{3} = 10 \quad volts$ and $v_{c_{2ref}} = \frac{2E}{3} = 20 \quad volts$.
Figures (5.20) and (5.21) show residual signals $\tilde{r}_1$, $\tilde{r}_2$ and $\tilde{r}_3$ generated respectively by (5.53), (5.56) and (5.58), in the case of the occurrence of the fault m_1 in both situation u_1 stuck

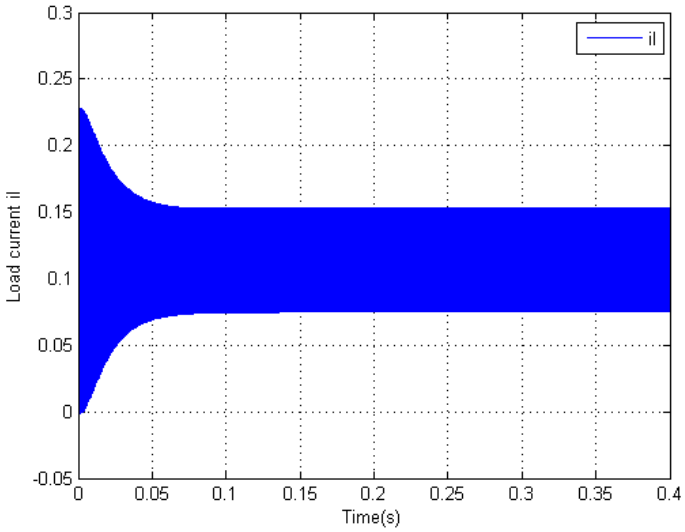

FIGURE 5.17: Load current *il*

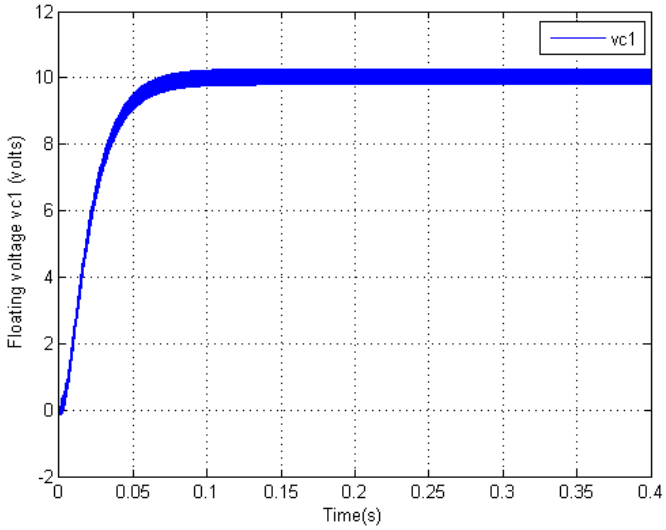

FIGURE 5.18: Floating voltage v_{c_1}

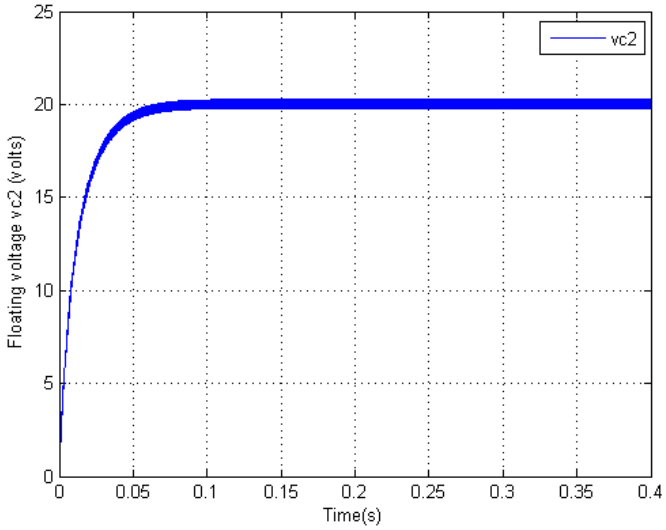

FIGURE 5.19: Floating voltage v_{c_2}

closed and u_1 stuck opened.

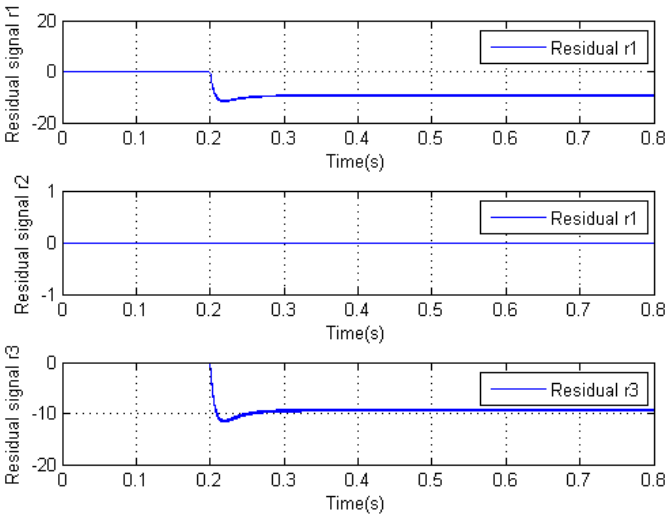

FIGURE 5.20: Residual signals $\tilde{r}_1$, $\tilde{r}_2$ and $\tilde{r}_3$ in the faulty mode u_1 stuck closed

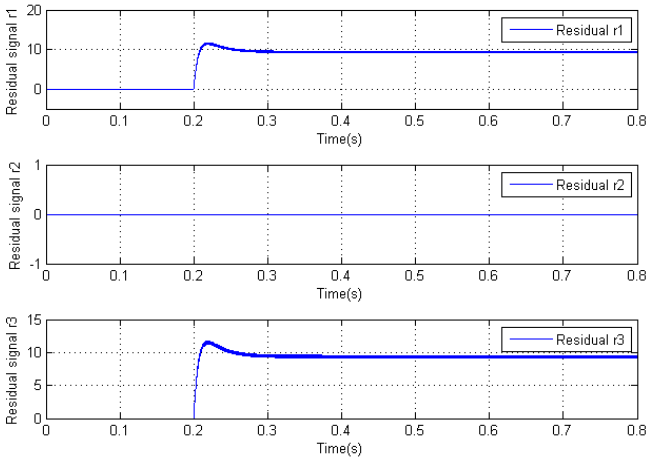

FIGURE 5.21: Residual signals $\tilde{r}_1$, $\tilde{r}_2$ and $\tilde{r}_3$ in the faulty mode u_1 stuck opened

Where we can notice that before the fault occurs, all residuals tend to zero. At $t = 0.2$ second, the fault m_1 occurs, the residuals $\tilde{r}_1$, $\tilde{r}_3$ detect the occurrence of the fault m_1. Whereas, the residual signal $\tilde{r}_2$ remains insensitive to the occurrence of the fault m_1. This is prove our analysis before.

Figures (5.22) and (5.23) show residual signals $\tilde{r}_1$, $\tilde{r}_2$ and $\tilde{r}_3$ generated respectively by (5.53), (5.56) and (5.58), in the case of the occurrence of the fault m_2 in both situation u_2 stuck closed and u_2 stuck opened. Where we can notice that before the fault occurs, all residuals tend to zero. At $t = 0.4$ second, the fault m_2 occurs, the residuals $\tilde{r}_1$, $\tilde{r}_2$ become sensitive to a fault m_2. While, residual signal $\tilde{r}_3$ remains insensitive to the occurrence of the fault m_2.

Figures (5.24) and (5.25) show residual signals $\tilde{r}_1$, $\tilde{r}_2$ and $\tilde{r}_3$ generated respectively by (5.53), (5.56) and (5.58), in the case of the occurrence of the fault m_3 in both situation u_3 stuck closed and u_3 stuck opened. Where we can notice that before the fault occurs, all residuals

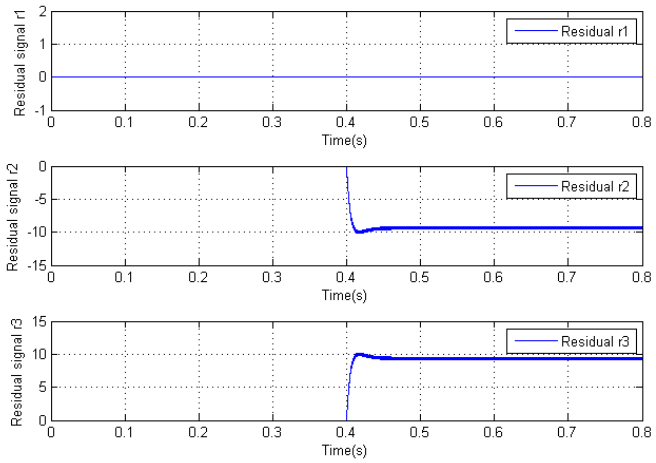

FIGURE 5.22: Residual signals $\tilde{r}_1$, $\tilde{r}_2$ and $\tilde{r}_3$ in the faulty mode u_2 stuck closed

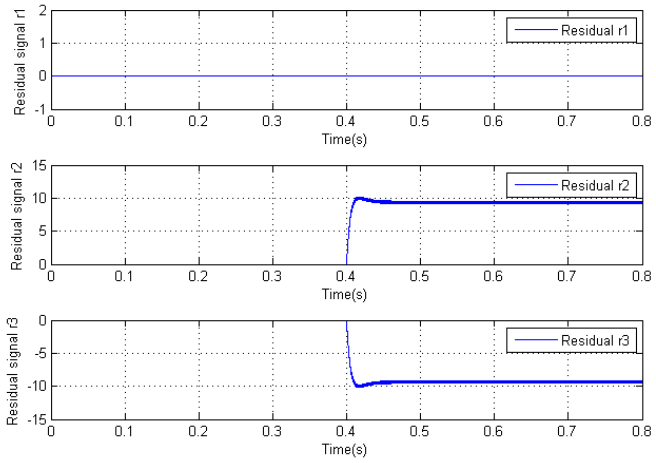

FIGURE 5.23: Residual signals $\tilde{r}_1$, $\tilde{r}_2$ and $\tilde{r}_3$ in the faulty mode u_2 stuck opened

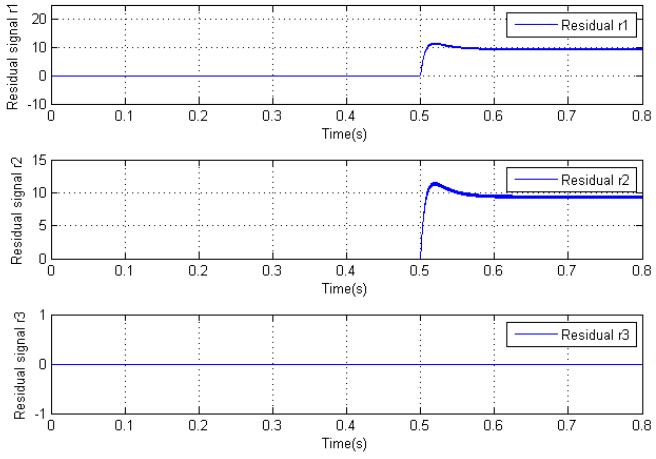

FIGURE 5.24: Residual signals $\tilde{r}_1$, $\tilde{r}_2$ and $\tilde{r}_3$ in the faulty mode u_3 stuck closed

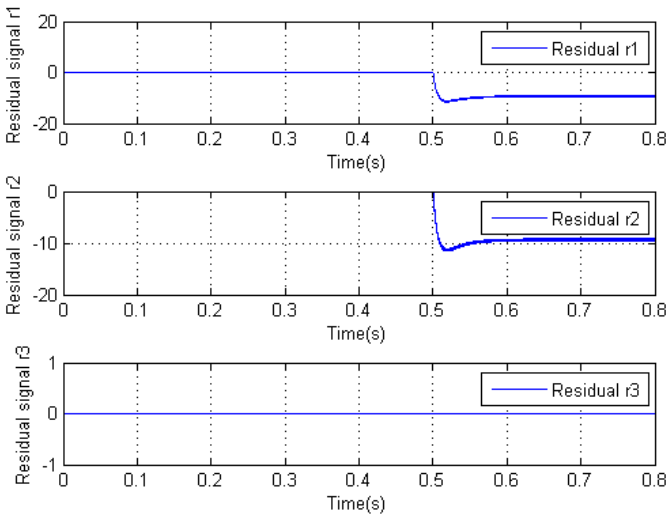

FIGURE 5.25: Residual signals $\tilde{r}_1$, $\tilde{r}_2$ and $\tilde{r}_3$ in the faulty mode u_3 stuck opened

tend to zero. At $t = 0.5$ second, the fault m_3 occurs, the residuals $\tilde{r}_2$, $\tilde{r}_3$ are sensitive to a fault m_3. While, residual signal $\tilde{r}_1$ remains insensitive to the occurrence of the fault m_2.

	m_1	m_2	m_3
$\tilde{r}_1^*$	1	0	1
$\tilde{r}_2^*$	0	1	1
$\tilde{r}_3^*$	1	1	0

TABLE 5.8: Table of residual signatures generated by Luenberger observer

Table (5.8) summarizes the sensitivity of the residual signals to faults m_1, m_2 and m_3. Note that 1 means that the corresponding residual is sensitive to a corresponding fault and 0 means insensitive. We can conclude from this table that the occurrence of a single fault can be isolated.

5.5.4 Residual generator based sliding mode observer

a- Sliding mode observer for states estimation of the 3-cell converter :

In previous section, we have assumed that all state variables of the three-cell converter are measured. In the case where only the load current $x_3 = i_l$ is measured, an observer should be designed to estimate the floating voltages in finite time. The state observability of three-cell converter is studied in chapter three and as reported in [2], [33], [40], [41] and [151]. In the following section, we design a sliding mode observer and from this observer we derive residual generators for fault detection and isolation procedure. The considered sliding mode observer to estimate the floating voltages of the three-cell converter $x_1 = v_{c_1}$ and $x_2 = v_{c_2}$ is given under following form [7], [33] and [34].

$$\begin{cases} \dot{\hat{x}}_1 &= \frac{1}{C_1}(u_2-u_1)\hat{x}_3+\alpha_1(u_2-u_1)sign(e_3) \\ \dot{\hat{x}}_2 &= \frac{1}{C_2}(u_3-u_2)\hat{x}_3+\alpha_2(u_3-u_2)sign(e_3) \\ \dot{\hat{x}}_3 &= -\frac{R}{L}\hat{x}_3+\frac{E}{L}u_3-\frac{1}{L}(u_2-u_1)\hat{x}_1-\frac{1}{L}(u_3-u_2)\hat{x}_2 \\ & \quad +\lambda_1|u2-u1||e_3|^{1/2}sign(e_3)+\lambda_2|u3-u2||e_3|^{1/2}sign(e_3) \\ \hat{y}_3 &= \hat{x}_3 \end{cases} \tag{5.60}$$

where $\hat{x}_1$, $\hat{x}_2$ and $\hat{x}_3$ represent the estimated of floating capacitor voltages and the load current respectively. e_3 represents the output estimation error, i.e, $e_3 = y_3 - \hat{y}_3$. The finite time convergence of the estimation errors is proved in [33]. Now, based on the designed sliding mode observer (5.60) and the previous analysis, we derive residual generators based sliding mode for each subsystem given by equations (5.24), (5.38) and (5.52).

b- Residual generator design sensitive to $\Delta_1 = \{m_1(t), m_3(t)\}$ and insensitive to $m_2(t)$:

Consider the model of the 3-cell converter (5.8), the sliding mode observer (5.60) and the decoupled subsystem sensitive to faults m_1 and m_3 and insensitive to fault $m_2(t)$ given by equation (5.24), then the following proposition can be stated.

Proposition 5.1 : Consider the model of the three-cell converter (5.8) and the sliding mode observer given by (5.60). Then the following filter

$$RG_4 : \begin{cases} \dot{\hat{z}}_1 &= \frac{1}{C_2}(u_3-u_1)\hat{y}_3+k_1(\frac{C_1}{C_2}\hat{x}_1+\hat{x}_2-\hat{z}_1) \\ &+ \frac{C1}{C2}\alpha_1(u_2-u_1)sign(e_3)+\alpha_2(u_3-u_2)sign(e_3) \\ \hat{r}_1 &= \frac{C_1}{C_2}\hat{x}_1+\hat{x}_2-\hat{z}_1, \end{cases} \tag{5.61}$$

is a residual generator with the following properties :

- The residual $\hat{r}_1$ is sensitive to the set of faults $\Delta_1 = \{m_1(t), m_3(t)\}$ and insensitive to $m_2(t)$.
- The residual signal $\hat{r}_1(t)$ converges exponentially to zero in the presence of initialization error and in the absence of faults $m_1(t)$ and $m_3(t)$.

Proof : The derivative of the residual signal $\hat{r}_1$ is :

$$\begin{aligned} \dot{\hat{r}}_1 &= \frac{C_1}{C_2}\dot{\hat{x}}_1+\dot{\hat{x}}_2-\dot{\hat{z}}_1 \\ &= \frac{C_1}{C_2}\{\frac{1}{C_1}(u_2-u_1)\hat{x}_3+\alpha_1(u_2-u_1)sign(e_3)\} \\ &\quad +\frac{1}{C_2}(u_3-u_2)\hat{x}_3+\alpha_2(u_3-u_2)sign(e_3)-\frac{1}{C_2}(u_3-u_1)\hat{y}_3 \\ &\quad -k_1\hat{r}_1-\frac{C1}{C2}\alpha_1(u_2-u_1)sign(e_3)-\alpha_2(u_3-u_2)sign(e_3), \end{aligned} \tag{5.62}$$

then

$$\dot{\hat{r}}_1 = -k_1\hat{r}_1, \qquad k_1 > 0. \tag{5.63}$$

It is clear that the residual signal $\hat{r}_1$ tends to zero once x_1 and x_2 are well estimated in the absence of faults. When the faults occur, their effects on the residual $\hat{r}_1$ are carried by the load current, and hence by $\hat{x}_1$ and $\hat{x}_2$. But the effect of the fault m_2 on the subspace defined by (5.61) is completely decoupled, due to the estimated output injection $\frac{C_1}{C_2}\hat{x}_1 + \hat{x}_2$.

c- Residual generator design sensitive to $\Delta_2 = \{m_2(t), m_3(t)\}$ and insensitive to $m_1(t)$:

Consider now the model of the 3-cell converter (5.8), the sliding mode observer (5.60) and the decoupled subsystem sensitive to faults m_2 and m_3 and insensitive to fault $m_1(t)$ given by equation (5.38), then the following proposition can be stated.

Proposition 5.2 : Consider the model of the three-cell converter (5.8) and the sliding mode observer (5.60). Then the following filter

$$RG_5 : \begin{cases} \dot{\hat{z}}_2 &= \frac{1}{C_2}(u_3 - u_2)\hat{y}_3 + k_2(\hat{x}_2 - \hat{z}_2) + \alpha_2(u_3 - u_2)sign(e_3) \\ \hat{r}_2 &= \hat{x}_2 - \hat{z}_2, \end{cases} \tag{5.64}$$

is a residual generator with the following properties :

— The residual r_2 is sensitive to m_2 and m_3 and insensitive to m_1.

— The residual signal $\hat{r}_2$ converges exponentially to zero in the presence of initialization error. and in the absence of faults m_2 and m_3.

Proof : The derivative of the residual signal is :

$$\begin{aligned} \dot{\hat{r}}_2 &= \dot{\hat{x}}_2 - \dot{\hat{z}}_2 \\ &= \frac{1}{C_2}(u_3 - u_2)\hat{x}_3 + \alpha_2(u_3 - u_2)sign(e_3) \\ &- \frac{1}{C_2}(u_3 - u_2)\hat{y}_3 - k_2(\hat{x}_2 - \hat{z}_2) - \alpha_2(u_3 - u_1)sign(e_3), \end{aligned} \tag{5.65}$$

we obtain

$$\dot{\hat{r}}_2 = -k_2\hat{r}_2, \qquad k_2 > 0. \tag{5.66}$$

Also, it is clear that the residual signal $\hat{r}_2$ tends to zero once x_1 and x_2 are well estimated in the absence of faults.

d- Residual generator design sensitive to $\Delta_3 = \{m_1(t), m_2(t)\}$ and insensitive to $m_3(t)$:

Consider again the model of the 3-cell converter (5.8), the sliding mode observer (5.60) and the decoupled subsystem sensitive to faults m_1 and m_2 and insensitive to fault $m_3(t)$ given by equation (5.52), then the following proposition can be stated.

Proposition 5.3 : Consider the model of the three-cell converter (5.8) and the sliding mode observer (5.60). Then the following filter

$$RG_6 : \begin{cases} \dot{\hat{z}}_3 &= \frac{1}{C_1}(u_2-u_1)\hat{y}_3 + k_3(\hat{x}_1-\hat{z}_3) + \alpha_1(u_2-u_1)sign(e_3) \\ \hat{r}_3 &= \hat{x}_1 - \hat{z}_3, \end{cases} \tag{5.67}$$

is a residual generator with the following properties :

- The residual $\hat{r}_3$ is sensitive to $m_1(t)$ and $m_2(t)$ and insensitive to $m_3(t)$.
- The residual signal $\hat{r}_3(t)$ converges exponentially to zero in the presence of initialization error and in the absence of faults $m_1(t)$ and $m_2(t)$.

Proof : The derivative of the residual signal is :

$$\begin{aligned} \dot{\hat{r}}_3 &= \dot{\hat{x}}_1 - \dot{\hat{z}}_3 \\ &= \frac{1}{C_1}(u_2-u_1)\hat{x}_3 + \alpha_1(u_2-u_1)sign(e_3) \\ &- \frac{1}{C_1}(u_2-u_1)\hat{y}_3 - k_3(\hat{x}_1-\hat{z}_3) - \alpha_1(u_2-u_1)sign(e_3), \end{aligned} \tag{5.68}$$

we obtain

$$\dot{\hat{r}}_3 = -k_3\hat{r}_3, \qquad k_3 > 0. \tag{5.69}$$

5.5.5 Simulation results

In this section, simulation results are carried out to show the effectiveness of the proposed residual generator based sliding mode observers. Figure (5.26) depicts a synoptic diagram of the proposed diagnosis procedure. Where, the different output injections are computed from the estimated states of the converter. Sliding mode observer parameters are $\lambda_1 = 1500, \lambda_2 = 1500, \alpha_1 = \frac{3}{4}, \alpha_2 = \frac{3}{4}$ and the residual generator gains are $k_1 = k_2 = k_3 = 150$.

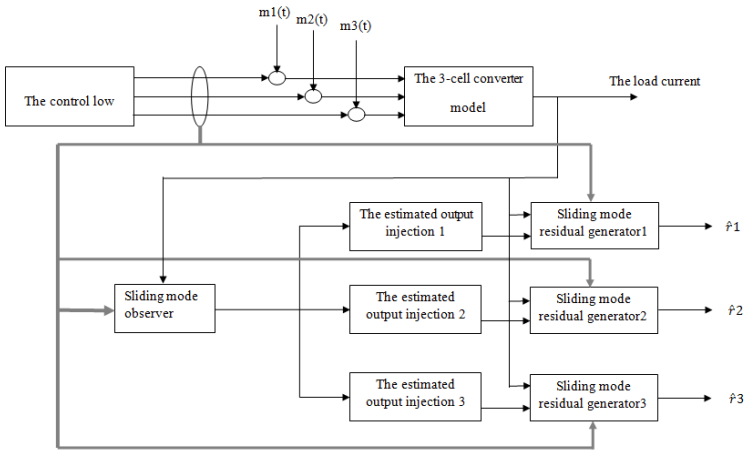

FIGURE 5.26: Synoptic diagram of the diagnostic procedure using sliding mode observer

Figure (5.27) depicts the obtained simulation results of the three-cell converter model (5.1) and the sliding mode observer (5.60). The convergence of the estimated states is established in finite time to their references $x_{1ref} = 10$ volts and $x_{2ref} = 20$ volts. Figure (5.28) shows the estimation errors, $e_1 = x_1 - \hat{x}_1$ and $e_2 = x_1 - \hat{x}_1$, converge to zero in the absence of faults. Figures (5.29) to (5.34) depict simulation results of residual signals $\hat{r}_1$, $\hat{r}_2$ and $\hat{r}_3$ based sliding observer, generated by (5.61), (5.64) and (5.67). Where all residuals are equal to zero in the

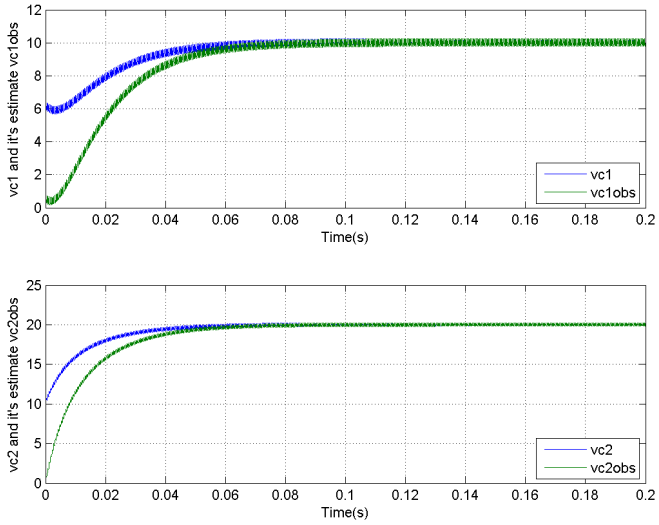

FIGURE 5.27: Floating voltages and their estimates a- x_1 and $\hat{x}_1$, b- x_2 and $\hat{x}_2$

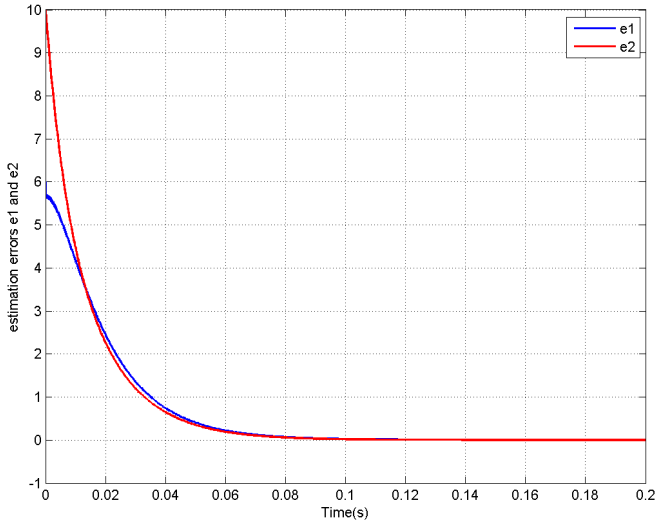

FIGURE 5.28: Estimation errors a- $e_1 = x_1 - \hat{x}_1$ and $e_2 = x_2 - \hat{x}_2$

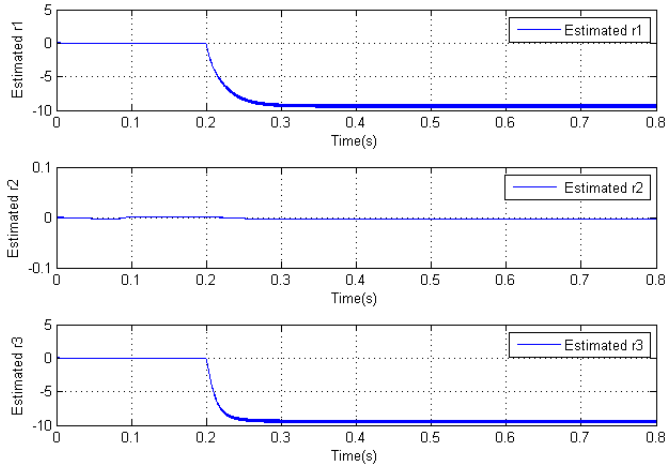

FIGURE 5.29: $\hat{r}_1$, $\hat{r}_2$ and $\hat{r}_3$ based sliding mode residual generator in the faulty mode u_1 stuck closed

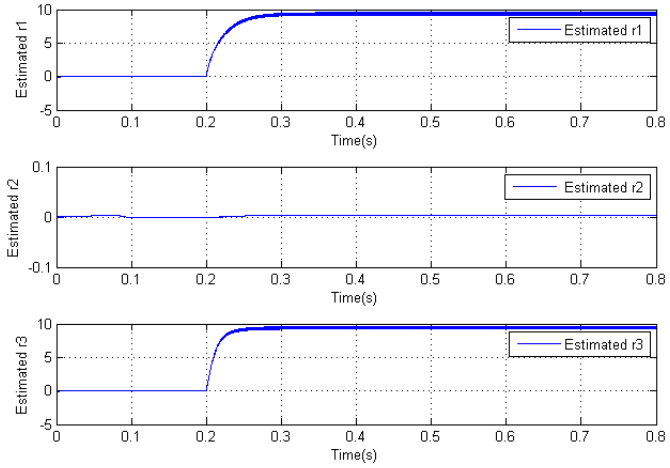

FIGURE 5.30: $\hat{r}_1$, $\hat{r}_2$ and $\hat{r}_3$ based sliding mode residual generator in the faulty mode u_1 stuck opened

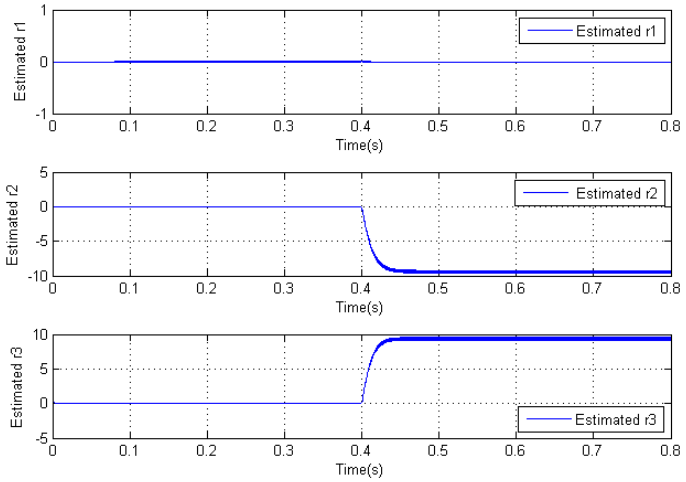

FIGURE 5.31: $\hat{r}_1$, $\hat{r}_2$ and $\hat{r}_3$ based sliding mode residual generator in the faulty mode u_2 stuck closed

absence of faults.

Figures (5.29) and (5.30) show respectively the obtained residual signals $\hat{r}_1$, $\hat{r}_2$ and $\hat{r}_3$ in the case of the occurrence of the fault m_1 causing u_1 stuck closed and u_1 stuck opened. Where, before the occurrence of the fault m_1 at $t = 0.2$ second, affects the residuals $\hat{r}_1$, $\hat{r}_3$ unlike the residual $\hat{r}_2$ which remains equal to zero.

Figures (5.31) and (5.32) show respectively the obtained residual signals $\hat{r}_1$, $\hat{r}_2$ and $\hat{r}_3$ in the case of the occurrence of the fault m_2 causing u_2 stuck closed and u_2 stuck opened. Where, before the occurrence of the fault m_2 at time $t = 0.4$ second, affects the residuals $\hat{r}_2$, $\hat{r}_3$ unlike the residual $\hat{r}_1$ which remains equal to zero.

Figures (5.33) and (5.34) show respectively the obtained residual signals $\hat{r}_1$, $\hat{r}_2$ and $\hat{r}_3$ in the case of the occurrence of the fault m_3 causing u_3 stuck closed and u_3 stuck opened. Where, before the occurrence of the fault m_3 at time $t = 0.4$ second, affects the residuals $\hat{r}_1$, $\hat{r}_2$ unlike the residual $\hat{r}_3$ which remains equal zero all the time.

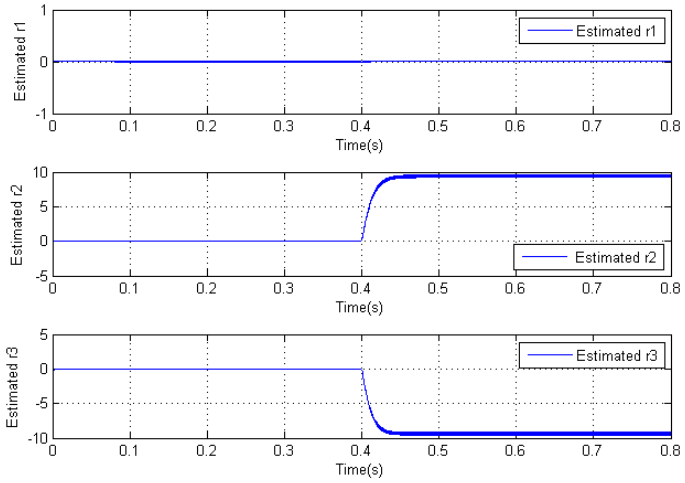

FIGURE 5.32: $\hat{r}_1$, $\hat{r}_2$ and $\hat{r}_3$ based sliding mode residual generator in the faulty mode u_2 stuck opened

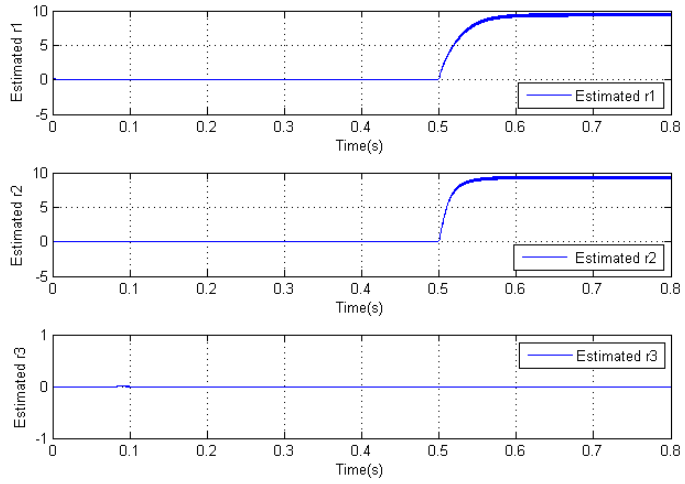

FIGURE 5.33: $\hat{r}_1$, $\hat{r}_2$ and $\hat{r}_3$ based sliding mode residual generator in the faulty mode u_3 stuck closed

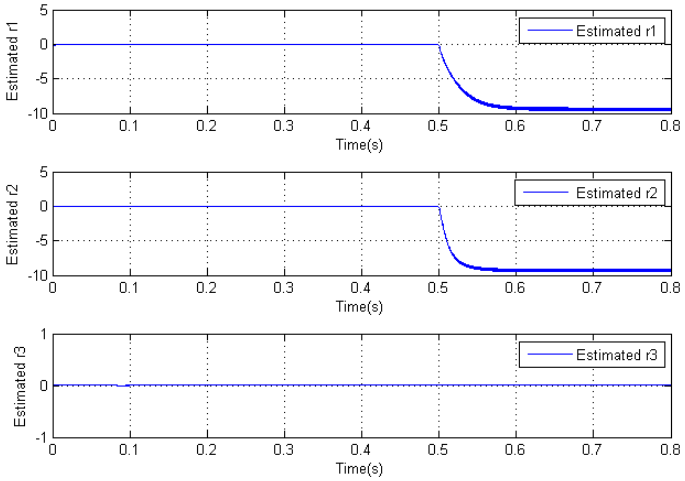

FIGURE 5.34: $\hat{r}_1$, $\hat{r}_2$ and $\hat{r}_3$ based sliding mode residual generator in the faulty mode u_3 stuck opened

	m_1	m_2	m_3
$\hat{r}_1^*$	1	0	1
$\hat{r}_2^*$	0	1	1
$\hat{r}_3^*$	1	1	0

TABLE 5.9: Table of residual signature based sliding mode observer

Table (5.9) summarizes the sensitivity of the residual signals to faults m_1, m_2 and m_3. Note that 1 means that the corresponding residual is sensitive to a corresponding fault and 0 means insensitive. We can conclude from this table that the occurrence of a single fault can be isolated.

5.6 Uncertainties studies

Model-based FDI methods are based on a mathematical model. However, a precise and accurate model of a real system cannot be obtained for several causes ; an unknown structure of disturbances, different noise effects, and uncertain parameters due to component aging. FDI methods that are able to handle these kind of uncertainties are referred to as robust. In order to highlight the effectiveness of the proposed residual signals that avoid false alarms against noises and parameter uncertainties, it is proposed to study the robustness of these residuals respect to measurement noise, resistance noise and capacitors degradation. A comparison between the robustness of the two strategies is then provided.

5.6.1 Robustness with respect to measurement noise

We test the robustness of the residual signals against measurement noise. For this end, we introduce noises on all state variables for the first diagnostic strategy (all states are assumed to be available to measurement). For the second diagnostic strategy using sliding mode observer, we consider a measurement noise only on the load current assumed to be the only measured

variable. The filter gains are $k_1 = k_2 = k_3 = 20$. The faults occurs at $t = 0.2$ second for m_1, at $t = 0.3$ second for m_2 and at $t = 0.4$ second for m_3. The obtained simulation results are depicted in figures (5.35), (5.36) and (5.37).
All the residuals generated by both Luenberger observer generator and sliding mode observer generator are affected by measurement noise without loss of fault detection and isolation performances. It is important to note that to avoid false alarms due to impulse noise, the residual signals magnitude can be adjusted by modifying the filter gains $k_i, \quad i = 1, 2, 3$.

5.6.2 Robustness with respect to resistance uncertainty

It is important to have an insensitivity of the residuals against the parametric uncertainties of the three-cell converter. According to, [149] the load resistance is the most disturbing elements in three cell converter systems. Figure(5.38) depicts a fast load resistance variation scenario used to test the robustness of the residual generators.
Figures (5.39) depicts the residual signals under resistance noise without the occurrence of any fault. As it can be seen, all residuals are not affected by the noise effect. Hence, the diagnosis performances are kept as it can be shown in figure (5.40) with the occurrence of the fault m_1 at $t = 0.2s$. This fact confirm that the residual generators (5.53), (5.56), (5.58), (5.61), (5.64) and (5.67) are completely decoupled from the resistance R variations. Note that in [149], the authors propose a statistical technique (Z-test) to overcome to the problem of false alarms due to resistance variations on generated residual.

5.6.3 Robustness with respect to capacitors degradation

In energy conversion systems, capacitors are often subject to degradation of their capacitances due to aging of the components. To show the robustness of the proposed residual signal against capacitors degradation (soft fault), we assume as in [6] that the capacitors C_1 and C_2 are described by a time varying capacitances,

$$C_1(t) = \begin{cases} C_1, & \text{if} \quad t < 0.3s \\ C_1 e^{-(t-0.3)}, & \text{if} \quad t \geq 0.3s \end{cases} \tag{5.70}$$

$$C_2(t) = \begin{cases} C_2, & \text{if} \quad t < 0.4s \\ C_2 e^{-(t-0.3)}, & \text{if} \quad t \geq 0.4s \end{cases} \tag{5.71}$$

The capacitor C_1 starts degrading at $t = 0.3s$ whereas the capacitor C_2 starts degrading at $t = 0.4s$. The degradation is assumed to be exponential as indicated by equations (5.70) and (5.71). Simulation results are depicted by figures (5.41) and (5.42).
Figure (5.41) shows that the residual signals $(\tilde{r}_1, \hat{r}_1)$, $(\tilde{r}_2, \hat{r}_2)$ and $(\tilde{r}_3, \hat{r}_3)$ subject to capacitor C_1 degradation. We can notice :

1- The sensitivity of $\tilde{r}_1, \tilde{r}_3$ generated by Luenberger residual generator.

2- The insensitivity of $\tilde{r}_2$ generated by Luenberger residual generator.

3- All residual signals $\hat{r}_1, \hat{r}_2, \hat{r}_3$ generated by sliding mode generator are insensitive to capacitor C_1 degradation.

Figure (5.42) depicts all residuals subject to capacitor C_2 degradation. It can be seen

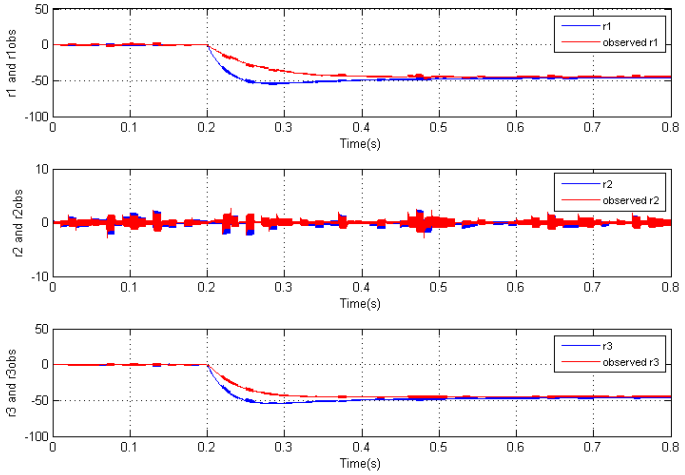

FIGURE 5.35: Measurement noise effect on residual signals for $u_1^f = 1$

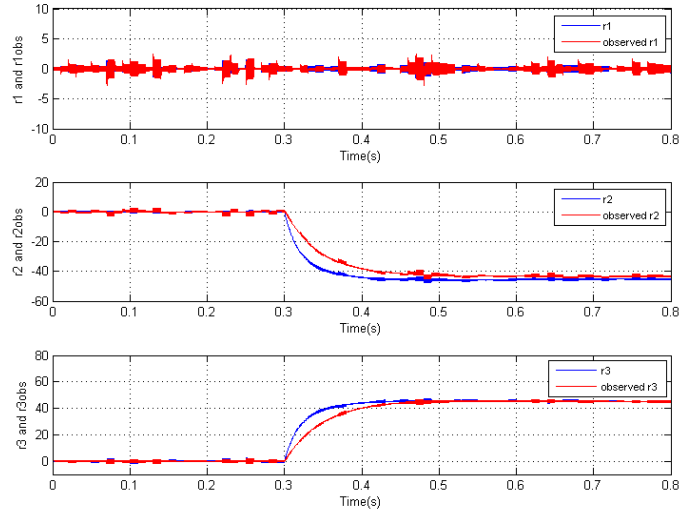

FIGURE 5.36: Measurement noise effect on residual signals for $u_2^f = 1$

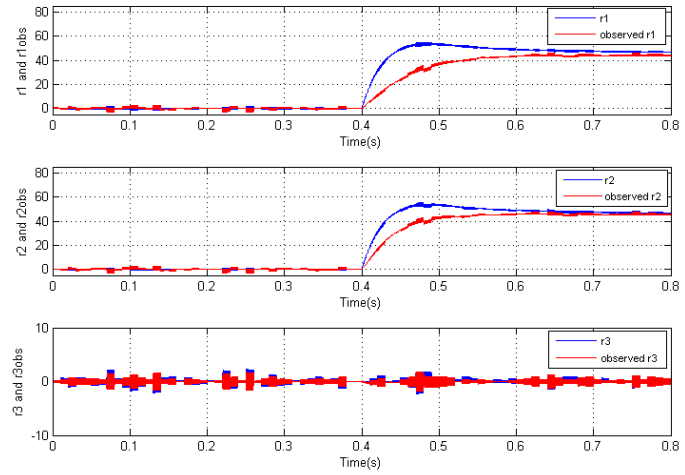

FIGURE 5.37: Measurement noise effect on residual signals for $u_3^f = 1$

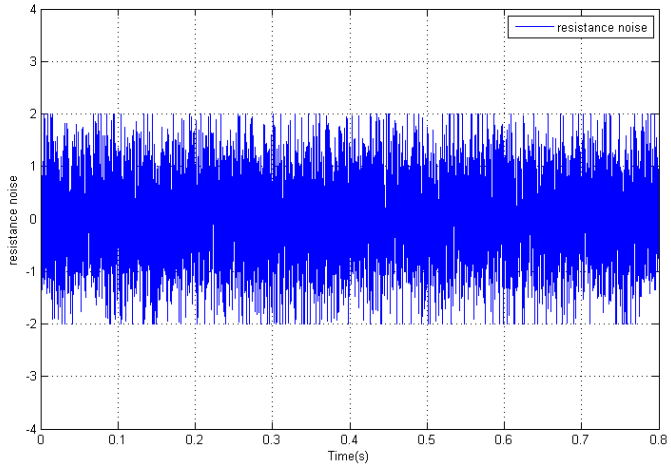

FIGURE 5.38: Noise added to resistance of the converter

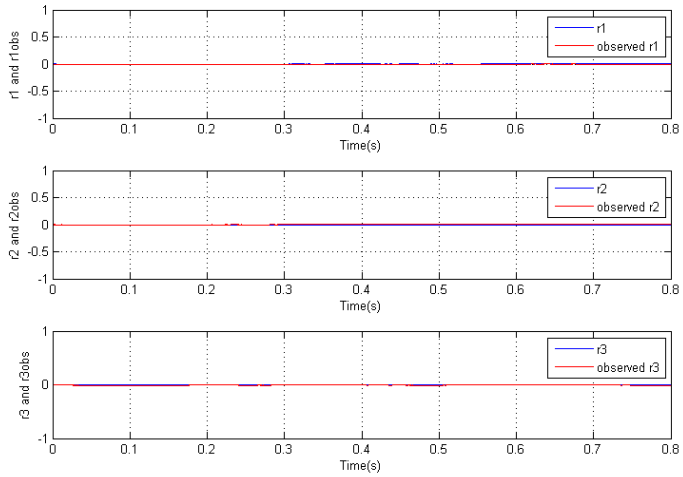

FIGURE 5.39: Resistance noise effect on residual signal without faults

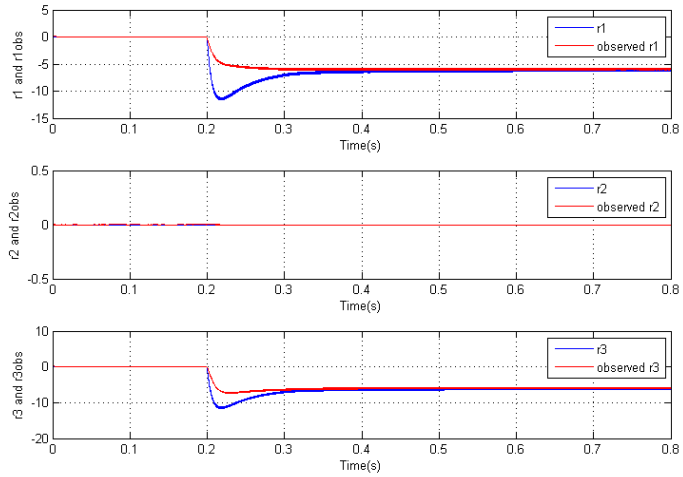

FIGURE 5.40: Resistance noise effect on residual signal for $u_1^f = 1$ and for $k_1 = k_2 = k_3 = 150$

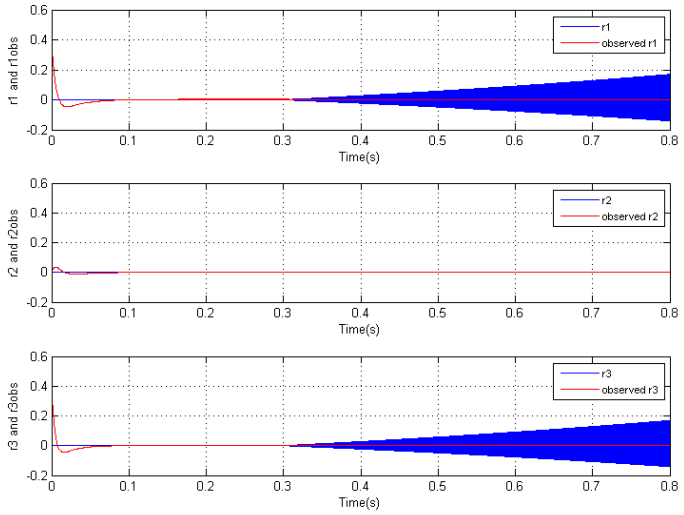

FIGURE 5.41: C_1 soft fault capacitor effect on residual signals

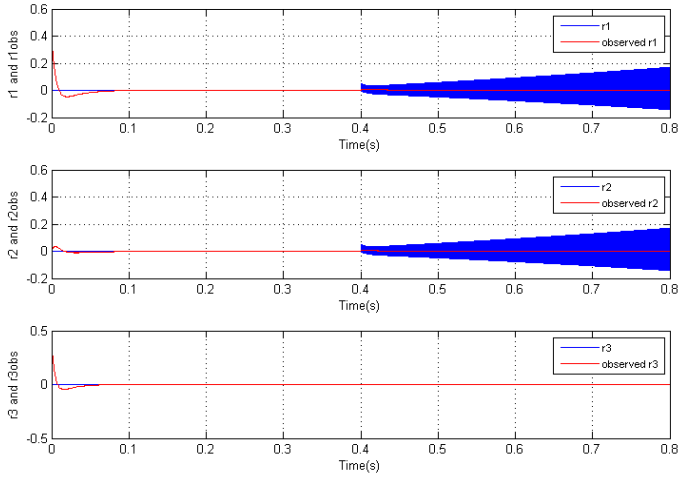

FIGURE 5.42: C_2 soft fault capacitor effect on residual signals

1- The sensitivity of $\tilde{r}_1, \tilde{r}_2$ generated by Luenberger residual generator.

2- The insensitivity of $\tilde{r}_3$ generated by Luenberger residual generator.

3- All residual signals $\hat{r}_1, \hat{r}_2, \hat{r}_3$ generated by sliding mode generator are insensitive to capacitor C_2 degradation.

5.6.4 Discussion on robustness tests

After designing the residual generators by the two diagnostic strategies, we proceed to the robustness tests against the multiple type of noises and uncertainties, namely, measurement noise, resistance noise, and degradation of two capacitors. The results of the sensitivity of the residual signals are summarized in Table (5.10), which represents the signature table of all the residuals generated by the two diagnostic strategies.

		1^{st} diagnosis strategy			2^{nd} diagnosis strategy		
		$\tilde{r}_1^*$	$\tilde{r}_2^*$	$\tilde{r}_3^*$	$\hat{r}_1^*$	$\hat{r}_2^*$	$\hat{r}_3^*$
Faults							
	Fault m_1	1	0	1	1	0	1
	Fault m_2	0	1	1	0	1	1
	Fault m_3	1	1	0	1	1	0
Uncertainties							
	Resistance noise	0	0	0	0	0	0
	C_1 degradation	1	0	1	0	0	0
	C_2 degradation	1	1	0	0	0	0
Measurement noises : All residual are sensitive without a loss of diagnosis performances							

TABLE 5.10: Residual signature table with respect to faults and uncertainties

We can deduce from this table that the two diagnostic strategies give good results in terms of detection and isolation of faults in the absence of different noises and uncertainties. In the presence of measurement noises, all residuals generated by the two strategies are sensitive, without the loss of detection and isolation performance, i.e., in the presence of this noise and a fault, both procedures can locate the faulty cell of the converter as shown in figures (5.35), (5.36) and (5.37). While, in the presence of resistance noise, the tests show that all residual generated by the two strategies are insensitive. This is a very important performance to avoid false alarms, as resistance is the most disturbing element of the converter. For the degradation of the two capacitors, we can notice that the residuals generated based on the sliding mode observers are insensitive. This is also a very important performance to avoid false alarms due to the aging of the capacitors. Unlike the second strategy, some residuals generated by the first diagnostic strategy are sensitive to the appearance of capacitor uncertainties. Indeed, the degradation of the capacitor C_1 generates a residual signature $(\tilde{r}_1^* \quad \tilde{r}_2^* \quad \tilde{r}_3^*) = (1 \quad 0 \quad 1)$, and this is also the residual signature in the presence of the fault m_1. The same thing for the degradation of the capacitor C_2, which generates a residual signature $(\tilde{r}_1^* \quad \tilde{r}_2^* \quad \tilde{r}_3^*) = (1 \quad 1 \quad 0)$ which is the same residual signature in the presence of the fault m_3. Therefore, false alarms and confusions can be generated by Luenberger's observer-based diagnostic procedure. As a

conclusion, the sliding mode observer-based diagnostic procedure is best suited to accomplish the task of detecting and isolating faults in the multicellular converter.

5.7 Conclusion

This chapter is devoted to the diagnosis of switch faults that are considered as discrete faults of the multicellular converter. A state of art have been presented about carried out works for the diagnosis of the converter. It seems that this is not sufficiently studied, especially for the diagnosis of simultaneous faults. The application of the geometric approach presented in chapter four, requires a fault model, for that we have presented a nonlinear model which takes into account the discrete faults in the 3-cell converter. Using this model, functional analysis has been presented for each fault situation. The application of the diagnosis approach to simultaneous switch faults detection and isolation of the converter is not possible, this is mainly due to the non-satisfaction of the isolation condition, consequently, a subsystem sensitive to a single fault and insensitive to the two others can not be obtained. To satisfy the conditions for the existence of a solution to a fundamental problem of residual generation, we have proposed to divide the faults into three subsets, each one contains two faults. In this case, isolation of each fault set from another single fault is being possible, and a geometric solution has been presented for each situation. Indeed, based on the observability co-distribution computed for each situation, three residual generators have been designed for two different diagnostic strategies based on observers. In the first strategy, we have assumed that all state variables of the converter are available to measurement, in this case, three residual generators based on the Luenberger observer have been proposed. While the second strategy, we have assumed that only the load current is available to measurement. In this case, a sliding mode observer has been designed for estimating the floating voltages. Sliding mode residual generators have been then proposed. The obtained simulation results in the absence of parametric uncertainties and measurement noise show the efficiency of the two diagnostic strategies. While in the presence of parametric uncertainties and measurement noise, the obtained simulations show the efficiency of residual generators based on sliding modes, and this is mainly due to the fact that sliding modes are known to be robust against parametric uncertainties.

General Conclusion

The works presented in this thesis concern the observability, observation, and diagnosis of the 3-cell converter. Due to its switching behavior, the multicellular converter is considered to be a hybrid system. However, several types of models have been developed, namely, the average model, the harmonic model, the instantaneous model, and the hybrid model. The use of one of them depends mainly on its application ; on control design, observability analysis, observer design, or on fault diagnosis.
Observability is a very important characteristic in the designing of an observer-based control system. The observability matrix of the hybrid model of the converter is never in full rank, but it does not imply the unobservability of the system. New approaches have been introduced recently for the analysis of the observability of hybrid systems, namely ZT_N-observability which is introduced by [4] and the geometrical approach introduced by [6]. The latter is based on the unobservable subspace along the hybrid time trajectory. Thus, the observability of the 3-cell converter is shown for a well-chosen control sequence, so that the floating voltages of the 3-cell converter can be estimated by an observer. Exploiting the obtained results from the observability analysis of the converter, a nonlinear switching model is obtained describing the behavior of the observable subspace of the converter. The important properties of the obtained observable sub-model are that it is observable along the hybrid time trajectory, and its nonlinear part is a function of the inputs and the outputs assumed known, that substantially simplified the issues of the observer design. The objective behind the determination of the observable sub-model is the reconstruction of the floating voltages of the converter. The idea is based on the designing of a sliding mode observer for the observable subspace of the converter, then reconstructing the floating voltages from an estimated variable provided by the observer. The convergence of the estimated variables to their references returns to the exponential stabilization of the estimation error, which has demonstrated using the Lyapunov formalism, and the issue is reformulated on the feasibility solution to the Linear Matrix Inequality problem, which is evident due to the observability property of the pair (A, C) along hybrid time trajectory. Consequently, the gain observer matrix and the sliding surface parameters of the observer are deduced. The reconstruction of the floating voltages is then evident from a variable estimated by the observer. The carried out simulation results show the efficiency of the proposed strategy of the reconstruction of the capacitor floating voltages.

The second part of this thesis concerns the fault diagnosis of the converter. Indeed, the three

cell converter operates in commutation mode, make it often subject to the switch faults. For that, it is necessary to have reliable diagnostic tools to ensure the good functioning of the converter and to protect not only the electrical devices that are connected to it and avoid the shutdown of the production but also to protect the human operators around. The considered fault affecting the converter cell is of type asymmetric, i.e., that causes the upper switch stuck opened (closed) and the lower switch stuck closed (opened). The choice of diagnosis approach is of paramount importance. We applied then the geometric approach which is based on the availability of a mathematical model. Thus, the nonlinear instantaneous model of the 3-cell converter is used since it is suitable for the chosen diagnostic approach. The existence of a solution to a fundamental problem of residual generation (FPRG) is related to the satisfaction of a necessary and sufficient condition, based on the unobservability co-distribution. Unfortunately, the FPRG using the geometrical approach has not a solution in the ideal case for faults isolation, i.e., generating three residuals, each one is sensitive to only one fault and each fault affects only one residual. Thus, simultaneous fault detection and isolation is not possible. This can be translated by the inexistence of an output injection which makes it possible to obtain a sub-system sensitive to a single fault and insensitive to two others. The idea that we have proposed, is to generate three residuals, each one sensitive to two faults and insensitive to only one. In this case, the necessary and sufficient condition to FPRG is checked, but the diagnosis performances are reduced to the occurrence of only one fault. The application of the approach has allowed the obtaining of three subsystems, each one being sensitive to two faults and completely decoupled from one fault. The fault detection and isolation procedure is then performed for two different strategies. The first assumes that all state variables of the converter model are available to measurement. Three residual generators based on the Luenberger observer are then designed for the three obtained subsystems. Whereas, the second strategy assumes that only the load current is available to measurement. Therefore, a sliding mode observer is designed to estimate the capacitor floating voltages. Thus, three sliding mode residual generators are proposed for each situation of faults. The convergence to zero of all generated residual signals is shown in the presence of initialization errors, as well as their sensitivity to a set of two faults and their insensitivity to a single fault. The carried out simulation results have shown the effectiveness of each diagnostic strategy for fault detection and isolation in the absence of uncertainties, and each blocking situation of the cell. Finally, to avoid false alarms, a robustness study is performed for uncertainty parameters and the measurement noises, namely the measurement noise, the resistance noise, and the capacitor's degradation over time. The obtained simulation results show the effectiveness of the residual generators based sliding mode observer and are more suitable in the presence of these parameter uncertainties and noises. This is since the sliding modes are known for their robustness to parametric uncertainties.

The work presented in this thesis has the potential to generate some future works that will further improve the research results either on observation or in fault diagnosis of the multi-cellular converter.

- The observable model of the 3-cell converter introduced in chapter three offers some interesting properties, and it is not yet sufficiently investigated. Indeed, this model can

be written as a hybrid LTI model, and the fact that all its modes are observable, other types of observation strategies can be applied, mainly those based on LMI strategies. Also, the reconstruction of the operating mode can be very interesting way for fault diagnosis using this model.

- The generalization of the diagnostic study using the geometric approach for n-cell converter can be very interesting. Indeed, the form of the output injections for a converter with n cells can be generalized, and can then be deduced directly for any p-cell converter.

- Simultaneous fault detection and isolation of the faulty cell of the 3-cell converter can enhance significantly the proposed diagnosis strategies proposed in the current work.
- To complete the diagnosis procedure, the insertion of a fault tolerant control (FTC) can also be a very interesting way to remedial to the occurrence of faults.

- Finally, the real implementation of the observation and the two fault diagnosis strategies can be a very interesting way to validate all obtained simulation results.

Bibliography

[1] Kouro. S, Malinowski. M, Gopakumar. K, Pou. J, Franquelo. L.G, Wu. B, Rodriguez. J, Perez. M, and Leon. J. I. Recent advances and industria applications of multilevel converters. *IEEE Transactions on Industrial Electronics*, 57(8) :2553–2580, 2010.

[2] Bejarano. F.J, Ghanes. M, and Barbot J.P. Observability and observer design for hybrid multicell choppers. *International journal of Control*, 83 :617–632, 2010.

[3] Benmiloud. M. Contribution to the analysis and control design of hybrid dynamical systems : Application to multicellular converters. *Phd thesis, university of Amar Telidji, Laghouat, Algeria*, 2017.

[4] Kang. W, Barbot. J.P, and Xu. L. On the observability of nonlinear and switched system. *Lecture note in control and information sciences*, pages 199–216, 2009.

[5] Liu. J, Laghrouche. S, Harmouche. M, and Wack. M. Adaptive gain second order sliding mode observer design for switching power converters. *Control Engineering practice*, pages 124–131, 2014.

[6] Tanwani. A, Dominguez-Garcia. A.D, and Liberzon. D. An inversion-based approach to fault detection and isolation in switching electrical networks. *IEEE transactions on control systems technology*, 19(5) :1059–1074, 2011.

[7] Meziane. H, Labarre. C, Lefteriu. S, Defoort. M, and Djemai. M. Fault detection and isolation for a multi-cellular converter based on sliding mode observer. *9th IFAC Symposium on Fault Detection, Supervision and Safety for Technical Processes SAFEPROCESS*, 2015.

[8] Koutroulis. E, Chatzakisa. J, Kalaitzakisa. K, Maniasb. S, and Voulgaris. N.C. A system for inverter protection and real-time monitoring. *Microelectronics Journal*, 34 (9), 2003.

[9] Richardeau. F, Baudesson. P, and Meynard. T.A. Faillures-tolerance and remedial strategies of a pwm multicell inverter. *IEEE Transactions on Power Electronics*, 17 (6) :125–247, 2002.

[10] Branicky. M. S, Borkar. V. S, and Mitter. S. K. A unified framework for hybrid control : Model and optimal control theory. *IEEE Transaction on Automatic Control*, 43(1) : 31–45, January 1998.

[11] Heemels. W. P. M. H, Lehmann. D, Lunze. J, and De Schutter. B. Introduction to hybrid systems. *Chapter 1 in Handbook of Hybrid Systems ControlTheory, Tools, Applications (J. Lunze and F. Lamnabhi-Lagarrigue, eds.), Cambridge, UK : Cambridge University Press*, ISBN 978-0-521-76505-3 :330, 2009.

[12] Johansson. K. H. Hybrid control systems. *Control Systems, Robotics and Automation, UNESCO Encyclopedia of Life Support Systems (eolss)*, XV.

[13] Riedinger. P. Contribution à la commande optimale des systèmes dynamiques hybrides. *Thèse de doctorat, Institut National Polytechnique de Lorraine, France*, 2000.

[14] Chaimowicz. L. Dynamic coordination of cooperative robots : A hybrid systems approach. *PhD thesis, University of Federal de Minas Gerais, Brazil*, June 2002.

[15] Liberzon. D. switching in systems and control. *Birkhäuser*, 2003.

[16] Chaib. S. Observation et diagnostic des systs hybrides. *Thèse de doctorat, Université d'Orléans, France*, 2007.

[17] Narasimhan. S. Model-based diagnosis of hynrid systems. *Phd thesis, Vanderbilt University, Tennessee, USA*, August 2007.

[18] David. R and Alla. H. On hybrid petri nets. *Discrete Event Dynamic Systems : Theory and Applications*, 11 :9–40, 2001.

[19] De Santis. E and Di Benedetto. M.D. Observability of hybrid dynamical systems. *Foundations and Trends in Systems and Control*, 3(4) :363–540, 2016.

[20] Petreczky. M, Tanwani. A, and Trenn. S. Observability of switched linear systems. *Springer International Publishing Switzerland, M. Djemai and M. Defoort (eds.), Hybrid Dynamical Systems, Lecture Notes in Control and Information Sciences*, 457, 2015.

[21] Balluchi. A, Benvenuti. L, Di Benedetto. M. D, and Sangiovanni-Vincentelli. A. L. Observability for hybrid systems. 42^{nd} *IEEE Conference on Decision and Control, Maui, Hawaii, USA*, 2003.

[22] Balluchi. A, Benvenuti. L, Di Benedetto. M. D, and Sangiovanni-Vincentelli. A. L. Design observers for hybrid systems. *In C. J. Tomlin and M. R. Greenstreet (Eds), Springer-Verlag Berlin Heidelberg*, 2289 :76–89, 2003.

[23] Chaib. S, Boutat. D, Benali. A, and Barbot. J. P. Algebraic and geometrical conditions for the observability of the discrete state of a class of hybrid systems. *Proceedings of the 2006 IEEE International Conference on Control Applications Munich, Germany*, October 2006.

[24] Chaib. S, Boutat. D, Benali. A, and Barbot. J. P. Algebraic and geometrical conditions for the observability of the discrete state of a class of hybrid systems. *Nonlinear Analysis : Hybrid systems and applications*, 63 :423 – 438, 2005.

[25] Vidal. R, Chiuso. A, Soatto. S, and Sastry. S. Observability of linear hybrid systems. *In A. Pnueli, O. Maler (Eds.), Lecture notes in computer science, Hybrid systems : Computation and control, Springer Verlag Berlin Heidelberg*, 2623 :526–539, 2003.

[26] De Santis. E, Di Benedetto. M. D, Di Gennaro. S, D'Innocenzo. A, and Pola. G. Critical observability of a class of hybrid systems and application to air traffic management. *Lecture Notes on Control and Information Sciences, Springer Verlag, Berlin*, 337 :141–170, 2005.

[27] Riosy. H, Davilaz. J, and Teel. A. R. Strong observability for a class of linear hybrid systems. *IEEE Conference on Decision and Control (CDC), Miami Beach, FL, USA*, December 2018.

[28] Kusters. F and Trenn. S. Switch observability for switched linear systems. *Automatica*, 87 :121–127, 2018.

[29] Kang. W and Barbot. J.P. Disscussion on observability and invertibility. *In proc. of IFAC, NOLCOS, Pretoria, South Africa*, pages 14–22, August 2007.

[30] Ghanes.M, Bejarano. F, and Barbot. J. P. On sliding mode and adaptive observers design for multicellconverter. *American Control Conferece, Hyatt Regency Riverfront, St. Louis, MO, USA*, June 2009.

[31] Hauroigne. P, Riedinger. P, and Lung. C. Observer based output feedback of a multicellular converter : control lyapunov fonction-sliding mode approach. *51st IEEE Conference on Decision and Control. Maui, Hawaii, USA*, December, 12-13, 2012.

[32] Benmansour. K. Réalisation d'un banc d'essai pour la commande et l'observation des convertisseurs multicellulaires serie : Approche hybride. *Thèse de doctorat, université de Cergy Pontoise*, Juin 2009.

[33] Defoort. M, Djemai. M, Floquet. T, and Perruquetti. W. Robust finite time observer design for multicellular converter. *International Journal of System Science*, 42(11) : 1859–1868, 2011.

[34] Jday. M, Vidal. P.E, Haggége. J, and Rotella. F. Observability and sliding mode observer design for multi-cell series converter. *6th International Conference on Control, Decision and Information Technologies (CoDIT19)*, pages 1486–1491, 2019.

[35] Defoort. M, Djemai. M, Floquet. T, and Perruquetti. W. On finit time observer design for multicellular converter. *International Workshop on variable Structure Systems, Mexico City, Mexico*, June 2010.

[36] Amghar. B. Modélisation, observabilité et commande de convertisseurs multicellulaires parallèles dans un environnement dédié. *Thèse de doctorat, Ecole Doctorale Cergy Pontoise*, Juillet 2013.

[37] Mrad. I, Barbot. J. P, and Sbita. L. Left invertibility for switched linear system based on $z(tn)$-observability and hosm observer. *IEEE, 15th International Multi-Conference on Systems, Signals Devices (SSD)*, 2018.

[38] Tanwani. A, Shim. H, and Liberzon. D. Observability implies observer design for switched linear systems. *Int Conference on hybrid systems : Computation and control, New york, USA*, 2011.

[39] Tanwani. A, Shim. H, and Liberzon. D. Observability for switched linear systems : Characterization and observer design. *IEEE Transactions on Automatic control*, 58 (4) :891–904, April 2013.

[40] Khelouat. S, Laleg Kirati. T.M, Benalia. A, Djemai. M, and Boukhetala. D. On sliding mode observer for a hybrid three-cell converter. *3rd International Conference on Systems and Control*, pages 613–618, 2013.

[41] Khelouat. S, Benalia. A, Laleg Kirati. T.M, and Boukhetala. D. Sliding mode observer design based linear matrix inequality approach for a three-cell converter. *6th International Conference on Control Engineering and Information Technologies*, pages 573–578, October 2018.

[42] Van Gorp. J, Defoort. M, and Djemai. M. Hybrid observer for the multicellular converter. *In Proceedings of the 4th IFAC Conference on Analysis and Design of Hybrid Systems, Eindhoven, Netherlands*, pages 259–264, Juin 2012.

[43] Arbib. C and De Santis. E. Almost always observable hybrid systems. *Nonlinear Analysis : Hybrid Systems*, 36, May 2020.

[44] Gazzam. N and Benalia. A. Voltage estimation of dc/dc converters. *Electrotehnicã, Electronicã, Automaticã (EEA)*, 66(1), 2018.

[45] Ameur. I, Gazzam. N, Benmiloud. M, and Benalia. A. Output feedback control of multicellular converters. *International Journal of Dynamics and Control*, November 2019. URL https://doi.org/10.1007/s40435-019-00592-z.

[46] Baglietto. M, Battistelli. G, , and Scardovi. L. Active mode observation of switching systems based on a-priori knowledge of the continuous state. *Proceedings of the 46th IEEE Conference on Decision and Control, New Orleans, LA, USA*, pages 12–14, December 2007.

[47] Van Gorp. J. Diagnosis and observation of a class of hybrid dynamical systems : Application to the serial multicellular converter. *Phd thesis, University of Valenciennes et du Hainaut-Cambresis*, December 2013.

[48] Isermann. R. Fault-diagnosis systems, an introduction from fault detection to fault tolerance. *Spriger-Verlag, Berlin*, 2006.

[49] Sayed-Mouchaweh. M. Fault diagnosis of hybrid dynamic and complex systems. *Springer International Publishing AG, part of Springer Nature*, https ://doi.org/10.1007/978-3-319-74014-0, 2018.

[50] Join. C, Ponsart. J.C, Sauter. D, and Theilliol. D. Nonlinear filter design for fault diagnosis : application to three-tank system. *Control Theory Application*, 152(1) :55–64, 2005.

[51] Gertler. D. J. Fault detection and diagnosis in engineering systems, marcel dekker, new york. 1998.

[52] Ichalal. D. Estimation and diagnosis of nonlinear systems described by a takagi-sugeno model. *Phd thesis, National Polytechnique of Lorraine, France*, November 2009.

[53] Ng. K.Y. Advancements in robust fault reconstruction using sliding mode observers. *Phd thesis, Monash University, south korea*, April 2009.

[54] Gateaux. G. Contribution to series multicells converters control : nonlinear and fuzzy control. *Phd thesis, Institut national polytechnique, Toulouse, France*, 1997.

[55] Benmansour. K, Benalia. A, Djemai M, and Deleon. J. Hybrid control of a multicellular converter. *In Nonlinear Analysis : Hybrid Systems*, 1 :16–29, 2007.

[56] Benzineb. O, Taibi. F, Laleg-Kirati. T. M, Boucherit. M. S, and Tadjine. M. Control and fault diagnosis based sliding mode observer of a multicellular converter : hybrid approach. *Journal of Electrical Engineering*, 64(1) :2553–2580, 2013.

[57] Benmiloud. M, Benalia. A, Djemai. M, and Defoort. M. On the local stabilization of hybrid limit cycles in switched affin systems. *in IEEE Transactions on Automatic Control.*, DOI : 10.1109/TAC.2018.2841806, 2018.

[58] Kamri. D, Bourdais. R, Buisson. J, and Larbes. C. Practical stabilization for piecewise-affine systems : A bmi approach. *Nonlinear Analysis : Hybrid Systems*, 6 :859–870, 2012.

[59] Patino. D, Riedinger. P, and Ruiz. F. A predictive control approach for dc-dc power converters and cyclic switched systems. *IEEE International Conference on Industrial Technology*, 2010.

[60] Trabelsi. M, Retif. J.M, Brun. X Lin-Shi. X, Morel. F, and Bevilacqua. P. Hybrid control of a three-cell converter associated to an inductive load. *IEEE Annual Power Electronics Specialists Conference*, 2008.

[61] Ben said. B, Ben saad. K, and Benrejeb. M. Sliding mode control for a multicell converters. *International Conference on Control, Engineering & Information Technology (CEIT'13), Proceedings Engineering & Technology*, 2 :39–44, 2013.

[62] Djemai. M, Busawon. K, Benmansour. K, and Marouf. A. High-order sliding mode control of a dc motor drive via a switched controlled multi-cellular converter. *International Journal of Systems Science (IJSS)*, 42(11) :1869–1882, November 2011.

[63] Baja. M, Patino. D, Cormerais. H, Riedinger. P, and Buisson. J. Hybrid control of a three-level three-cell dc-dc converter. *American Control Conference*, 2007.

[64] Franquelo. L. G, Rodriguez. J, Leon. J.I, Kouro. S, Portillo. R, and Prats Maria. A.M. The age of multilevel converter arrives. *IEEE Industrial Electronics Magazine*, pages 28–39, June 2008.

[65] Malinowski. M. Multilevel voltage source converter topologies for industrial medium voltage drives. *Bulletin of the Polish Academy of Sciences Technical Sciences*, 65(5) : 567–578, 2017.

[66] Leredde. A. Study and design of multilevel converters for high power applications. *Phd thesis, Institut national polytechnique, Toulouse, France*, 2011.

[67] Meynard. T.A, Foch. H, Thomas. P, Courault. J, Jakob. R, , and Nahrstaedt. M. Multicell converter : Basic concepts and industry application. *IEEE Transactions on industrial electronics*, 49(5) :955–964, 2002.

[68] Gazzam. N and Benalia. A. Voltage estimation of dc/dc converters. *Electrotehnica, Electronica, Automatica (EEA)*, 66(1) :73–79, 2017.

[69] Bejarano. F. J and Pisano. A. Switched observers for switched linear systems with unknown inputs. *IEEE Transactions On Automatic Control*, 56(3) :681–686, March 2011.

[70] Arichi. F, Djemai. M, Cherki. B, , and Manamanni. N. Continuous and discrete state estimation for a class of nonlinear switched systems. *IEEE Transactions On Circuits And SystemsII : Express Briefs*, 62(7) :691–695, July 2015.

[71] Bako. L and Lecoeuche. S. A new state observer for switched linear systems using a non smooth optimization approach. *50th IEEE conference on Decision and Control and European Control Conference (CDC-ECC), Orlando, FL, USA*, pages 5329–5336, December 2015.

[72] Rios. H, Davila. J, and Fridman. L. High-order sliding modes observers for linear autonomous-switched systems with unknown inputs. *12th IEEE Workshop on Variable Structure Systems, VSS12, Mumbai*, pages 428–433, January 2012.

[73] Rios. H, Davila. J, Fridman. L, and Efimov. D. State estimation for linear switched systems with unstable invariant zeros and unknown inputs. *51st IEEE Conference on Decision and Control, Maui, Hawaii, USA*, December 2012.

[74] Rios. H, Efimov. D, Davila. J, Raissi. T, Fridman. L, and Zolghadri. A. State estimation for linear switched systems with unknown inputs. *Proceedings of the 4th IFAC Conference on Analysis and Design of Hybrid Systems, Eindhoven, The Netherlands*, June 2012.

[75] Orani. N, Pisano. A, Franceschelli. M, Giua. A, and Usai. E. Robust reconstruction of the discrete states for a class of non linear uncertain switched systems. *Nonlinear Analysis : Hybrid Systems*, 5 :220–232, 2011.

[76] Barbot. J. P, Saadaoui. H, Djemai. M, and Manamanni. N. Nonlinear observer for autonomous switching systems with jumps. *Nonlinear Analysis :Hybrid Systems*, 1(4) : 537–547, December 2007.

[77] Saadaoui. H, Manamanni. N, Djemai. M, Barbot. J. P, and Floquet. T. Exact differentiation and sliding mode observer for switched lagrangian systems. *Nonlinear Analysis*, 65(5) :1050–1069, september 2006.

[78] Pettersson. S. Designing switched observers for switched systems using multiple lyapunov functions and dwell-time switching. *Analysis and Design of Hybrid Systems, Alghero, Italy*, 2006.

[79] Balluchi. A, Benvenuti. L, Di Benedetto. M. D, and Sangiovanni-Vincentelli. A. The design of dynamical observers for hybrid systems : Theory and application to an automotive control problem. *Automatica*, 49 :915–925, 2013.

[80] Huang. G. J and Wu-Hua Chen. W-H. A revisit to the design of switched observers for switched linear systems with unknown inputs. *International Journal of Control, Automation, and Systems*, 12(5) :954–962, 2014.

[81] Ifqir. S, Ait-Oufroukh. N, Ichalal. D, and Mammar. S. Synchronous interval observer design for switched lpv systems using multiple quadratic iss-lyapunov functions. *25th Mediterranean Conference on Control and Automation, Valletta, Malta*, July 2017.

[82] Hou. Y, Zhu. F, Zhao. X, and Guo. S. Observer design and unknown input reconstruction for a class of switched descriptor systems. *IEEE Transactions on Systems, Man, and Cybernetics : Systems*, 48(8) :1411–1419, August 2018.

[83] Liu. L. J and Zhao. X. Design of multiple-mode observer and multiple-mode controller for switched positive linear systems. *IET Control Theory Applications*, 13(9) :1320–1328, June 2019.

[84] Davila. A, Moreno. J. A, and Fridman. L. Optimal lyapunov function selection for reaching time estimation of super twisting algorithm. *In Proceedings of the 48th IEEE Conference On Decision and Control, Shanghai, P.R. China*, pages 8405–8410, December 2009.

[85] Moreno. J and Osorio. M. A lyapunov approach to second order sliding mode controler and observers. *in proceeding of the IEEE Conference on Decision and Control, New Orleans, USA*, pages 2856–2861, 2008.

[86] Benmansour. K, Djemai. M, Tadjine. M, and Boucherit. M.S. On sliding mode observer for hybrid three cells converter : Experimental results. *IEEE International workshop on variable structure systems*, pages 373–377, June 2008.

[87] Benmansour. K, Tlemçani. A, Djemai. M, and De Leon. J. A new interconnected observer design in power converter : Theory and experimentation. *Nonlinear Dynamics and Systems Theory*, 10(3) :211–224, 2010.

[88] Ghanes. M, Trabelsi. M, Lin-Shi. X, Barbot. J. P, Retif. J. M, and Busawon. K. High gain observer for a three-cell chopper : Design and experimental results. *International Journal of Robust and Nonlinear Control*, DOI : 10.1002/rnc.3063, 2013.

[89] Walcott. B. L and Zak. S.H. State observation of nonlinear uncertain dynamical systems. *IEEE Transactions on Automatic Control*, AC-32(2), February 1987.

[90] Alessandri. A. Sliding-mode estimators for a class of non-linear systems affected by bounded disturbances. *International Journal of Control*, 76(3) :226–236, 2003.

[91] Massoumnia. M.A. A geometric approach to the synthesis of failure detection filters. *IEEE Transactions on Automatic Control*, 31(9) :839–846, 1986.

[92] De Persis. C and Isidori. A. On the observability co-distributions of nonlinear systems. *System & Control letters*, 40 :297–304, 2000.

[93] Paone. N, Cristalli. C, and Rodriguez. R.M. Comparative study between laser vibrometer and accelerometer measurements for mechanical fault detection of electric motors. *Proceedings of SPIE - The International Society for Optical Engineering*, 2002.

[94] Cristalli. C, Paone. N, and Rodriguez. R.M. Mechanical fault detection of electric motors by laser vibrometer and accelerometer measurements. *Mechanical Systems and Signal Processing*, 20(6) :1350–1361, 2006.

[95] Mohanty. A. R and Fatima. S. Shaft misalignment detection by thermal imaging of support bearings. *International Federation of Automatic Control, Hosting by Elsevier Ltd.*, pages 554–559, 2015.

[96] Azamfar. M, Singh. J, Bravo-Imaz. I, and Lee. J. Multisensor data fusion for gearbox fault diagnosis using 2-d convolutional neural network and motor current signature analysis. *Mechanical Systems and Signal Processing*, 144, October 2020.

[97] Li. D, Wang. Y, Wang. J, Wang. C, and Duanf. Y. Recent advances in sensor fault diagnosis : A review. *Sensors and Actuators A : Physical*, 309, July 2020.

[98] Mansouri. M, Harkat. M. F, Nounou. H. N, and N. Nounou. M. N. Data-driven and model-based methods for fault detection and diagnosis. *Copyright 2020 Elsevier Inc.*, 2020.

[99] S. Yi. S, Lai. Z, He. Z, Cheung. Y, and Liu. Y. Joint sparse principal component analysis. *Pattern Recognit*, 61 :524–536, January 2017.

[100] Muradore. R and Fiorini. P. A pls-based statistical approach for fault detection and isolation of robotic manipulators. *IEEE Transactions On Industrial Electronics*, 59(8) : 3167–3175, August 2012.

[101] Do. V. L. Statistical detection and isolation of cyber-physical attacks on scada systems. *43rd Annual Conference of the IEEE Industrial Electronics Society (IECON)*, 2017.

[102] Zadkarami. M, Shahbazian. M, and Salahshoor. K. Pipeline leakage detection and isolation : An integrated approach of statistical and wavelet feature extraction with multi-layer perceptron neural network (mlpnn). *Journal of Loss Prevention in the Process Industries*, 43 :479–487, 2016.

[103] Sobhani-Tehrani. E and Khorasani. K. Fault diagnosis of nonlinear systems using a hybrid approach. *Lecture Notes in Control and Information Sciences, Springer Science and Business Media*, 2009.

[104] Rai. A and Upadhyay. S. H. A review on signal processing techniques utilized in the fault diagnosis of rolling element bearings. *Tribology International*, 96 :289–306, 2016.

[105] Kia. S. H, Henao. H, and Capolino. G-A. Diagnosis of broken-bar fault in induction machines using discrete wavelet transform without slip estimation. *IEEE Transactions On Industry Applications*, 45(4) :1395–1404, 2009.

[106] Heydarzadeh. M, Zafarani. M, Nourani. M, and Akin. B. A wavelet-based fault diagnosis approach for permanent magnet synchronous motors. *IEEE Transactions On Energy Conversion*, 34(2), 2019.

[107] Palleti. V. R, Chong. T. Y, and Samavedham. L. A mechanistic fault detection and isolation approach using kalman filter to improve the security of cyber physical systems. *Journal of Process Control*, 68 :160–170, August 2018.

[108] Gautam. S, Tamboli. P, Roy. K, Patankar. V. H, and Duttagupta. S. P. Sensors incipient fault detection and isolation of nuclear power plant using extended kalman filter and kullbackleibler divergence. *ISA Transactions*, 92 :180–190, September 2019.

[109] Zoljic-Beglerovic. S, Stettinger. G, Luber. B, and Horn. M. *10th IFAC Symposium on Fault Detection, Supervision and Safety for Technical Processes, Warsaw, Poland*, pages 1330–1335, August 2018.

[110] Pourasghar. M, Combastel. C, Puig. V, and Ocampo-Martinez. C. Fd-zkf : A zonotopic kalman filter optimizing fault detection rather than state estimation. *Journal of Process Control*, 2018.

[111] Das. M, Sadhu. S, and Ghoshal. T. K. Fault detection and isolation using an adaptive unscented kalman filter. *Third International Conference on Advances in Control and Optimization of Dynamical Systems, Kanpur, India*, pages 326–332, March 2014.

[112] Rigatos. G, Serpanos. D, Siadimas. V, Siano. P, and Abbaszadeh. M. Fault diagnosis of gas-turbine power units with the derivative-free nonlinear kalman filter. *Electric Power Systems Research*, 174, September 2019.

[113] Wang. X and Syrmos. V. L. Fault detection, identification and estimation in the electro-hydraulic actuator system using ekf-based multiple-model estimation. *16th Mediterranean Conference on Control and Automation Congress Centre, Ajaccio, France*, June 2008.

[114] Huang. Y, Jing. Y, and shi. Y. Multi-sensor node fusion localization using unscented kalman filter in rough environments. *2018 Chinese Control And Decision Conference (CCDC)*, 2018.

[115] Jing. C. S and Pebrianti. D. Fault detection and identification in quadrotor system (quadrotor robot). *IEEE International Conference on Automatic Control and Intelligent Systems, Shah Alam, Malaysia*, October 2016.

[116] Patton. R.J. and Chen. J. A review of parity space approaches to fault diagnosis. *Prec. IFAC SAFEPROCESS Symp*, pages 65–81, 1991.

[117] Ding. X, Guo. L, and Jeinsch. T. A characterization of parity space and its application to robust fault detection. *IEEE Transactions on Automatic Control*, 44(2) :337–343, February 1999.

[118] Gertler. J. Fault detection and isolation using parity relations. *Control Engeneering Practice*, 5(5) :653–661, 1997.

[119] Cho. S and Jiang. J. A fault detection and isolation technique using nonlinear support vectors dichotomizing multi-class parity space residuals. *Journal of Process Control*, 82 :31–43, 2019.

[120] Blesa. J, Jiménez. P, Rotondo. D, Nejjari. F, and Puig. V. An interval nlpv parity equations approach for fault detection and isolation of a wind farm. *IEEE Transactions On Industrial Electronics*, 62(6) :3794–3805, June 2015.

[121] Cocquempot. V, Staroswiecki. M, and El Mezyani. T. Switching time estimation and fault detection for hybrid systems using structured parity residuals. *IFAC Fault Detection, Supervision and Safety of Technical Processes, Washington, D.C., USA*, 2003.

[122] Hammouri. H, Kinnaert. M, and El Yaagoubi. E. H. Application of nonlinear observers to fault detection and isolation. *A book chapter in New Directions in Nonlinear Observer Design, Springer, Berlin/Heidelberg*, pages 423–443, 1999.

[123] Hammouri. H, Kinnaert. M, and El Yaagoubi. E. H. Observer-based approach to fault detection and isolation for nonlinear systems. *IEEE Transactions on Automatic Contro*, 44(10) :1879–1884, 1999.

[124] Nijmeijer. H and Fossen. T. I. New directions in nonlinear observer design. *Lecture notes in control and information sciences, Springer-verlag London*, 1999.

[125] Edwards. C, Spurgeon. S. K, and Patton. R. J. Sliding mode observers for fault detection and isolation. *Automatica*, 36 :541–553, 2000.

[126] Gou. L, Shen. Y, Zheng. H, and Zeng. X. Multi-fault diagnosis of an aero-engine control system using joint sliding mode observers. *IEEE Access*, 8 :10186–10197, 2020. URL doi:10.1109/ACCESS.2020.2964572.

[127] Baldi. P, Blanke. M, Castaldi. P, Mimmo. N, and Simani. S. Fault diagnosis for satellite sensors and actuators using nonlinear geometric approach and adaptive observers. *International Journal of Robust and Nonlinear Control*, April 2018. URL https://doi.org/10.1002/rnc.4083.

[128] Makni. S, Bouattour. M, El Hajjaji. A, and Chaabane. M. Robust adaptive proportional integral observer for faults estimation : Application to bioreactor. *19th International Conference on Sciences and Techniques of Automatic Control and Computer Engineering (STA)*, 2019.

[129] Li. X and Yang. G. Fault diagnosis for non-linear single output systems based on adaptive high-gain observer. *IET Control Theory Applications*, 7(16) :1969–1977, November 2013.

[130] Chu. Z, Meng. D, Zhu. D, and Luo. C. Fault reconstruction using a terminal sliding mode observer for a class of second-order mimo uncertain nonlinear systems. *ISA Transactions*, 97 :67–75, February 2020.

[131] Chua. W. S, Chan. J. C. L, Tan. C. P, Chong. E. K. P, and Saha. S. Robust fault reconstruction for a class of nonlinear systems. *Automatica*, 113, March 2020.

[132] Li. T, Dai. Z, Songa. G, and Dub. H. Simultaneous disturbance estimation and fault reconstruction using probability density functions. *Applied Mathematics and Computation*, 362, December 2019.

[133] Yu. Y, Peng. M. J, Wang. H, Ma. Z. G, and Li. W. Improved pca model for multiple fault detection, isolation and reconstruction of sensors in nuclear power plant. *Annals of Nuclear Energy*, 148, December 2020.

[134] Han. M, Li. J, Han. B, and Zhong. K. Fault subspace decomposition and reconstruction theory based online fault prognosis. *Control Engineering Practice*, 85 :121–131, April 2020.

[135] De Persis. C and Isidori. A. A geometric approach to nonlinear fault detection and isolation. *IEEE Transactions on automatic control.*, 46(6) :853–865, 2001.

[136] De Persis. C, De Santis. R, and Isidori. A. Actuator fault detection and isolation for a vtol aircraft. *Proceedings of the American Control Conference*, 2001.

[137] Lootsma. T.F. Observer based fault detection and isolation for nonlinear systems. *Phd thesis, Aalborg University*, 2001.

[138] Espinoza Trejo D.R and Campos Delgado D.U. Detection and isolation of actuator faults for a class of non linear systems with application to electric drives. *IET Control theory and application*, 3(10) :1317–1329, 2009.

[139] Aguilera F., De la Barrera P.M., De Angelo C.H., and Espinoza Trejo D.R. Current-sensor fault diagnosis in induction-motor drives using a geometric approach. *Control Engineering Practice*, 53 :35–46, 2016.

[140] Khelouat. S, Benalia. A, Boukhetala. D, and Laleg Kirati. T.M. A geometric approach for fault detection and isolation of stator short circuit failure in a single asynchronous machine. *American Control Conference*, pages 5138–5145, june 2012.

[141] Mashreghi. A and Namvar. M. Geometric-based fault diagnosis in a grid-connected inverter. *IEEE Conference on Decision and Control*, 2018.

[142] Peng. T, Tao. H, Yang. C, Chen. Z, Yang. C, Gui. W, , and Karimi. H. R. A uniform modeling method based on open circuit faults analysis for npc-three-level converter. *IEEE Transactions on circuit and systems II*, 2018. URL DOI:10.1109/TCSII.2018.2856862.

[143] Tanwani. A and Liberzon. D. Invertibility of switched nonlinear systems. *Automatica*, 46 :1962–1973, 2010.

[144] Levin. K. T, Hope. E. M, and Dominguez-Garcia. A. D. Observer-based fault diagnosis of power electronics systems. *IEEE Energy Conversion Congress and Exposition*, 2010.

[145] Ding. X, Poon. J, Celanovic. I, and Dominguez-Garcia. A. D. Fault detection and isolation filters for three-phase ac-dc power electronics systems. *IEEE Transactions on Circuits and Systems I*, 60(4) :1038–1051, 2013.

[146] Ren. H, Zong. G, and Karimi. H. R. Asynchronous finite-time filtering of networked switched systems and its application : an event-driven method. *IEEE Transactions on circuit and systems*, 66(1) :391–402, 2019.

[147] Uzunova. M, Ould-Bouamama. B, and Djemai. M. Hybrid bond graph diagnostic and localisation-signal signature study of three-cell converter. *in Mediterranean Conference on Control & Automation (MED)*, 2012.

[148] Louajri. H. Centralized and decentralized fault diagnosis of a class of hybrid dynamic systems : Application to three cell converter. *Phd thesis, Lille university, France*, 2015.

[149] Louajri. H and Sayed-Mouchaweh. M. Decentralized approach for fault diagnosis of three cell converters. *Annual conference of the Prognostics and Health Management society*, 5 :265–277, 2014.

[150] Toubakh. H, Sayed-Mouchaweh. M, Benmiloud. M, Defoort. M, and Djemai. M. Self adaptive learning scheme for early diagnosis of simple and multiple switch faults in multicellular power converters. *ISA Transactions*, March 2020. URL https://doi.org/10.1016/j.isatra.2020.03.025.

[151] Gazzam. N and Benalia. A. Observability analysis and observer design of multicellular converters. *8th International Conference on Modelling, Identification and Control ICMIC*, pages 763–767, 2016.

Annexes

Annexe A

Notions on Differential Geometry

Let consider an affine nonlinear system of the form

$$\begin{cases} \dot{x}(t) = f(x) + \sum_{i=1}^{m} g_i(x)u_i \\ y(t) = h(x) \end{cases} \tag{A.1}$$

where $x \in \mathbb{R}^n$ is the state, $u \in \mathbb{R}^m$ is the input control and $y \in \mathbb{R}^p$ is the output. f, g and h are smooth vector of appropriate dimensions.

Lie derivative :

The Lie derivative of the function h along f, often written as $L_f h(x)$ is given by

$$L_f h(x) = \frac{\partial h(x)}{\partial x} f(x) \tag{A.2}$$

repeated use of this operation is possible, thus by tacking the derivative of h first along of vector field f and then along of vector field g defines the new function as

$$L_g L_f h(x) = \frac{\partial (L_f h(x))}{\partial x} g(x). \tag{A.3}$$

If h being differentiated k times along f, the notation L_f^k is used ; it is given by

$$L_f^k h(x) = \frac{\partial (L_f^{k-1} h(x))}{\partial x} f(x), \tag{A.4}$$

with $L_f^0 h(x) = h(x)$.

Lie Bracket :

The Lie bracket of two vector fields f and g is the new smooth vector field v defined as :

$$v = [f, g] = \frac{\partial g}{\partial x} f - \frac{\partial f}{\partial x} g, \tag{A.5}$$

with $\frac{\partial g}{\partial x}$ and $\frac{\partial f}{\partial x}$ denoted the Jacobian matrices of the mapping g and f respectively. Of course, repeated bracketing of vector field g with the same vector field f is possible, and

in order to avoid a notation $[f,[,...,[f,g]]]$, that could generate confusion, it is preferable to define such an operation recursively, as

$$ad_f^k = [f, ad_f^{k-1} g], \tag{A.6}$$

for any $k \geq 1$, and where $ad_f^0 g(x) = g(x)$.

Co-vector derivative :

Let $w_1, ..., w_n$ be smooth real valued function of real variables $x_1, ..., x_n$, and consider the row vector $(w_1(x_1, ..., x_n), w_2(x_1, ..., x_n), ..., w_n(x_1, ..., x_n))$, then the derivative of the co-vector along of the vector field f is given as :

$$L_f w(x) = f^T(x)(\frac{\partial w^T(x)}{\partial x})^T + w(x)\frac{\partial f}{\partial x}. \tag{A.7}$$

Distribution of vector field :

A distribution is an application that assigns each point $x \in X$, a set of vector fields $f_1, ..., f_d$ that span a vector space, denoted as :

$$\Delta(x) = span f_1, ..., f_d. \tag{A.8}$$

- Let Δ_1 and Δ_2 be distributions, then $\Delta_1 + \Delta_2$ is defined by tacking pointwise the sum of the subspaces $\Delta_1(x)$ and $\Delta_2(x)$, namely,

$$(\Delta_1 + \Delta_2)(x) = \Delta_1(x) + \Delta_2(x) \tag{A.9}$$

- The intersection $\Delta_1 \cap \Delta_2$ is defined as :

$$(\Delta_1 \cap \Delta_2)(x) = \Delta_1(x) \cap \Delta_2(x) \tag{A.10}$$

- A distribution Δ_1 contains Δ_2, and is written $\Delta_2 \subset \Delta_1$ if $\Delta_2(x) \subset \Delta_1(x)$ for all x.

- A vector field f belongs to a distribution Δ, and is written $f \in \Delta$, if $f(x) \in \Delta(x)$ for all x.
- The dimension of a distribution at a point x is the dimension of the subspace $Delta(x)$.
- A singular distribution is a distribution of variable dimension.

Involutive distribution :

A distribution Δ is involutive if the Lie Bracket $[\tau_1, \tau_2]$ of any pair of vector field τ_1 and τ_2 belonging to Δ is a vector field belongs to Δ, i.e., if

$$\tau_1 \in \Delta, \tau_2 \in \Delta_2 \Rightarrow [\tau_1, \tau_2] \in \Delta. \tag{A.11}$$

-The distribution Δ is nonsingular if and only if it is involutive. If Δ is not involutive, we can defined its involutive closure.

- The involutive closure distribution of a distribution Δ, noted $\overline{\Delta}$ is the smallest involutive distribution containing Δ. Noted that $\overline{\Delta}$ can be constructed from the iterated Lie Bracket of vector field $f_1, ..., f_d$.
- A distribution is conditioned invariant, if it satisfies the following condition :

$$[f, \Delta \cap kerdh] \in \Delta. \tag{A.12}$$

- The codistribution of the distribution Δ, noted $\Delta^{\perp}$ id defined as :

$$\Delta^{\perp} = \{w^*(x) \in (R^n)^*; < w^*(x), v(x) >= 0, \forall v \in \Delta\} \tag{A.13}$$